Technische Universität München

Max-Planck-Institut für Quantenoptik

Cavity cooling and spectroscopy of a bound atom-cavity system

Peter L. W. Maunz

Vollständiger Abdruck der von der Fakultät für Physik
der Technischen Universität München
zur Erlangung des akademischen Grades eines

Doktors der Naturwissenschaften (Dr. rer. nat.)

genehmigten Dissertation.

Vorsitzender :		Univ.-Prof. Dr. W. Weise
Prüfer der Dissertation :	1.	Hon.-Prof. Dr. G. Rempe
	2.	Univ.-Prof. Dr. St. Paul (Schriftliche Beurteilung)
		Univ.-Prof. Dr. Dr. h. c. A. Laubereau (Mündliche Prüfung)

Die Dissertation wurde am 14. 12. 2004
bei der Technischen Universität München eingereicht
und durch die Fakultät für Physik am 10. 2. 2005 angenommen.

Abstract

Cooling is indispensable for trapping and observing single free atoms. In atomic physics, this can be achieved efficiently by laser cooling. Conventional methods to laser cool atoms are based on repeated optical pumping cycles followed by spontaneous emission of a photon from the atom. Such pumping schemes can only be applied to certain atomic species, which have a closed optical transition. Drawbacks caused by photons spontaneously emitted from the atom can be avoided in the strongly coupled atom-cavity system in which energy and entropy can be removed by photons lost from the cavity.

This thesis reports on the first observation of this cooling mechanism which does not rely on spontaneous emission. In the experiment, a single atom is captured in an intracavity dipole trap. Illuminating the system with a weak, slightly blue-detuned light beam extends the storage time of the atom in the trap. The observed cooling force is at least five times larger than the force achieved by free-space cooling methods at comparable excitation of a two-level atom.

Utilising cavity cooling, single atoms are prepared strongly-coupled to the mode of a high-finesse cavity. This allows to observe two well-resolved normal-mode peaks in both the cavity transmission as well as in the trap lifetime. The experiment is in agreement with a Monte Carlo simulation, demonstrating the localisation of the atom to within a tenth of a wavelength. The ability to individually excite the normal modes opens new possibilities to use this system for applications in quantum information science, including the realisation of quantum-logic gates.

In the future cavity cooling might be applied to systems which cannot be cooled by conventional methods as for instance molecules or an atom carrying a quantum bit.

Zusammenfassung

Das Kühlen einzelner Atome ist die Voraussetzung dafür, sie in einer Lichtfalle einfangen und beobachten zu können. Mit der Laserkühlung steht der Atomphysik eine effiziente Methode dafür zur Verfügung. Deren Nachteil besteht jedoch darin, daß sie auf der wiederholten Absorption und spontanen Emission von Photonen beruht. Daher ist diese Methode nur für wenige Atomsorten, die einen geschlossenen Übergang aufweisen, anwendbar. Im stark gekoppelten Atom-Resonator-System kann die spontane Emission von Photonen vom Atom vermieden werden, indem Energie und Entropie durch aus der Resonatormode transmittierte Photonen abgeführt werden.

In dieser Arbeit wird diese neue Kühlmethode, die nicht auf spontaner Emission beruht, erstmals verwirklicht. Im Experiment wird ein einzelnes Atom in einer Resonator-Dipolfalle eingefangen. Beleuchtet man dieses System mit einem schwachen, leicht blau verstimmten Laserstrahl, so wird die Speicherzeit des Atoms in der Falle verlängert. Die beobachtete Kühlkraft ist mehr als fünfmal stärker als die Kühlkraft, die bei vergleichbarer Anregung eines Zwei-Niveau-Atoms, mit Laserkühlmethoden im freien Raum, erreicht wird.

Mittels dieser Resonator-Kühlmethode werden einzelne Atome in der Mode des Hochfinesse-Resonators lokalisiert. Dadurch können die Normalmoden des gekoppelten Systems sowohl in der Transmission als auch in der Lebensdauer der Falle aufgelöst werden. Das Experiment wird durch eine Monte-Carlo-Simulation beschrieben, welche zeigt, daß das Atom auf ein Zehntel der Wellenlänge lokalisiert werden kann. Die unabhängige Anregung der beiden Normalmoden eröffnet neue Anwendungsmöglichkeiten in der Quanteninformationsverarbeitung, beispielsweise die Realisierung Quantenlogischer Gatter.

In der Zukunft könnte die Resonatorkühlung auch auf Systeme angewandt werden, die mittels konventioneller Methoden nicht gekühlt werden können, wie etwa Moleküle oder ein Atom, in welchem ein Quantenbit gespeichert ist.

Contents

Chapter 1

Introduction

The quantum nature of physical systems is not apparent in every day life. To investigate quantum phenomena it is desirable to experimentally realise small model systems, which are governed by the laws of quantum mechanics. The basic system of matter light interaction consists of a single atom coherently interacting with a single mode of the light field within a cavity. Built from two well known parts the system can be described from first principles. Nonetheless, the combined system shows a wealth of effects that can be studied. The coupling of the system to the environment leads to a loss of photons transmitted through the cavity mirrors and scattered by the atom. This disturbs the coherent dynamics of the system, but on the other hand the emitted photons can be detected and allow to continuously observe the system. This renders the system suitable for the investigation of the conditional dynamics of an open quantum system (Wiseman and Milburn, 1993; Carmichael *et al.*, 2000). The position-dependent strength of the interaction between the atom and the light field in principle allows to observe the atomic position and motion (Rempe, 1995). Furthermore, the strong coupling between matter and light provided by the cavity can be used as a matter-light interface for quantum information science and might allow to map a quantum state from an atom onto a photon and vice versa (Cirac *et al.*, 1997) or to implement a quantum gate between single photon quantum bits (Duan and Kimble, 2004).

In order to realise this system in the laboratory, it is necessary to place a single atom in a cavity and isolate the system from interactions with its environment to the extend that quantum coherence is maintained over dynamically relevant timescales. For a long time, experiments with single molecules or atoms were unimaginable. In the realm of atomic and optical physics, experiments with single atoms were first realised in the pioneering experiments on trapping and cooling of single ions (Neuhauser *et al.*, 1980; Wineland and Itano, 1981). The invention of laser cooling (Letokhov and Minogin, 1981; Chu, 1998; Cohen-Tannoudji, 1998; Phillips, 1998) also

opened up the possibility to efficiently cool neutral atoms to very low temperatures and enabled the observation of a single atom in a magneto-optical trap (MOT) (Hu and Kimble, 1994; Ruschewitz *et al.*, 1996; Haubrich *et al.*, 1996) and in dipole traps (Frese *et al.*, 2000; Schlosser *et al.*, 2001). In free space the atomic motion can also be deliberately manipulated (Kuhr *et al.*, 2001).

Coupling an atom to a single mode of the radiation field and achieving a coherent exchange of the excitation between the atom and the light field requires a tiny cavity composed of mirrors with ultrahigh reflectivity. In the optical domain, a milestone on this way was the realisation of strong coupling for atoms from an atomic beam to a cavity mode in the experiment of Thompson *et al.* (1992). In strong coupling, the exchange rate of an excitation between atoms and the cavity mode, g, is larger than the decay rates of the atomic polarisation, γ, and the cavity field, κ. In this regime the interaction with a single atom can dramatically influence the transmission of the cavity. The oscillatory exchange of the excitation can be observed using a homodyne measurement of the transmitted field conditioned on the detection of a transmitted photon Foster *et al.* (2000). However, the atoms of an atomic beam are too fast to be observed one by one. Combining the technology of high-finesse cavities with laser cooling methods allowed to considerably extend the time an atom needs to traverse the tiny cavity mode and enabled the observation of single atoms (Mabuchi *et al.*, 1996; Münstermann *et al.*, 1999b; Sauer *et al.*, 2004). Now the time an atom spends in the cavity was long enough to observe the effect of radiative forces from a few-photon light field which are altered by the presence of the cavity (Hood *et al.*, 1998; Münstermann *et al.*, 1999a). The forces generated by a single intracavity photon can even be strong enough to control the atomic motion. In the experiments of Pinkse *et al.* (2000) and Hood *et al.* (2000), a single atom was captured in the light field of only a single photon. The cavity transmission allowed to simultaneously trace the atomic motion in real time. A feedback scheme which relayed on the observation of the atomic motion was realised by Fischer *et al.* (2002) to extend the storage time of a single atom in the cavity. However, the symmetry of the fundamental cavity mode allows only to observe the distance of the atom from the cavity axis. Information on the angle of the atom in a plane perpendicular to the cavity axis can be obtained by utilising higher-order transversal modes (Horak *et al.*, 2002; Maunz *et al.*, 2003; Puppe *et al.*, 2004).

The experiment performed in this thesis uses an auxiliary far-detuned dipole trap to capture and store an atom within the cavity mode, a system first realised by Ye *et al.* (1999). The far-detuned trap allows to substantially extend the storage time of a single atom compared to near-resonant traps used before. There, the atomic motion is severely disturbed by spontaneous scattering of photons and fluctuations of the dipole force while the low atomic excitation and momentum diffusion in the far-detuned quasi-

conservative trap allows for an oscillatory motion of the atom. This enables the observation of the radial and the axial motion of an individual atom.

A main result achieved in the framework of this thesis is cooling of the axial motion of a single atom in the trap using a new "cavity cooling" mechanism (Horak *et al.*, 1997). Like other conventional cooling mechanisms, cavity cooling involves a dissipative process to remove entropy from the system. In laser cooling, this is usually spontaneous emission of photons from the atom. Cavity cooling reduces this ubiquitous process. In the strongly coupled atom-cavity system, the role of spontaneous emission is replaced by the escape of photons from the cavity. For cooling, the atom's kinetic energy is transfered to the photons which leave the cavity with more energy than when they entered. This cavity cooling scheme is demonstrated to be at least five times more efficient than free-space laser cooling mechanisms of a two-level atom with equal excitation of the atom (Maunz *et al.*, 2004). Furthermore it might be applied in the future to systems that cannot be cooled by conventional methods — molecules which do not have a closed transition (Vuletić and Chu, 2000) or even an atom carrying a quantum bit (Griessner *et al.*, 2004). For larger atomic samples, there are variations of cavity cooling that show favourable collective effects (Chan *et al.*, 2003; Nagorny *et al.*, 2003; Kruse *et al.*, 2003; Zippilli *et al.*, 2004).

The ability to cool a single atom in the intracavity trap allows to compensate for heating and to localise an atom at a region of strong coupling. This can be applied to measure the distinctive splitting of the two normal modes of the atom-cavity system, both in the cavity transmission and in the lifetime of an atom in the trap. Although normal-mode spectroscopy of atomic ensembles has a long tradition, a spectrum for a single trapped atom was never observed before. This result demonstrates the excellent control over the atomic motion and shows the reliable localisation of an atom in the regime of strong coupling (Maunz *et al.*, 2005). The measurement of the normal-mode splitting in this thesis was followed up by measurements of normal-mode splittings in solid state systems (Chiorescu *et al.*, 2004; Wallraff *et al.*, 2004; Reithmaier *et al.*, 2004; Yoshie *et al.*, 2004).

In conclusion, the three experiments performed in this thesis, real-time observation of the axial and radial atomic motion, cavity cooling and the normal-mode spectroscopy, document the progress towards the experimental realisation of the archetype system of matter light interaction. A first application of the atom-cavity system for quantum information science was already realised by the generation of single photons on demand (Kuhn *et al.*, 2002; McKeever *et al.*, 2004a; Keller *et al.*, 2004) which are the essential ingredient of linear optical quantum computation schemes (Knill *et al.*, 2001). Spectacular advances have recently been achieved in quantum information processing with trapped ions interacting via phonons (Riebe *et al.*, 2004; Barrett *et al.*, 2004; Chiaverini *et al.*, 2004). While ions were recently coupled to cavities (Guthörlein *et al.*, 2001; Kreuter *et al.*, 2004), strong coupling

of an ion to a cavity mode is not realised yet. The progress in the control of the motion of an atom inside the optical cavity prepares the foundation for applications of this system in quantum information science.

This thesis is organised as follows: In chapter 2 an overview of the theoretical description of the atom-cavity system is given. Analytical expressions for the radiative forces are used to numerically simulate the motion of single atoms in the cavity as described in chapter 3. The experimental apparatus is introduced in chapter 4. The results obtained with this apparatus are presented in chapters 5-7: In chapter 5 the observation of the individual motion of a single atom is investigated. Chapter 6 elaborates Maunz *et al.* (2004) and focuses on cavity cooling of a single atom stored in the trap. In chapter 7 (Maunz *et al.*, 2005) this cooling mechanism is used to measure the distinctive splitting of the normal-modes of the atom-cavity system. Chapter 8 concludes the experimental results and gives an outlook on experiments that could be feasible in the future based on the results of this work.

Chapter 2

Theory of the atom-cavity system

In the experiment, a single atom which is strongly coupled to the light field of a high-finesse cavity is investigated (figure 2.1). The atomic motion is observed via the cavity transmission. Radiative forces are induced by the interaction of the atom with two cavity fields. One of them is near-resonant with the atomic transition and is used to observe the atom. The other is a far-detuned and serves to capture and trap the atom.

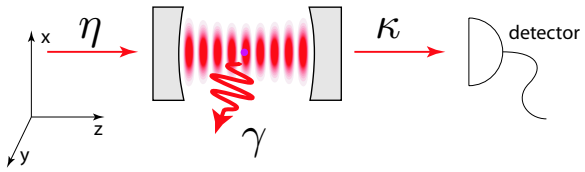

Figure 2.1: Schematic of the atom-cavity system

In this chapter, the theoretical description of the atom-cavity-trap system is introduced. The for the experiment most relevant progress of the theoretical description of this system is outlined in section 2.1. The theory of the interaction of a single atom with a single cavity mode is summarised in section 2.2. Here the Jaynes-Cummings model is introduced and the theory is extended to the open quantum system interacting with its environment. The master equation describing the open quantum system is solved for weak atomic excitation where analytical expressions for the radiative forces are obtained. In section 2.3, these expressions are approximated for large detuning as applicable to describe the radiative forces of the far-detuned trap. The theory of the combined interaction of the atom with the near-resonant and the far-detuned light fields which was developed within this thesis is presented in section 2.4. Along the lines of Hechenblaikner *et al.* (1998) analytical expressions for the dipole force, the momentum diffusion and fric-

tion coefficient are derived for weak atomic excitation. The addition of the far-detuned trap leads to additional terms in the dipole force, friction and diffusion coefficients. The atomic motion in the light fields can be described by means of the Fokker-Planck equation as will be discussed in section 2.5.

2.1 Introduction

Experimental progress in the observation of single laser-cooled atoms (Mabuchi *et al.*, 1996; Münstermann *et al.*, 1999b) allowed to observe radiative forces on a single atom in real time and triggered extensive theoretical investigations of the forces generated by the strong interaction of an atom with the light field of a high-finesse cavity. Doherty *et al.* (1997) investigated the mechanical effect of the optical potential of the cavity field on the atomic motion in the limit of a resonantly driven cavity. In close analogy to Doppler heating in a standing wave field, they found heating mechanisms which lead to high kinetic energies and short storage times of the atom. In the same year, Horak *et al.* (1997) and Hechenblaikner *et al.* (1998) proposed a novel cooling mechanism which is mediated by the combined atom-cavity dynamics. This effect emerges in the strong coupling regime and can be explained as a Sisyphus type cooling mechanism generated by the delayed adaption of the intracavity photon number to the position of the atom. Their analytical solution for the radiative forces and excitation of a single atom interacting with a single cavity mode was extended by Fischer *et al.* (2001) and Fischer (2002) to cover the interaction of many atoms with many degenerate cavity modes.

Recent experiments (Ye *et al.*, 1999; McKeever *et al.*, 2003; Maunz *et al.*, 2004) employ an additional far-detuned intracavity dipole trap to store a single atoms in the cavity mode. The simultaneous interaction of an atom with a near-resonant and a strong far-detuned light field, which is realised in these systems, was first investigated numerically by van Enk *et al.* (2001). In this thesis, analytical expressions for the radiative forces in the atom-cavity-trap system in the limit of weak atomic excitation are derived. The expressions for the dipole force, momentum diffusion and friction coefficient allow to interpret the origin of these forces and to efficiently simulate the motion of an atom in the combined atom-cavity-trap system.

In all aforementioned publications, the atom was treated as a point-like particle. A theoretical analysis of the atom-cavity system including the wave packet dynamics of the atomic motion can be found in Vernooy and Kimble (1997). Recently, the influence of the finite localisation of an atom on the autocorrelation function of transmitted photons was investigated by Leach and Rice (2004).

2.2 Quantum theory of the atom-cavity system

2.2.1 The atom-cavity system

The basic interaction of a single atom with a single mode of the electromagnetic field was first investigated by Jaynes and Cummings (1963). The simplified system consisting of a single point-like two-level atom at rest, coupled to a single quantised mode of the cavity without losses is described in the dipole and rotating wave approximations by the Hamiltonian

$$H_{JC} = \hbar\omega_a \sigma^+\sigma^- + \hbar\omega_c a^+ a + \hbar g(a^+\sigma^- + \sigma^+ a). \tag{2.1}$$

Where a^+, a are the creation and annihilation operators of a photon in the cavity mode, respectively. They obey the canonical commutation relation

$$[a, a^+] = 1. \tag{2.2}$$

The resonance frequency of the cavity is $\omega_c/2\pi$. The number of photons stored in the cavity is given by the expectation value of the photon number operator a^+a. The energy difference between the atomic excited and ground state is $\hbar\omega_a$. The operator of the atomic excitation is $\sigma^+\sigma^-$ and the operators σ^+, σ^- and σ_z are the pseudo-spin operators fulfilling the algebra

$$[\sigma^+, \sigma^-] = \sigma_z, \quad [\sigma_z, \sigma^\pm] = \pm 2\sigma^\pm. \tag{2.3}$$

The third term of the Hamiltonian (2.1) describes the exchange of one quantum of excitation between the atom and the cavity mode. The rate of exchange of the excitation is determined by the coupling constant

$$g = \sqrt{\frac{\omega_c}{2\epsilon_0 V\hbar}}\, d_{ge}, \tag{2.4}$$

of atom and light field which is proportional to the dipole matrix element of the atomic transition, d_{ge}, and inversely proportional to the square root of the cavity mode volume, V. (ϵ_0 is the vacuum permittivity).

The energy eigenvalues and eigenstates of this system can be calculated analytically. The ground state of this system $|g, 0\rangle$ is an energy eigenstate. The other energy eigenstates of the system are superpositions of the states $|g, n\rangle$ with the atom in the ground state and n intracavity photons and $|e, n-1\rangle$ with an excited atom and $n-1$ photons

$$\begin{array}{rcrcl} |+, n\rangle &=& \cos\theta|e, n-1\rangle &+& \sin\theta|g, n\rangle \\ |-, n\rangle &=& -\sin\theta|e, n-1\rangle &+& \cos\theta|g, n\rangle. \end{array} \tag{2.5a}$$

The transformation from the basis $\{|e, n-1\rangle, |g, n\rangle\}$ to the "dressed state" basis $\{|+, n\rangle, |-, n\rangle\}$ is a rotation in the Hilbertspace of the system by the

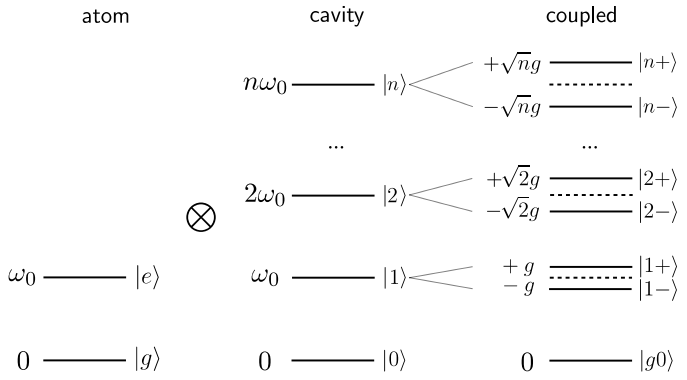

Figure 2.2: Dressed states of the coupled atom-cavity system for the resonant case $\Delta = \omega_c - \omega_a = 0$.

"mixing angle" θ which is determined by the coupling g and the atom-cavity detuning $\Delta = \omega_c - \omega_a$. The mixing angle θ is given by

$$\theta = \arctan \frac{g}{-\Delta/2 + \sqrt{g^2 + (\Delta/2)^2}}. \tag{2.6}$$

For the detunings $\Delta/g = (-\infty, 0, \infty)$ the mixing angle is $\theta = (0, \pi/4, \pi/2)$, respectively. The energy eigenvalues are

$$E_{+,n} = n\hbar\omega_c - \hbar\frac{\Delta}{2} + \frac{\hbar}{2}\sqrt{\Delta^2 + 4g^2 n} \tag{2.7}$$

$$E_{-,n} = n\hbar\omega_c - \hbar\frac{\Delta}{2} - \frac{\hbar}{2}\sqrt{\Delta^2 + 4g^2 n}. \tag{2.8}$$

The coupling-induced shift of the energy levels is $E_{+,n} - E_{-,n} - \hbar\Delta = \hbar\sqrt{\Delta^2 + 4g^2 n} - \hbar\Delta$ and reaches a maximum of $2\hbar g\sqrt{n}$ for $\Delta = 0$. The energy eigenstates of the uncoupled and coupled system are depicted in figure 2.2.

2.2.2 Open quantum systems

In the previous section, the Jaynes-Cummings system, a closed system without losses was presented. While this simple model explains the basic phenomena of the strongly-coupled atom-cavity system, in most experimental situations the interaction of the system with the environment cannot be neglected and leads to an exchange of energy and to a loss of phase coherence. In the optical regime, where the environment is to very good approximation in its vacuum state, the coupling to the environment is well described by spontaneous emission from the atom and a loss of photons from the cavity. These damping mechanisms allow to collect information on the system under investigation and provide the dissipation which is essential for cooling.

To develop a quantum mechanical description of a system S interacting with a reservoir R the total system is considered. The Hilbert space of the total system is the tensor product of the Hilbert spaces of system and reservoir $\mathcal{H} = \mathcal{H}_{\mathcal{S}} \otimes \mathcal{H}_{\mathcal{R}}$. To replenish the lost excitation, the system is driven by coherent radiation with frequency $\omega_p/2\pi$ introduced in the Hamiltonian by a pump term exciting the cavity mode

$$H_P = i\hbar\eta \left(a^+ e^{-i\omega_p t} - a e^{i\omega_p t}\right). \tag{2.9}$$

The total Hamiltonian is the sum of the Hamiltonians describing the Jaynes-Cummings system, the reservoir, the interaction of atom and cavity with the reservoir and the coherent pumping:

$$H_T = H_{JC} + H_R + H_{AR} + H_{CR} + H_P. \tag{2.10}$$

The reservoir can be modelled as a bath of harmonic oscillators with frequencies ω_k and creation and annihilation operators b_k^+ and b_k, respectively. The Hamiltonian of the reservoir reads

$$H_R = \sum_k \hbar\omega_k \left(b_k^+ b_k + \frac{1}{2}\right). \tag{2.11}$$

The interaction of the system with the reservoir consists of the interaction of the atom with the reservoir modes,

$$H_{AR}(\mathbf{r}) = \sum_k g_{ar,k}(\mathbf{r}) \left(\sigma^+ b_k + b_k^+ \sigma\right), \tag{2.12}$$

and the coupling of the cavity mode to the reservoir modes outside the resonator

$$H_{CR} = \sum_k g_{cr,k}(b_k^+ a + a^+ b_k). \tag{2.13}$$

With the coupling $g_{ar,k}(\mathbf{r})$ of the atom and $g_{cr,k}$ of the cavity mode to the kth mode of the reservoir, respectively. For weak interaction between the system and the reservoir, the interaction can be treated in the Born approximation, which neglects terms higher than second order in the interaction. In this approximation, the interaction of the system with the reservoir can be interpreted as an exchange of photons between the atom and the reservoir modes (H_{AR}) and the cavity mode and the reservoir modes (H_{CR}), respectively.

The time evolution of the total system is given by the van-Neumann equation for the density operator of the total system, χ,

$$\dot{\chi} = -\frac{i}{\hbar}[H, \chi]. \tag{2.14}$$

This is a complex equation for a huge system. Using the following approximation the time evolution of the system density operator ρ can be extracted by tracing over the degrees of freedom of the reservoir.

In a huge reservoir, correlations within the reservoir decay on a timescale which is much faster than the timescale of the interaction with the system. Therefore the state of the reservoir does not depend on the state of the system, it has effectively no memory of the system state at earlier times. Thus, the influence of the reservoir on the system depends only on the current state of the system and not on its history (Markov approximation).

2.2.3 Master equation for the driven atom-cavity system

Applying Born and Markov approximations (Carmichael, 1999) and tracing over the degrees of freedom of the reservoir

$$\rho = \mathrm{Tr}_R\{\chi\} \tag{2.15}$$

yields the master equation for the reduced density operator of the system, ρ,

$$\begin{aligned}\dot{\rho} = -\frac{i}{\hbar}[H_{JC} + H_P, \rho] &-\gamma(\bar{n}+1)(\sigma^+\sigma^-\rho + \rho\sigma^+\sigma^- - 2\sigma^-\rho\sigma^+) \\ &-\gamma\bar{n}(\sigma^-\sigma^+\rho + \rho\sigma^-\sigma^+ - 2\sigma^+\rho\sigma^-) \\ &-\kappa(\bar{n}+1)(a^+a\rho + \rho a^+a - 2a\rho a^+) \\ &-\kappa\bar{n}(aa^+\rho + \rho aa^+ - 2a^+\rho a),\end{aligned} \tag{2.16}$$

where γ is the decay rate of the atomic polarisation and κ is the cavity field decay rate. Here the state of the reservoir enters the time evolution of the system only via the mean occupation of its oscillator states. For a reservoir with absolute temperature T, the mean occupation of these oscillator states is

$$\bar{n}(\omega_k, T) = \frac{e^{-\hbar\omega_k/k_BT}}{1 - e^{-\hbar\omega_k/k_BT}}. \tag{2.17}$$

Here, k_B is the Boltzmann constant. The terms of equation 2.16 which are proportional to $(\bar{n}+1)$ describe induced emissions of an energy quantum from the system to the reservoir, those proportional to $\bar{n}$ describe the absorption of one excitation from the reservoir. At room temperature and for optical frequencies, the mean occupation of the oscillator states of the reservoir is very small ($\bar{n} \lll 1$). Therefore the master equation for the atom-cavity system can be approximated by

$$\begin{aligned}\dot{\rho} = \mathcal{L}\rho = -\frac{i}{\hbar}[H_{JC} + H_P, \rho] &-\gamma(\sigma^+\sigma^-\rho + \rho\sigma^+\sigma^- - 2\sigma^-\rho\sigma^+) \\ &-\kappa(a^+a\rho + \rho a^+a - 2a\rho a^+).\end{aligned} \tag{2.18}$$

Here $\mathcal{L}$ is called the Liouville super operator. Without an atom in the cavity the master equation (2.18) can be solved analytically. The mean intracavity photon number in this case is

$$\left\langle a^{+}a\right\rangle_{e} =: n_e = \frac{\eta^2}{\kappa^2 + \Delta_c^2}, \tag{2.19}$$

where $\Delta_c = \omega_p - \omega_c$ is the cavity detuning.

2.2.4 Two-time averages and the quantum regression theorem

In principle, the master equation can be solved and the reduced density operator ρ of a system interacting with a reservoir can be obtained. Using this density operator, the time-dependent expectation values of system operators can be calculated as

$$\langle \dot{O} \rangle = \mathrm{Tr}_S\{O\dot{\rho}\} = \mathrm{Tr}_S\{O\mathcal{L}(\rho)\}. \tag{2.20}$$

In order to calculate correlation functions of system operators, two-time expectation values of products of arbitrary system operators, O_1, O_2, of the form $\langle O_1(t)O_2(t+\tau)\rangle$ must be calculated. This can be done using the Quantum Regression Theorem (Carmichael, 1999):

$$\langle O_1(t)O_2(t+\tau)\rangle = \mathrm{Tr}_S\left\{O_2(0)e^{\mathcal{L}\tau}[\rho(t)O_1(0)]\right\} \tag{2.21}$$

$$\langle O_1(t+\tau)O_2(t)\rangle = \mathrm{Tr}_S\left\{O_1(0)e^{\mathcal{L}\tau}[O_2(0)\rho(t)]\right\}. \tag{2.22}$$

These formal equations can also be reduced to a form which is more convenient for calculations. Essentially, the equations of motion for expectation values of system operators (one-time averages) are also the equations of motion for correlation functions (two-time averages) as will be shown in the following.

We assume, that for a complete set of system operators $\{A_\mu\}_{\mu=1,2,\ldots}$ and an arbitrary operator O, and for each A_μ holds

$$\mathrm{Tr}_S\{A_\mu(\mathcal{L}O)\} = \sum_\lambda M_{\mu\lambda}\,\mathrm{Tr}_S\{A_\lambda O\}, \tag{2.23}$$

where the $M_{\mu\lambda}$ are constants. Then it follows, that

$$\langle \dot{A}_\mu \rangle = \sum_\lambda M_{\mu\lambda}\,\langle A_\lambda \rangle\,. \tag{2.24}$$

Thus the expectation values $\langle a_\mu \rangle\,,\ \mu = 1, 2, \ldots,$ obey a coupled set of linear equations where the evolution matrix $\mathbf{M}$ is defined by the coefficients $M_{\mu\lambda}$. In matrix notation

$$\langle \dot{\mathbf{A}} \rangle = \mathbf{M}\,\langle \mathbf{A} \rangle\,. \tag{2.25}$$

Using (2.21) and (2.23), the equation of motion for two-time averages can be calculated. For $\tau \geq 0$ one gets

$$\frac{\mathrm{d}}{\mathrm{d}\tau} \langle O_1(t)\mathbf{A}(t+\tau)\rangle = \mathbf{M} \langle O_1(t)\mathbf{A}(t+\tau)\rangle \tag{2.26a}$$

$$\frac{\mathrm{d}}{\mathrm{d}\tau} \langle \mathbf{A}(t+\tau)O_2(t)\rangle = \mathbf{M} \langle \mathbf{A}(t+\tau)O_2(t)\rangle . \tag{2.26b}$$

Here O can be an arbitrary system operator, not necessarily one of the A_μ. Using this result, the expectation values of correlation functions can be calculated easily.

2.2.5 Light forces

To calculate the light forces in this system, the motional degrees of freedom must be included in the Hamiltonian. In a near-planar Fabry-Perot cavity, the photon creation and annihilation operators a^+ and a refer to the cavity mode with the spatial modefunction

$$\phi(\mathbf{r}) = \cos(kz)e^{-(x^2+y^2)/\mathrm{w}_0^2}. \tag{2.27}$$

Here, k is the wave vector and w_0 the waist of the cavity mode. Together with the kinetic energy $\mathbf{P}^2/2m$ of the atom with mass m the Hamiltonian reads

$$H = \frac{\mathbf{P}^2}{2m} + \hbar\omega_a\sigma^+\sigma^- + \hbar\omega_c a^+a + \hbar g\phi(\mathbf{r})(a^+\sigma^- + \sigma^+a) + H_P + H_R + H_{CR} + H_{AR}(\mathbf{r}). \tag{2.28}$$

The force operator can be calculated from this Hamiltonian using the Heisenberg equation of the atomic momentum

$$\mathbf{F} = \dot{\mathbf{P}} = \frac{i}{\hbar}[H, \mathbf{P}]. \tag{2.29}$$

For the expectation value of the force we get

$$\langle \mathbf{F}\rangle = -\hbar(\nabla\phi(\mathbf{r}))\left\langle a^+\sigma^- + \sigma^+a\right\rangle . \tag{2.30}$$

The other terms do not contribute to the average force, but they contribute to the fluctuations of the force and therefore lead to a spreading of the atomic wavepacket and contribute to the momentum diffusion coefficient discussed below.

2.2.6 Solution for weak atomic excitation

Starting from the master equation (2.18) the dynamical equations for the expectation values of the system operators σ^- and a can be calculated using (2.20). With the definitions (Murr, 2003), (but note the different sign convention)

$$\Delta_a := \omega_p - \omega_a \qquad \tilde{\Delta}_a := \Delta_a + i\gamma \tag{2.31}$$

$$\Delta_c := \omega_p - \omega_c \qquad \tilde{\Delta}_c := \Delta_c + i\kappa, \tag{2.32}$$

the dynamical equations for the expectation values $\langle a \rangle$ and $\langle \sigma^- \rangle$ can be written as

$$\langle \dot{a} \rangle = i\tilde{\Delta}_c \langle a \rangle - ig(\mathbf{r}) \langle \sigma^- \rangle + \eta \tag{2.33}$$

$$\langle \dot{\sigma}^- \rangle = ig(\mathbf{r}) \langle \sigma_z a \rangle + i\tilde{\Delta}_a \langle \sigma^- \rangle \tag{2.34}$$

$$\langle \dot{\sigma}_z \rangle = ig(\mathbf{r}) \langle a^+\sigma^- - \sigma^+ a \rangle - 2\gamma \langle \sigma^+\sigma^- \rangle . \tag{2.35}$$

An analytical solution for this system of non-linear differential equations leads to optical bistability (Lugiato, 1984). In the case of weak atomic excitation, the algebra of the pseudo-spin operators (2.3) can be approximated by the algebra of the harmonic oscillator (2.2). Within this approximation, the commutator has the value $[\sigma^+, \sigma^-] = -1$ and $\sigma_z a$ in equation (2.34) is replaced by $-a$. Thus the differential equations are linearised:

$$\begin{aligned} \langle \dot{a} \rangle &= i\tilde{\Delta}_c \langle a \rangle - ig(\mathbf{r}) \langle \sigma^- \rangle + \eta \\ \langle \dot{\sigma}^- \rangle &= -ig(\mathbf{r}) \langle a \rangle + i\tilde{\Delta}_a \langle \sigma^- \rangle . \end{aligned} \tag{2.36}$$

With the definitions

$$\mathbf{Y} = \begin{pmatrix} a \\ \sigma^- \end{pmatrix}, \qquad \mathbf{Z} = \begin{pmatrix} i\tilde{\Delta}_c & -ig \\ -ig & i\tilde{\Delta}_a \end{pmatrix}, \qquad \mathbf{I}_\eta = \begin{pmatrix} \eta \\ 0 \end{pmatrix}, \tag{2.37}$$

the approximated system of linear differential equations (2.36) can be written in compact matrix notation

$$\langle \dot{\mathbf{Y}} \rangle = \mathbf{Z} \langle \mathbf{Y} \rangle + \mathbf{I}_\eta. \tag{2.38}$$

The steady state solution of this system of linear differential equations is given by

$$\langle \mathbf{Y} \rangle = -\mathbf{Z}^{-1}\mathbf{I}_\eta. \tag{2.39}$$

The result reads

$$\langle a \rangle_0 = \frac{i\tilde{\Delta}_a \eta}{g^2 - \tilde{\Delta}_a \tilde{\Delta}_c} \tag{2.40}$$

$$\langle \sigma^- \rangle_0 = \frac{ig\eta}{g^2 - \tilde{\Delta}_a \tilde{\Delta}_c}. \tag{2.41}$$

In the coupled oscillator model the expectation value of normally ordered products of operators factorise (Fischer, 2002, page 27). Therefore, the steady state expectation values for the intracavity photon number $\langle a^+a\rangle = \langle a^+\rangle\langle a\rangle$, the atomic excitation $\langle\sigma^+\sigma^-\rangle = \langle\sigma^+\rangle\langle\sigma^-\rangle$ and the dipole force can be calculated from the solution (2.40), (2.41) of (2.36). The results are

$$\left\langle a^+a\right\rangle_0 = \eta^2\frac{|\tilde{\Delta}_a|^2}{|g^2-\tilde{\Delta}_a\tilde{\Delta}_c|^2} = \eta^2\frac{\Delta_a^2+\gamma^2}{|g^2-\tilde{\Delta}_a\tilde{\Delta}_c|^2} \tag{2.42}$$

$$\left\langle\sigma^+\sigma^-\right\rangle_0 = \eta^2\frac{g^2}{|g^2-\tilde{\Delta}_a\tilde{\Delta}_c|^2} \tag{2.43}$$

$$\left\langle a^+\sigma^- + \sigma^+a\right\rangle_0 = \eta^2\frac{2\Delta_a g}{|g^2-\tilde{\Delta}_a\tilde{\Delta}_c|^2}. \tag{2.44}$$

These expressions are identical to those first calculated by Hechenblaikner *et al.* (1998). The dipole force acting on an atom at rest is obtained using (2.29)

$$\mathbf{F}(\mathbf{r}) = \dot{\mathbf{P}} = \frac{i}{\hbar}[H,\mathbf{P}] = -\hbar\nabla g(\mathbf{r})(a^+\sigma^- + \sigma^+a) \tag{2.45}$$

$$\langle\mathbf{F}(\mathbf{r})\rangle_0 = -\hbar\eta^2(\nabla g(\mathbf{r}))\frac{2\Delta_a g(\mathbf{r})}{|g^2-\tilde{\Delta}_a\tilde{\Delta}_c|^2} \tag{2.46}$$

2.2.7 Force fluctuations and momentum diffusion

Equation (2.46) gives the expectation value of the dipole force. Fluctuations of this force lead to a spreading of the atomic momentum distribution. The time evolution of the variance of the atomic momentum distribution

$$(\Delta P)^2(t) = \left\langle[\mathbf{P}(t)-\langle\mathbf{P}(t)\rangle]^2\right\rangle. \tag{2.47}$$

is characterised in first order by the diffusion coefficient

$$2D = \frac{\mathrm{d}}{\mathrm{d}t}(\Delta P)^2(t). \tag{2.48}$$

The diffusion coefficient can be calculated following its definition as

$$\begin{aligned}\frac{\mathrm{d}}{\mathrm{d}t}\left\langle[\mathbf{P}(t)-\langle\mathbf{P}(t)\rangle]^2\right\rangle &= \frac{\mathrm{d}}{\mathrm{d}t}\left\langle\mathbf{P}^2\right\rangle - 2\left\langle\mathbf{P}\right\rangle\frac{\mathrm{d}}{\mathrm{d}t}\left\langle\mathbf{P}\right\rangle \\ &= \left\langle\mathbf{F}\cdot\mathbf{P}+\mathbf{P}\cdot\mathbf{F}\right\rangle - 2\left\langle\mathbf{P}\right\rangle\cdot\left\langle\mathbf{F}\right\rangle.\end{aligned} \tag{2.49}$$

Inserting the formal solution

$$\mathbf{P}(t) = \int_0^\infty \mathrm{d}\tau\ \mathbf{F}(t-\tau) + \mathbf{P}(0) \tag{2.50}$$

for the atomic momentum and (2.49) into (2.48) yields

$$\begin{aligned} 2D &= 2\,\mathcal{R}e \int_0^\infty \mathrm{d}\tau \;\left(\langle \mathbf{F}(t)\cdot\mathbf{F}(t-\tau)\rangle - \langle\mathbf{F}(t)\rangle\cdot\langle\mathbf{F}(t-\tau)\rangle\right) \\ &= 2\,\mathcal{R}e \int_0^\infty \mathrm{d}\tau \;\langle \delta\mathbf{F}(t)\cdot\delta\mathbf{F}(t-\tau)\rangle\,. \end{aligned} \tag{2.51}$$

The equation (2.51) can be used to calculate the momentum diffusion coefficient. For a fixed atom and weak atomic excitation, the momentum diffusion coefficient was calculated by Hechenblaikner *et al.* (1998). The result reads

$$D = D_{se} + D_{dp} \tag{2.52}$$

$$D_{se} = \hbar^2 k^2 \gamma \left\langle \sigma^+\sigma^-\right\rangle = \hbar^2 k^2 \gamma \frac{\eta^2 g^2}{|g^2 - \tilde{\Delta}_a\tilde{\Delta}_c|^2} \tag{2.53}$$

$$\begin{aligned} D_{dp} &= \hbar^2(\nabla g)^2 \frac{\eta^2\gamma}{|g^2-\tilde{\Delta}_a\tilde{\Delta}_c|^2}\left(1+\frac{4\Delta_a g^2}{\gamma}\frac{\Delta_c\gamma+\Delta_a\kappa}{|g^2-\tilde{\Delta}_a\tilde{\Delta}_c|^2}\right) \\ &= D_{\mathrm{free}}\left(1+\frac{4\Delta_a g^2}{\gamma}\frac{\Delta_c\gamma+\Delta_a\kappa}{|g^2-\tilde{\Delta}_a\tilde{\Delta}_c|^2}\right). \end{aligned} \tag{2.54}$$

Here, the momentum diffusion coefficient D_{se} is generated by spontaneous emission of photons from the atom, while D_{dp} is due to fluctuations of the dipole force.

$$D_{\mathrm{free}} = \hbar^2(\nabla g)^2 \frac{\eta^2\gamma}{|g^2-\tilde{\Delta}_a\tilde{\Delta}_c|^2} \tag{2.55}$$

is the diffusion coefficient for an atom in a free-space standing wave light field (Cohen-Tannoudji, 1992, equation (5.44)).

2.2.8 Velocity-dependent forces

A point-like atom moving within the cavity mode experiences a locally varying coupling. The steady state of the atom-cavity system depends on the coupling strength. Its value is not established instantaneously but on the timescale of the atomic and cavity decay. In the case of a moving atom, the system does not reach the steady state corresponding to the actual atomic position but lags behind it. To describe this effect the dipole force for a resting atom (2.46) must be extended by a velocity-dependent correction.

For an atom which moves only a small fraction of a wavelength during the relaxation time of the system, $\mathbf{k}\cdot\mathbf{v} \ll (\Gamma,\kappa)$, the velocity-dependent force can be approximated by a term linear in the velocity. This can be reached by expanding the density operator of the system in powers of the atomic velocity: $\rho = \rho_0 + \rho_1 + \cdots$. To calculate the expectation values up to first order of the atomic velocity, the total derivative of the density matrix can be split into partial derivatives (hydrodynamic derivative)

$$\frac{\mathrm{d}}{\mathrm{d}t}\rho = \frac{\partial}{\partial t}\rho + \mathbf{v}\cdot\nabla\rho. \tag{2.56}$$

In the same way the total derivative of $\langle \mathbf{Y} \rangle$ can be written as

$$\left\langle \dot{\mathbf{Y}} \right\rangle = \left(\frac{\partial}{\partial t} + \mathbf{v} \cdot \nabla \right) \langle \mathbf{Y} \rangle . \tag{2.57}$$

It is assumed that there is no explicit (external) time-dependence of the Hamiltonian and therefore $\frac{\partial}{\partial t} \langle \mathbf{Y} \rangle = 0$. Using equation (2.38) and considering only the first order in the atomic velocity, the first order correction for the expectation values is

$$\langle \mathbf{Y} \rangle_1 = \mathbf{Z}^{-1} \mathbf{v} \cdot \nabla \langle \mathbf{Y} \rangle_0 \tag{2.58}$$

where $\langle \mathbf{Y} \rangle_0$ is the steady-state solution for a fixed atom. This result can be used to calculate the expectation value of the force operator in first order of the velocity $\mathbf{v}$,

$$\langle \mathbf{F} \rangle_1 = -\hbar (\nabla g) \left(\langle a^+ \rangle_0 \langle \sigma^- \rangle_1 + \langle a^+ \rangle_1 \langle \sigma^- \rangle_0 \right) + c.c. \tag{2.59}$$

$$=: -\beta \mathbf{v} \tag{2.60}$$

The coefficient β is called friction coefficient. The analytic result for this velocity-dependent force is lengthy and can be found in Hechenblaikner *et al.* (1998).

2.2.9 Interpretation using dressed states

In the previous sections the excitation and radiative forces of the atom-cavity system were calculated using the Heisenberg equations for the photon annihilation operator a and the atomic lowering operator σ^-. Starting with the coupled harmonic oscillator model used for the solution in the case of weak atomic excitation, it is also possible to transform from the operator basis $\{a, \sigma^-\}$ to the basis of annihilation operator of an excitation in the energy eigenstate (2.5) of the closed atom-cavity system. Solving the system in this basis is more complicated, because in general, the eigenstates vary spatially. On the other hand this dressed states approach provides an illustrative understanding of the excitation of the dressed states and the radiative forces in the atom-cavity system as was demonstrated for the radiation forces on an atom in free space by (Dalibard and Cohen-Tannoudji, 1985). In the limit of well-resolved lines, the excitation of a dressed state is determined by two contributions: First the dressed state is only excited if the detuning of the driving laser from the dressed state is smaller than its linewidth. Secondly, the contribution of the cavity state to the dressed state is important. If only the cavity is pumped, the driving strength of the dressed state is proportional to the contribution of the cavity state. In the dressed state picture, the dipole force is given by summation over the population of each dressed state times its energy gradient.

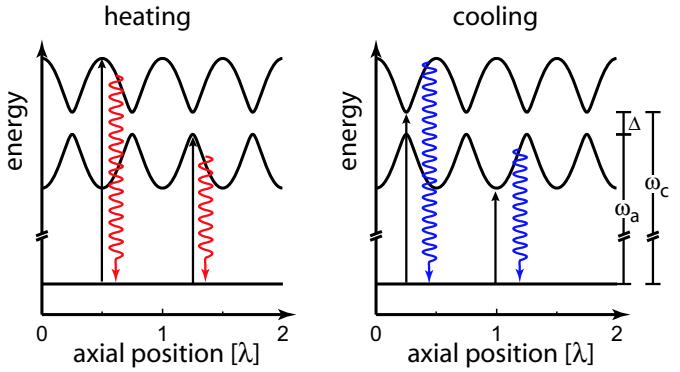

Figure 2.3: Energy eigenstates of the atom-cavity system (dressed states) as a function of the axial position of the atom.

The velocity-dependent force can also be understood from the quantum-mechanical energy-level structure of the coupled atom-cavity system (figure 2.3). A dressed state is only excited if it is resonant with the driving laser. For a laser resonant with the maximum of the upper dressed state and a moving atom, the system is mainly excited when the atom is near an antinode of the field. The system then adiabatically follows the dressed state before the excitation is lost. In this case, a red-detuned photon is emitted and the kinetic energy of the atom is increased. The same situation occurs if the system is excited at a maximum of the lower dressed state at a node.

For different parameters this sisyphus effect can cool the atom. To achieve this, the system is excited near a minimum of one of the dressed states (figure 2.3 b)). After beeing excited in a potential valley, the atom has to invest kinetic energy in climbing the potential hill. If the excitation is lost, a blue-detuned photon is emitted which removes part of the kinetic energy and the entropy from the system. If the system is made to cycle through this scheme many times, the atomic motion is cooled.

2.2.10 Spatial dependency of the radiative forces

The radiative forces calculated in the previous sections strongly depend on the atomic position within the standing wave light field. As an example, the friction and dipole momentum diffusion coefficients are plotted in figure 2.4 as a function of the atomic position. Both vanish near an antinode of the field since each is proportional to $(\nabla g)^2$. The friction coefficient also vanishes near a node of the field while the diffusion coefficient has a small non-zero value at a node.

To select detunings which are experimentally advantageous for observation and cooling, it is necessary to estimate the average friction and diffusion coefficients that an atom will experience in the cavity. The simplest

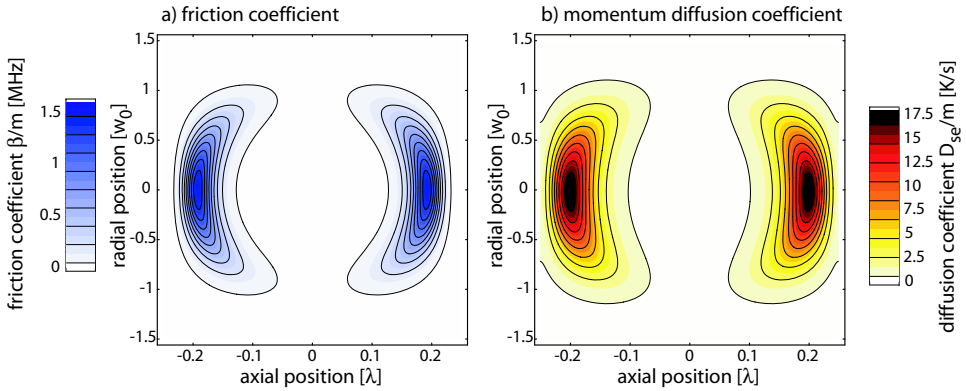

Figure 2.4: Friction coefficient a), and momentum diffusion coefficient b) as a function of the axial and radial position of the atom. Friction and diffusion coefficient vanish near an antinode of the standing-wave light field. The friction coefficient vanishes near a node while the diffusion coefficient reaches a small but non-zero value at a node. Both reach their maximum between nodes and antinodes. The parameters are $(g, \gamma, \kappa, \Delta_a) = 2\pi \times (16, 3, 1.4, 35)$ MHz and $\eta^2 = \kappa^2$ corresponding to one empty cavity photon $n_e = 1$.

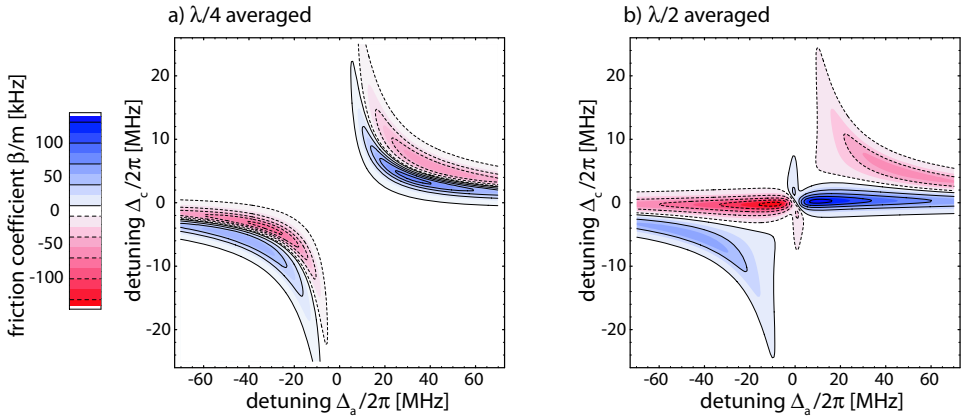

Figure 2.5: Friction coefficient for an atom averaged over the interval a) $[-\lambda/8, \lambda/8]$ and b) $[-\lambda/4, \lambda/4]$ on the cavity axis. The maximal cooling rate is 80 kHz around the antinode a), and 140 kHz averaged over a range of $\lambda/2$. The parameters are $(g, \gamma, \kappa) = 2\pi \times (16, 3, 1.4)$ MHz and $n_e = 1$. Heating, cooling regions are indicated by dashed, solid contour lines, respectively.

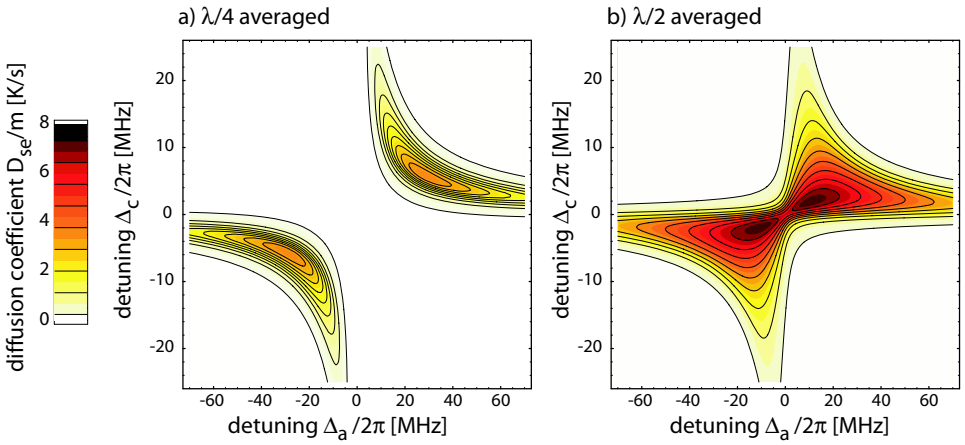

Figure 2.6: Momentum diffusion coefficient for an atom averaged over the interval a) $[-\lambda/8, \lambda/8]$ and b) $[-\lambda/4, \lambda/4]$ on the cavity axis. The maximal heating rate is 3.5 K/s in plot a), and 8 K/s averaged over a range of $\lambda/2$. The parameters are $(g, \gamma, \kappa) = 2\pi \times (16, 3, 1.4)$ MHz and $n_e = 1$.

approach is to spatially average the coefficients. Figure 2.5 and 2.6 show the friction and diffusion coefficients averaged along the cavity axis. In each case two different averages are calculated. Plot a) shows the average over a length of $\lambda/4$, centred at an antinode of the field, while b) shows an average over the whole region between two antinodes ($\lambda/2$). The average values which are obtained differ significantly for the two averaging strategies. If the coefficients are averaged near an antinode, the forces are strong for detunings close to the normal-mode resonances: By scanning the frequency of the probe laser for a fixed atom-cavity detuning Δ, — represented in figure 2.5 by the straight line $\Delta_c = \Delta_a + \Delta$ — cooling is found for red detuning from the normal modes while for blue detuning from the normal modes heating is obtained. In contrast, an average over the whole range between two nodes, leads to a different result. Here cooling is found only for red detuning with respect to the lower nomal-mode resonance and in case of $\Delta_a > 0$ for $\Delta_c = 0$.

In conclusion, it is not clear which axial and radial range schould be chosen to average the forces. Since the friction and diffusion coefficients seen by the atom depend on the atomic motion, which in turn is determined by the forces, the relevant range to average the coefficients over depends on the detunings. Thus the most conclusive approach to solve this problem is to numerically calculate the trajectory of single atoms and average the forces over these trajectories. This approach will be taken in the simulations presented in chapter 3.

2.2.11 Beyond weak excitation

The analytic solution of the atom-cavity system for weak excitation of the atom is a reasonable approximation as long as the atomic excitation stays below 10%. In the experiments the atomic excitation is kept well below this limit. Thus the analytical solution described above can be applied for parameter optimisation and numerical simulations. For higher atomic excitation, the steady state of the system can be calculated numerically by integration of the master equation. If the number of dressed states to include in the calculation is large, wavefunction Monte Carlo methods can be more efficient. Both possibilities were realised in Maunz (1999).

Recently Murr (2003) presented a solution of the atom-cavity system which goes beyond the coupled oscillator model. Here equation (2.36) is solved by using a generalised factorisation assumption to replace $\langle \sigma_z a \rangle$ by $\langle \sigma_z \rangle_p \langle a \rangle$, where p is called the referred state. In the first step $\langle \sigma_z \rangle_p$ is approximated to be -1. In an iterative scheme, the expectation value deduced for $\langle \sigma_z \rangle$ is then used to calculate the expectation values for nonvanishing saturation of the atomic transition.

2.3 Dipole forces and dipole trap

Near-resonant light is well suited to detect and observe a single atom in the cavity. However, the dipole force generated by this light field is accompanied by strong fluctuations and leads to a significant excitation of the atom. The heating generated by these effects limits the available storage time. The relative fluctuations of the dipole force and the atomic excitation can be reduced by increasing the detuning of the laser from the atomic resonance.

In this section the radiative forces generated by a far-detuned intracavity light field will be analysed. The expressions for the radiative forces which were obtained in section 2.2.6 are also valid in the far-detuned case with a stronger laser since the atomic excitation is kept very low and can be used to calculate the radiative forces.

In most cases the considered atomic species has more than two energy levels and for large detunings additional atomic transitions can significantly contribute to the light shift of the atomic ground and excited state. For certain atomic species a “magic wavelength” of the trap can be found for which the ground state and the excited state experience the same light shift and thus the atom sees the same trapping potential irrespective of its state (Hidetoshi Katori and Kuwata-Gonokami, 1999; Ido *et al.*, 2000). However for rubidium a magic wavelength can only be found very far detuned at a wavelength of about $1.4\,\mu$m and for blue detuning of the trap.

2.3.1 Radiative forces in the far-detuned trap

For large detuning from the atomic resonance $\Delta_a \gg \gamma$ and

$$|\tilde{\Delta}_a| \gg \frac{g^2}{|\tilde{\Delta}_c|} \quad \text{or asymptotically} \quad |\Delta_a| \gg \frac{g^2}{\sqrt{\Delta_c^2+\kappa^2}}, \tag{2.61}$$

the expressions calculated for the dipole force (2.46) and the momentum diffusion (2.54) can be simplified. Using the approximation

$$|g^2 - \tilde{\Delta}_a\tilde{\Delta}_c|^2 \approx \Delta_a^2(\kappa^2+\Delta_c^2) \tag{2.62}$$

for the denominator, the dipole force can be written as

$$F \approx -\hbar\eta^2 \frac{g(\mathbf{r})\nabla g(\mathbf{r})}{\Delta_a(\kappa^2+\Delta_c^2)} \propto \frac{1}{\Delta_a}. \tag{2.63}$$

and is inversely proportional to the detuning Δ_a. In this limit the intracavity photon number

$$\langle a^+ a\rangle = \frac{\eta^2}{\kappa^2+\Delta_c^2} \tag{2.64}$$

is approximated by its value without an atom. Thus, in this limit, the intracavity photon number is not affected by the atom. The potential generated by the dipole force can be integrated to obtain the trapping potential

$$V_{\text{trap}} \approx -\frac{\eta^2}{\kappa^2}\frac{\hbar\, g(\mathbf{r})^2}{\Delta_a(1+\Delta_c^2/\kappa^2)} = -n_{\text{trap}}\frac{\hbar\, g(\mathbf{r})^2}{\Delta_a(1+\Delta_c^2/\kappa^2)}. \tag{2.65}$$

Here $n_{\text{trap}} = \eta^2/\kappa^2$ is the number of intracavity photons of the trapping field. The momentum diffusion coefficients for spontaneous emission (2.53) and dipole force fluctuations (2.54) can be approximated as

$$D_{se} \approx \hbar^2 k^2 \gamma \frac{\eta^2\, g(\mathbf{r})^2}{\Delta_a^2(\kappa^2+\Delta_c^2)} \propto \frac{1}{\Delta_a^2} \tag{2.66}$$

$$D_{dp} \approx \hbar^2(\nabla g(\mathbf{r}))^2 \frac{\eta^2\,\gamma}{\Delta_a^2(\kappa^2+\Delta_c^2)}\left(1+4\frac{g(\mathbf{r})^2}{\gamma\kappa}\frac{\kappa^2}{\kappa^2+\Delta_c^2}\right) \propto \frac{1}{\Delta_a^2}. \tag{2.67}$$

Both are proportional to $1/\Delta_a^2$ and therefore the heating rate for fixed depth of the dipole potential is proportional to $1/\Delta_a$. Hence by detuning the trapping laser from the atomic resonance and increasing its power linearly, the trap depth can be kept constant while the heating is inversely proportional to the detuning.

For an intracavity dipole trap which is resonant with one of the modes of the cavity ($\Delta_c = 0$) the momentum diffusion coefficient generated by dipole force fluctuations has the form (2.54)

$$D_{dp} = D_{\text{free}}(1+8C). \tag{2.68}$$

Thus an atom which is strongly coupled to the intracavity dipole trap, experiences an intrinsic heating rate which is amplified by a factor $8C$ compared to a free space dipole trap of equal depth. The strong heating is a fundamental limitation imposed by fluctuations of the intracavity field. For the parameters of this experiment, the heating rate is about a factor 240 stronger than in free space.

2.3.2 Trapping potential for multi-level atoms

All the above calculations are only valid for a two-level atom which is realised in the experiment. Magnetic sublevels of the considered atomic transition can have different transition strengths and thus experience a different trapping potential. Figure 2.7 depicts the trapping potential for the Zeeman

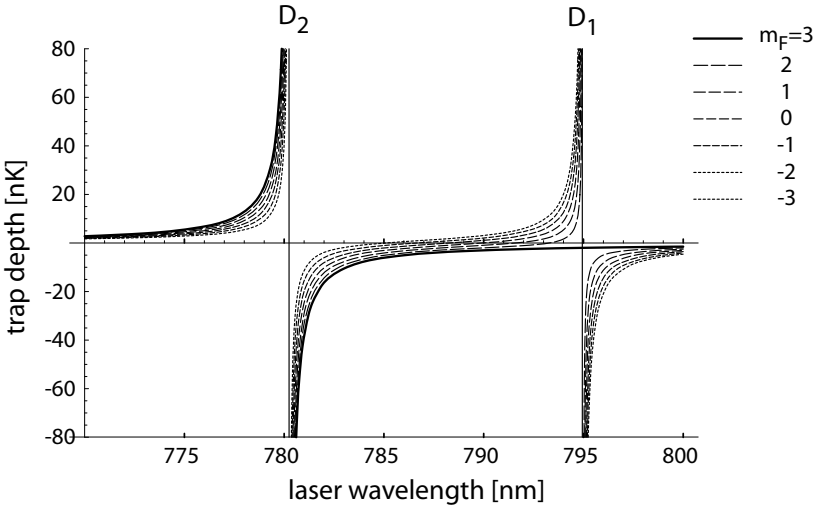

Figure 2.7: Trap depth for an atom in the states $5S_{1/2}, F = 3, m_F = -3 \ldots 3$ as a function of the wavelength of the trapping laser for a light field containing one photon in the cavity on average ($n_{\mathrm{trap}} = 1$). Due to the selection rules for σ^+ polarised light the $5S_{1/2}, F = 3, m_F = 3$ experiences no shift by the D_1 line of ^{85}Rb at 795 nm.

substates $m_F = -3 \ldots 3$ of the ^{85}Rubidium $5S_{1/2}, F = 3$ ground state and a circularly polarised trap. All Zeeman substates are coupled to the $5P_{3/2}$ state with a transition wavelength of 780.243 nm (D_2-line). In contrast, the $m_F = 3$ substate does not couple to the $5S_{1/2}$ state (D_1-line). Thus the trapping potential of this state is not shifted by the coupling to the D_1-line as can be seen in figure 2.7. An atom in this state in a right circularly polarised dipole trap represents an effective two-level system and is optically pumped to the $m_F = 3$ state by the trapping light itself. In the experiment the probe laser also optically pumps the atom to this state. Hence, the atom

can be treated as a two-level system and the expressions calculated above can be applied. In this way a deeper trapping potential is achieved compared to a linearly polarised trap. On the other hand the unequal trapping potential of the different Zeeman substates can lead to additional heating if the atom is pumped between different Zeeman substates.

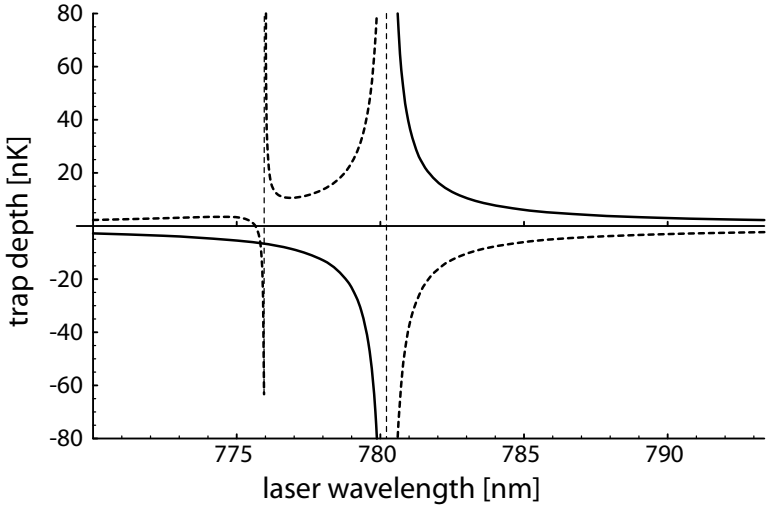

Figure 2.8: Light shift of the $5S_{1/2}, F = 3, m_F = 3$ ground state (solid line) and $5P_{3/2}, F = 4, m_F = 4$ excited state (dashed line) of ^{85}Rb as a function of the wavelength of the right circularly polarised trapping light. The calculation includes the following relevant transitions: $5S_{1/2} \leftrightarrow 5P_{3/2}$ @ 780.24 nm, $5P_{3/2} \leftrightarrow 5D_{5/2}$ @ 775.97 nm, $5P_{3/2} \leftrightarrow 4D_{5/2}$ @ 1529.31 nm (see figure A.1).

In the case of a far-detuned trapping field, the Stark shift of the ground and excited state can be significantly shifted due to the coupling to other atomic energy levels. For the $5S_{1/2}, F = 3, m_F = 3$ ground state of ^{85}Rb which is used in the experiment, the transitions $5P_{3/2} \leftrightarrow 5D_{5/2}$ with a wavelength of 775.97 nm and $5P_{3/2} \leftrightarrow 4D_{5/2}$ at 1529.31 nm generate the leading corrections. These are included in the calculation of the Stark shifts of the ground and excited state shown in figure 2.8. At 785.28 nm, the wavelength used in the experiment, the upper state is shifted up by almost the same amount that the ground states is shifted down in energy. The contribution from other levels leads to a correction of less than 1%.

At a wavelength of about 775.823 nm the excited and ground state experience identical light shifts. This wavelength is called a "magic wavelength". In a trap with a magic wavelength ground and excited state have the same trapping potential and the transition frequency of an atom is not shifted and hence independent of the atomic position. Unfortunately, the magic wavelength at 775.823 nm is blue detuned from the atomic resonance and thus cannot be used for trapping in three dimensions.

In caesium a red-detuned magic wavelength is available and allows to achieve extremely long storage times (McKeever *et al.*, 2003). In a configuration in which the potential of the excited state is even tighter than the ground state, a particle moving in the trap is expected be to cooled by the trap light.

2.4 Theory of the atom-cavity-trap system

Up to now the interaction of the atom with only one cavity mode was considered and the effect of the near-resonant probe field and the far-detuned trapping field were calculated independently. In the experiment both light fields are employed simultaneously to observe and to trap the atom. In this case, the light shift induced by the far-detuned trap leads to a modification of the cavity transmission, the atomic excitation and the radiative forces.

2.4.1 The atom-cavity-trap system

The interaction of an atom with two cavity modes of different frequency is rather complex and a general analytical solution is not known. For large detuning of cavity mode and atomic resonance, there is no back action of the atom on the intracavity intensity (2.64). Thus the intracavity strength of the far-detuned light field is fixed and determined by the coherent driving. The interaction with a two-level atom results in a position-dependent Stark shift

$$\Delta_S(\mathbf{r}) = -\frac{g_{\mathrm{trap}}^2(\mathbf{r})\, n_{\mathrm{trap}}}{\Delta_{\mathrm{trap}}}. \tag{2.69}$$

Here $g_{\mathrm{trap}}(\mathbf{r})$ is the position-dependent coupling of the far-detuned cavity mode and Δ_{trap} is the detuning of this mode from the atomic resonance. The energy of the atomic ground state is lowered by Δ_S and the excited state is increased by Δ_S. Thus the atomic resonance is shifted by $2\Delta_S$. Due to the large detuning, the atomic excitation generated by this light field is low.

Since only the Stark shift has a measurable influence on the interaction of an atom with the near-resonant light field, the theory developed above for the interaction of an atom with the near-resonant cavity field can be extended by including the Stark shift Δ_S of the far-detuned light field in the Jaynes-Cummings Hamiltonian (2.1). The Hamiltonian of the closed

system in a frame rotating with the frequency of the pump laser ω_p reads

$$\begin{aligned} H &= -\hbar\Delta_a\sigma^+\sigma^- - \hbar\Delta_c a^+a + \hbar g(\mathbf{r})(\sigma^+a + a^+\sigma^-) \\ &\quad + 2\hbar\Delta_S(\mathbf{r})\left(\sigma^+\sigma^- - \frac{1}{2}\right) \end{aligned} \tag{2.70}$$

$$\begin{aligned} &= -\hbar(\Delta_a - 2\Delta_S(\mathbf{r}))\sigma^+\sigma^- + \hbar\Delta_c a^+a \\ &\quad + \hbar g(\mathbf{r})(\sigma^+a + a^+\sigma^-) - \hbar\Delta_S(\mathbf{r}). \end{aligned} \tag{2.71}$$

The second expression (2.71), for the Hamiltonian shows that apart from a position dependent energy shift, the Hamiltonian has the same form as the Jaynes-Cummings Hamiltonian (2.1), with the atom-probe detuning Δ_a replaced by the "effective detuning"

$$\Delta_{a,\mathrm{eff}}(\mathbf{r}) := \Delta_a - 2\Delta_S(\mathbf{r}) \tag{2.72}$$

$$\Delta_{\mathrm{eff}}(\mathbf{r}) := \Delta_{a,\mathrm{eff}}(\mathbf{r}) - \Delta_c = \Delta_a - 2\Delta_S(\mathbf{r}) - \Delta_c. \tag{2.73}$$

2.4.2 Intracavity photon number and atomic excitation

The formal equivalence of the Hamiltonians (2.71) and (2.1) can be used to calculate the expectation values of system operators which do not include spatial derivatives. The expectation values of the intracavity photon number and atomic excitation can thus be obtained from (2.42) and (2.43) by replacing Δ_a with $\Delta_{a,\mathrm{eff}}$.

The transmission of the cavity with an atom at the central antinode of the light field is depicted in figure 2.9 a) as a function of the detunings Δ_a and Δ_c. It shows the two normal-mode resonances which are discussed in detail in section 7.6. For a Stark shift of Δ_S the atomic transition is blue shifted by $2\Delta_S$ and the transmission at a atom-probe detuning $\Delta_{a,\mathrm{eff}}$ with Stark shift is the same as the transmission at $\Delta_a - 2\Delta_S$ without Stark shift. In figure 2.9 b) the cavity transmission is shown for the parameters used in the experiment for atom detection. If the atom is located near the antinode of the probe field, the transmission drops distinctly. For $\Delta_a = \Delta_c = 0$ and maximal coupling the transmission is 0.002% of the transmission without an atom (empty cavity transmission). For $\Delta_a = 2\pi \times 35\,\mathrm{MHz}$ it is 4% of the empty cavity transmission. With a Stark shift of $2\Delta_S = 2\pi \times 16\,\mathrm{MHz}$ and blue detuning of the cavity mode and probe laser with respect to the atomic resonance $\Delta_a > \Delta_S$ and $\Delta_c = 0$, the Stark shift reduces the effective detuning. The minimal effective detuning between atom and cavity is reached at an antinode of the far-detuned field. Since the transmission drop is more pronounced for small effective detuning, the visibility of an atom is increased in the centre of the cavity where the antinodes of both fields overlap (to 1% of the empty cavity transmission).

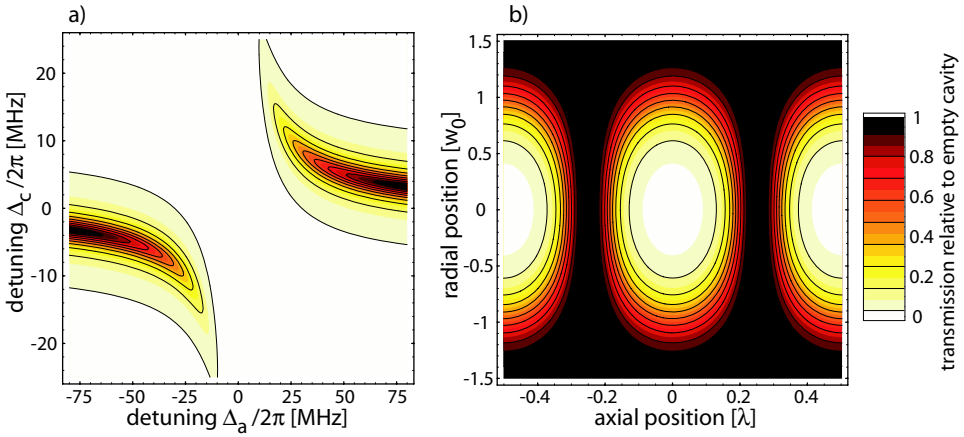

Figure 2.9: Cavity transmission. a) as a function of the detunings Δ_a and Δ_c for an atom at an antinode of the light field and $\Delta_S = 0$. Since an atom at an antinode is considered, the Stark shift only changes $\Delta_{a,\text{eff}}$ and thus the plot is shifted horizontally if the far-detuned field is switched on. b) shows the cavity transmission as a function of the position of the atom in the central antinodes for $\Delta_S = 2\pi \times 16\,\text{MHz}$. The parameters are $(g, \gamma, \kappa, \Delta_a, \Delta_c) = 2\pi \times (16, 3, 1.4, 35, 0)\,\text{MHz}$.

The atomic excitation is plotted in figure 2.10 a) for a pump strength producing one intracavity photon in the empty resonant cavity ($n_e = 1$). The maximal atomic excitation on the normal modes for $n_e = 1$ and an atom at an antinode is about 12%. For the parameters used for atom detection (figure 2.10 b)), the atomic excitation stays below 2%. This maximum is reached between the nodes and the antinodes of the field, as at the antinodes the intensity vanishes while the atom-cavity system is out of resonance with the incident laser for an atom at a node.

2.4.3 Force on a resting atom

The dipole force that an atom experiences in the combined dipole and probe fields can be calculated in the limit of weak atomic excitation using (2.29). The resulting expression

$$\langle F \rangle = -\hbar(\nabla\Delta_S)\left(2\left\langle\sigma^+\sigma^-\right\rangle - 1\right) - \hbar(\nabla g)\left\langle a^+\sigma^- + \sigma^+ a\right\rangle \tag{2.74}$$

for the dipole force has two terms. The first can be recast as

$$\langle F \rangle_{\text{far}} = -\hbar(\nabla\Delta_S)(P_e - P_g) \tag{2.75}$$

where P_e and P_g are the probability to find the atom in the excited and ground state, respectively. In the case $P_e = 0$ and $P_g = 1$ this expression is well known and is equal to the force (2.63) obtained for the far-detuned field. The interaction with the near-resonant light can excite the atom and

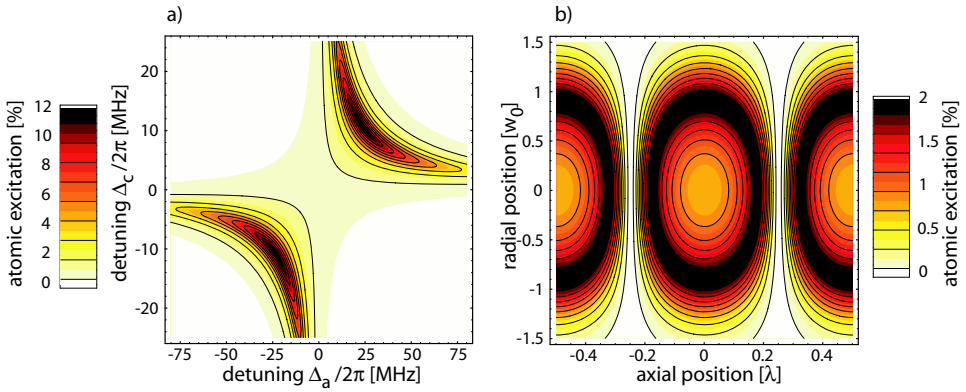

Figure 2.10: Atomic excitation: a) as a function of the detunings Δ_a and Δ_c for an atom at an antinode of the light field ($\Delta_S = 0$). b) shows the atomic excitation as a function of the position of the atom for the parameters used in the experiment for atom detection ($2\Delta_S = 2\pi \times 16\,\mathrm{MHz}$). The other parameters are $(g, \gamma, \kappa, \Delta_a, \Delta_c) = 2\pi \times (16, 3, 1.4, 35, 0)\,\mathrm{MHz}$ and $n_e = 1$.

thus effectively reduces the dipole force. The second term corresponds to the dipole force (2.46) of the atom-cavity system in which Δ_a is replaced by $\Delta_{a,\mathrm{eff}}$. In conclusion the far-detuned field changes the near-resonant force by shifting the atomic resonance. The near-resonant field affects the force of the far-detuned field by exciting the atom.

2.4.4 Momentum diffusion

The momentum diffusion coefficient for an atom in the combined atom-cavity-trap system is calculated in the same way as in the atom-cavity system (Fischer, 2002). There the diffusion coefficient is calculated from the force correlations (2.51)

$$D = \mathcal{R}e \int_0^\infty \mathrm{d}\tau \ \langle \delta\mathbf{F}(t) \cdot \delta\mathbf{F}(t-\tau) \rangle \,. \tag{2.76}$$

The two terms proportional to ∇g and $\nabla \Delta_{a,\mathrm{eff}}$ in the expression for the dipole force (2.74) lead to three terms proportional to $(\nabla g)^2$, $(\nabla \Delta_{a,\mathrm{eff}})^2$ and $(\nabla g)(\nabla \Delta_{a,\mathrm{eff}})$ in the momentum diffusion coefficient:

$$\begin{aligned} D_{dp} = \frac{\hbar^2 \eta^2}{|g(\mathbf{r})^2 - \tilde{\Delta}_{a,\mathrm{eff}} \tilde{\Delta}_c|^4} \Big(\Big(\gamma\, g(\mathbf{r})^4 + \gamma \ \left({\Delta_c}^2 + \kappa^2\right) \ \left(\gamma^2 + {\Delta_{a,\mathrm{eff}}}^2\right) \\ + 2\, g(\mathbf{r})^2 \ \left(\gamma^2 \kappa + \gamma\, \Delta_c\, \Delta_{a,\mathrm{eff}} + 2\, \kappa\, {\Delta_{a,\mathrm{eff}}}^2\right) \Big) \ (\nabla g(\mathbf{r}))^2 \\ - 2\, g(\mathbf{r}) \ \Big(\gamma \ \left({\Delta_c}^2 + \kappa^2\right) \ \Delta_{a,\mathrm{eff}} + g(\mathbf{r})^2 \ \left(\gamma\, \Delta_c + 2\, \kappa\, \Delta_{a,\mathrm{eff}}\right) \Big) \ \nabla g(\mathbf{r})\, \nabla \Delta_{a,\mathrm{eff}} \\ + g(\mathbf{r})^2 \ \Big(\gamma \ \left({\Delta_c}^2 + \kappa^2\right) + \kappa\, g(\mathbf{r})^2 \Big) \ (\nabla \Delta_{a,\mathrm{eff}})^2 \Big) \,. \end{aligned} \tag{2.77}$$

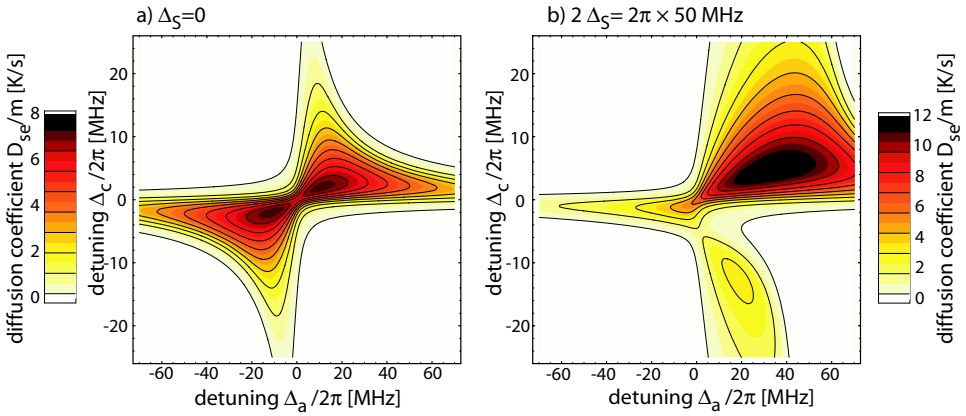

Figure 2.11: Momentum diffusion generated by force fluctuations averaged over one wavelength on the cavity axis. a) without trapping field and, b), with a trapping field with a maximal Stark shift of $2\Delta_S = 2\pi \times 50\,\mathrm{MHz}$. The parameters are $(g, \gamma, \kappa) = 2\pi \times (16, 3, 1.4)\,\mathrm{MHz}$ and $\eta^2 = \kappa^2$.

The first term is generated by the fluctuations of the dipole force of the near-resonant field ($\propto (\nabla g)^2$). The third term, which is proportional to $(\nabla \Delta_{a,\mathrm{eff}})^2$ is generated by fluctuations of the force in the far-detuned light field. These are generated by the excitation of the atom by the near-resonant probe beam. The term proportional to $(\nabla g)(\nabla \Delta_{a,\mathrm{eff}})$ originates in correlations between the two aforementioned force fluctuations and can be positive or negative. In figure 2.11 the diffusion coefficient (2.77) is compared with the diffusion coefficient (2.54) without trapping field. By adding the trapping potential, the diffusion coefficient averaged over the cavity axis is increased for detunings for which the near-resonant dipole forces are large.

2.4.5 Velocity-dependent force

Along the same line as in section 2.2.8, the dipole force in first order of the atomic velocity can be calculated. The expressions that are obtained are lengthy and are therefore given in appendix B. In figure 2.12, the velocity-dependent force in the centre of the cavity averaged over one wavelength with and without trapping field are compared. By adding the trapping potential, the maximal averaged cooling rate is increased from 140 kHz to 200 kHz. For the parameters used for atom detection ($\Delta_a = 2\pi \times 35\,\mathrm{MHz}$, $\Delta_c = 0$), only cooling is found in the central antinode. Spatially, the friction force is strongest between antinodes and nodes as illustrated in figure 2.13 a). The maximal cooling rate is about 1.5 MHz.

Figure 2.13 b) shows the friction coefficient, again averaged over one wavelength, as a function of the shift between the trapping and probe field and the maximal Stark shift $2\Delta_S$. For a maximal Stark shift $2\Delta_S$ which

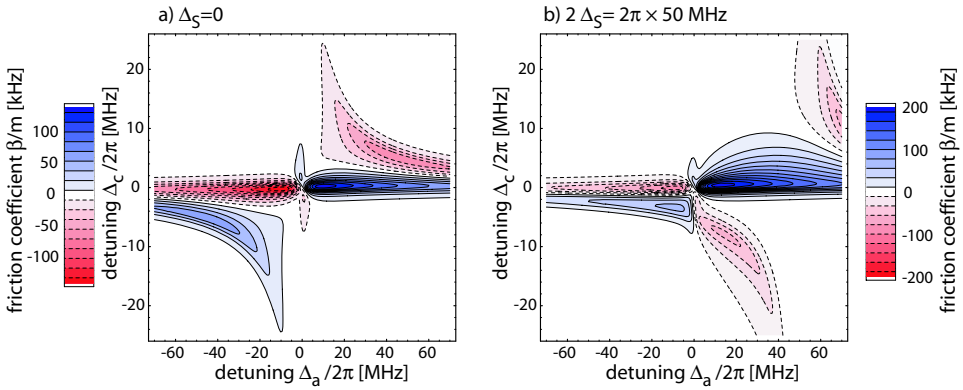

Figure 2.12: Friction coefficient β/m for an atom on the cavity axis, averaged over one wavelength in the centre of the cavity. a) without trapping field. The maximal cooling and heating rate is 140 kHz. b) with trapping field with a maximal Stark shift of $2\Delta_S = 2\pi \times 50\,\mathrm{MHz}$. The maximal cooling rate is 200 kHz, the maximal heating rate is 100 kHz. The parameters are $(g, \gamma, \kappa) = 2\pi \times (16, 3, 1.4)\,\mathrm{MHz}$ and $\eta^2 = \kappa^2$. Heating and cooling regions are indicated by dashed and solid contour lines, respectively.

exceeds the atom-probe detuning Δ_a, cooling which is found in the centre of the cavity can be turned to heating if the two modes are displaced. This behaviour can also be seen in figure 2.14 where the friction coefficient is depicted as a function of the axial position and the radial position. This illustration shows that the heating and cooling occurs in narrow spatial regions. The pronounced spatial variation of the velocity-dependent forces has a strong impact on the motion of an atom in the light fields. A conclusive average of these forces can only be achieved by spatially averaging over the trajectory of an atom which moves according to these forces. This will be done in the numerical simulations presented in chapter 3.

An atom which is subject to heating and cooling will on average reach an axial equilibrium temperature which is given by

$$T = \frac{\bar{D}}{\bar{\beta}}, \tag{2.78}$$

where $\bar{x}$ denotes the average over the atomic trajectory. The momentum diffusion in axial direction is the sum of two contributions

$$D = \frac{2}{5} D_{se} + D_{dp}, \tag{2.79}$$

the momentum diffusion generated by spontaneous emission in axial direction and the dipole diffusion coefficient which is directed along the cavity axis. The friction coefficient β is also directed along the cavity axis. An estimate of the equilibrium temperature is given by first spatially averaging

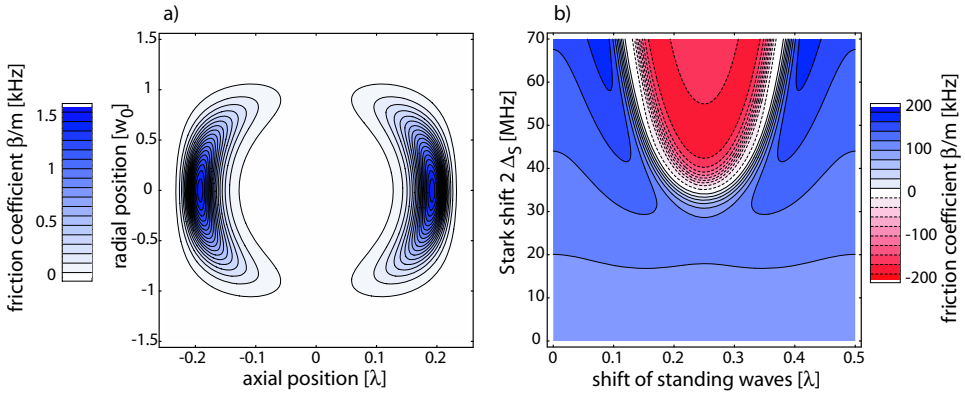

Figure 2.13: Friction coefficient β/m a) as a function of the spatial position of an atom, and b) as a function of the maximal Stark shift and the relative shift of the antinodes of the two standing waves. The parameters are $(g, \gamma, \kappa, \Delta_a, \Delta_c, \Delta_S) = 2\pi \times (16, 3, 1.4, 35, 0, 0)$ MHz and $\eta^2 = \kappa^2$. Heating and cooling regions are indicated by dashed and solid contour lines, respectively.

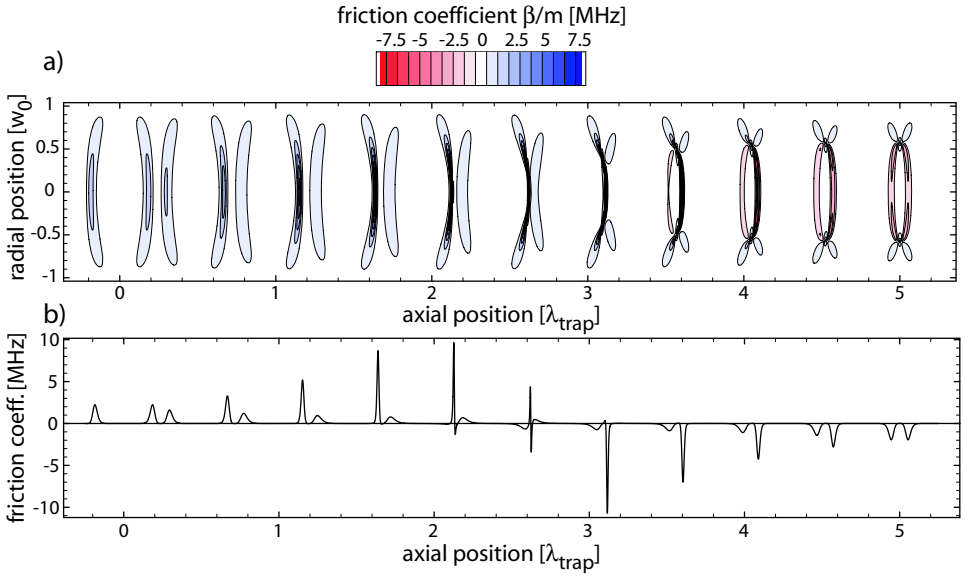

Figure 2.14: a) Friction coefficient β/m as a function of "squeezed axial position" and radial position of the atom. To visualise the effect of the displacement of the two standing wave fields, the spatial displacement of the fields is increased. At $x = 0$ the fields match, while a node of the probe field coincides with an antinode of the trapping field at $x = 5\lambda_{\text{trap}}$. As shown in figure 2.13 the regions with high friction are spatially localised. b) Shows the friction coefficient presented in a) as a function of the position on the cavity axis. The parameters are $(g, \gamma, \kappa, \Delta_a, \Delta_c, \Delta_S) = 2\pi \times (16, 3, 1.4, 35, 0, 50)$ MHz and $\eta^2 = \kappa^2$.

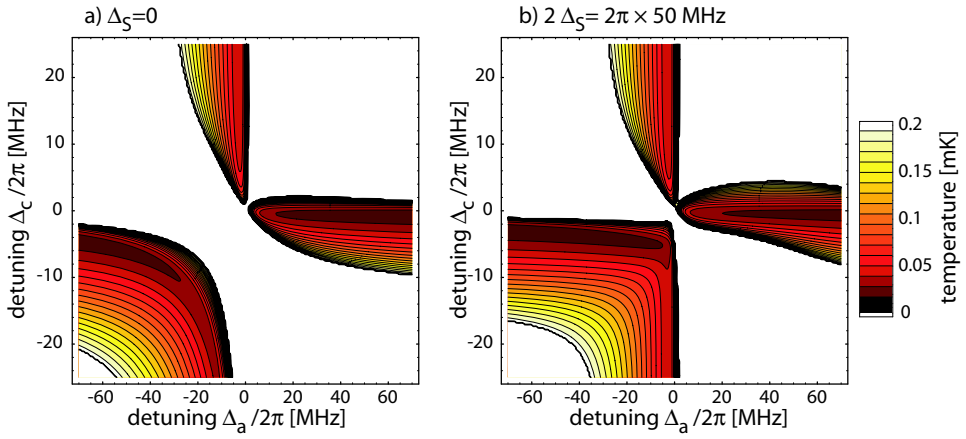

Figure 2.15: Axial equilibrium temperature $T = \bar{D}/\bar{\beta}$ in the centre of the cavity averaged over one wavelength. a) Without trapping potential, the minimal temperature is $20\,\mu$K. b) With a trapping potential of $2\Delta_S = 2\pi \times 50\,$MHz, b), the minimal temperature is $19\,\mu$K.

the friction and diffusion coefficients over one wavelength and then taking the ratio. The result is shown in figure 2.15. The equilibrium temperature which can be achieved is only weakly influenced by the Stark shift of the trap. For certain detunings the equilibrium temperature is small compared to the trap depth.

Figure 2.16 shows the axial equilibrium temperature for $\Delta_c = 0$ as a function of the detuning Δ_a and the radial position of the atom. It shows that an equilibrium temperature of about $20\,\mu$K can be achieved in wide range of detunings up to a radius of about $0.8w_0$. The equilibrium temperature is compared with the trap depth in figure 2.16 b). The equilibrium temperature is below 10% of the trap depth for a radial distance of up to $0.8w_0$.

2.4.6 Interpretation using the dressed states

In the atom-cavity-trap system, the velocity-dependent forces can also be visualised using the dressed-states depicted in figure 2.17. In this system, cavity cooling arises when a ground-state atom moves away from an antinode, thereby climbing a potential hill at the expense of kinetic energy. When the atom reaches the top of the hill at a node, the cavity becomes resonant with the probe laser and can absorb a photon. Atom and cavity are uncoupled at this position, so that the probability to excite the atom vanishes. While the atom continues to move, the system follows the excited state adiabatically until the excitation is emitted and the system returns to its ground state. This decay process is dominated by the escape of a photon

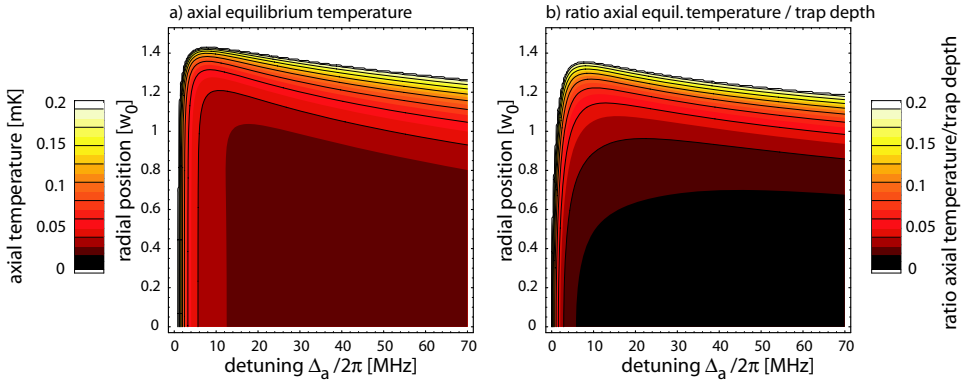

Figure 2.16: a) Axial equilibrium temperature $T = \bar{D}/\bar{\beta}$ as a function of the detuning Δ_a and the radial position. The momentum diffusion and friction coefficients are averaged over one wavelength on a straight line parallel to the cavity axis. b) depicts the ratio of the equilibrium temperature and the trap depth. The parameters are $(g, \gamma, \kappa, 2\Delta_S, \Delta_c) = 2\pi \times (16, 3, 1.4, 50, 0)$ MHz.

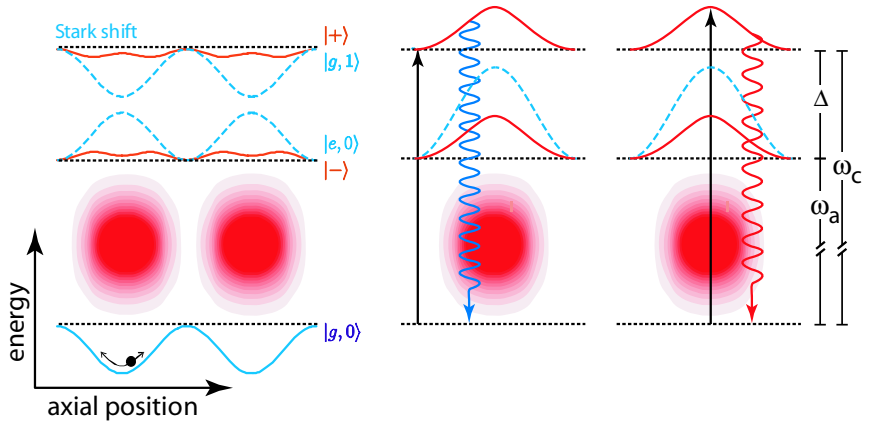

Figure 2.17: Dressed states of the atom-cavity-trap system as function of the atomic axial position. a) The ground state $|g, 0\rangle$ is shifted down by the Stark shift near an antinode while the excited state $|e, 0\rangle$ is shifted up by the same amount (dashed lines). The state $|g, 1\rangle$ has one intracavity photon more than the state $|g, 0\rangle$. The dressed states $|+\rangle$ and $|-\rangle$ effectively repel each other and are given by the solid lines. b) For easier interpretation this plot shows the energy difference of each state to the ground state. Now, by construction the ground state is flat and energy differences between excitation and emission of a photon can easily be deduced.

from the cavity, because the atomic contribution to the excited state close to a node is very small. In the cooling cycle, kinetic energy is reduced because the emitted photon has a higher frequency than the absorbed photon. This asymmetry between absorption and emission holds for an average cycle and increases with the lifetime of the cavity field. It is emphasised that excitation of the atom by the probe light is also suppressed away from the nodes because of the frequency mismatch. Therefore only the cavity is excited by the weak probe laser.

2.5 Fokker-Planck equation

The atomic motion in the light field is determined by the dipole force, velocity-dependent force and momentum diffusion due to force fluctuations. Thus the differential equation for the atomic trajectory is a stochastic differential equation, which is also known as Langevin equation. The atomic motion can also be described by the time evolution of a (classical) probability density function in phase space. The time evolution of this probability distribution is given by the corresponding Fokker-Planck equation. An introduction to this subject can be found in Gardiner (1985).

The general Fokker-Planck equation for our system is a partial differential equation on the six-dimensional phase space. As the coefficients of this partial differential equation are a function of the phase-space point the problem is very complex and a solution can only be obtained numerically. Despite its complexity some general properties of the dynamical behaviour can be deduced from the Fokker-Planck equation, which will be done in section 2.5.1. The Fokker-Planck equation for two simple one-dimensional models of the diffusion process can be solved exactly. These are presented in sections 2.5.2 and 2.5.3 and will give some insight on the storage time and momentum distribution of an atom in the trap.

2.5.1 Fokker-Planck equation for an atom in the cavity

The motion of an atom under fluctuating light forces is described by the stochastic differential equation for the atomic motion in phase space

$$\frac{\mathrm{d}}{\mathrm{d}t}\dot{\mathbf{x}} = \mathbf{A}(\mathbf{x},t) + \mathbf{D}(\mathbf{x},t)\,\xi(t). \tag{2.80}$$

Here $\xi(t)$ is a rapidly fluctuating force with vanishing mean value and $\mathbf{D}(\mathbf{x},t)$ is the diffusion coefficient. The drift coefficient $\mathbf{A}(\mathbf{x},t)$ describes the forces. By integration it can be shown (Gardiner, 1985) that the stochastic differential equation (2.80) is equivalent to the Fokker-Planck equation for the (classical) probability density $w(\mathbf{x})$ to find an atom at the phase-space point $\mathbf{x}$. The solution of the Fokker-Planck equation (summation over the phase

space degrees of freedom)

$$\partial_t w(\mathbf{x},t) = -\sum_i \partial_i \left(A_i(\mathbf{x}) w(\mathbf{x},t)\right) + \frac{1}{2}\sum_{i,j} \partial_i \partial_j \left(D_{ij}(\mathbf{x}) w(\mathbf{x},t)\right) \qquad (2.81)$$

describes the time evolution of the probability density function $w(\mathbf{x})$.

Let us assume the function $w(\mathbf{x},t)$ solves the Fokker-Planck equation (2.81) for given drift coefficients $A_i(x,p,t)$ and diffusion coefficients $D_{ij}(x,p,t)$. Scaling the drift coefficients $A_i(x,p,t)$ and the diffusion coefficients $D_{ij}(x,p,t)$ by the same factor α leads to an equation which is solved by $w(\mathbf{x},\alpha t)$. Thus in this case the timescale of the evolution of the probability density function is scaled by the factor α. In contrast, if there exists a (quasi-)stationary probability distribution, it does not change by this scaling.

This result can be used to investigate the change of the storage time of an atom upon a change of the probe power: In this case the atom moves in a potential of finite depth which defines a part of phase space and will be lost if it leaves this volume. The loss can be modelled by solving the Fokker-Planck equation with absorbing boundary conditions. The probability $p(t)$ to find the atom in the region of interest R at time t is given by the integral

$$p(t) = \int_R w(\mathbf{x},t)\,\mathrm{d}\mathbf{x}\,. \qquad (2.82)$$

If only forces of the probe light are relevant and the power of the probe light is scaled by a factor α (maintaining low atomic saturation), the timescale of the solution of the diffusion process $\tilde{w}(\mathbf{x},t)$ is scaled by the same factor $\tilde{w}(\mathbf{x},t) = w(\mathbf{x},\alpha t)$. Thus the probability to find an atom in the scaled trap $\tilde{p}(t)$ is $\tilde{p}(t) = p(\alpha t)$.

In conclusion by increasing the probe power by a factor α, the average storage time of an atom in the trap will drop by the same factor α.

2.5.2 Lifetime of an atom in the dark trap

In general an exact solution for the Fokker-Planck equation (2.81) in the six-dimensional phase space does not exist. However exact solutions for some one-dimensional diffusion processes do exist. In the following we consider a plausible one-dimensional model of the diffusion process.

First we will approach the motion of an atom in the far-detuned dipole trap without probe light. In this system, diffusion is not compensated by friction and the drift term vanishes. Since the fluctuations of the light generate a diffusion process in momentum space, we will restrict the analysis to a one-dimensional momentum space. To model the escape of an atom from the trap we will assume absorbing boundary conditions at the points $\pm p_{\max}$ with $p_{\max}^2/2m = E_{\mathrm{trap}}$. Furthermore, a constant, spatially averaged

diffusion coefficient is used. Applying these approximations, the Fokker-Planck equation is reduced to the Wiener process

$$\partial_t w(p,t) = \frac{1}{2} D\, \partial_p^2\, w(p,t) \tag{2.83}$$

which has an exact solution. In the following, the absorbing boundary conditions $w(0,t) = w(1,t) = 0$ are chosen for simplicity. Using these boundary conditions, the solution of equation (2.83) can be written as a Fourier sine series

$$w(p,t) = \sum_{n=1}^{\infty} b_n(t) \sin(n\pi p). \tag{2.84}$$

For a particle initially localised at p_0 ($w(p,0) = \delta(p - p_0)$) the solution is

$$w(p,t) = 2 \sum_{n=1}^{\infty} e^{-\frac{1}{2} n^2 \pi^2 D t} \sin(n\pi p_0) \sin(n\pi p). \tag{2.85}$$

The Fourier coefficients in this solution are exponentially damped on a timescale

$$\tau_n = \frac{2}{n^2 \pi^2 D}. \tag{2.86}$$

In this problem $\tau_1 = \frac{2}{\pi^2 D}$ is the longest timescale and determines the asymptotic behaviour. As higher Fourier coefficients are damped on a timescale much shorter than τ_1, the diffusion process (2.83) rapidly approaches the quasi-stationary state

$$w_{qs}(p,t) = 2 e^{-t/\tau_1} \sin(\pi p_0) \sin(\pi p). \tag{2.87}$$

The process can be depicted in the following way: The initially narrow momentum distribution spreads on a timescale fast compared to τ_1. After this time the system has reached the quasi-stationary state, which is given by the fundamental sine ($n = 1$). Subsequently the shape of the distribution is preserved and only the amplitude decays.

The probability to find the atom in the trap as a function of time is given by

$$p(t) = \int_{-p_{\max}}^{p_{\max}} \mathrm{d}p \;\; w(p,t) \tag{2.88}$$

and can be approximated for $t \gg \tau_1$ as

$$p(t) \approx p_1(t) := \frac{4}{\pi} e^{-t/\tau_1}. \tag{2.89}$$

As $p_1(0) = 4/\pi > 1$, the contribution from higher Fourier coefficients to the integral (2.88) is negative. Thus the function $p(t)$ initially shows a reduced decay and approaches $p_1(t)$ on the timescale $t \geq \tau_1$.

For an atom in the far-detuned trap this means, once the momentum distribution has reached the quasi-stationary distribution, the probability to find an atom in the trap drops exponentially with the decay rate $\tau_1 = \frac{2}{\pi^2 D}$. If the atomic momentum distribution is better localised than w_{qs} to start with, the decay rate is initially lower and approaches the value $\frac{1}{2}\pi^2 D$ on a timescale τ_1. A repeated re-localisation of the atomic momentum distribution can thus lead to an extended storage time.

2.5.3 Momentum distribution including cooling

In this section we will approach the description of the motion of an atom in the presence of the near-resonant probe light. This light field adds additional momentum diffusion and eventually also a friction force which can compensate for momentum diffusion and thus lead to a steady state of the momentum distribution. Since in this case we are not interested in trap lifetimes we will not use boundary conditions.

In the corresponding Fokker-Planck equation this leads to a non-vanishing drift term A. For the velocity-dependent force $F = -\beta v$ the differential equation reads

$$\partial_t w(p,t) = \partial_p \left[\beta p w(x,t)\right] + \frac{1}{2} D \partial_p^2 w(p,t). \tag{2.90}$$

The stationary solution of this Ornstein-Uhlenbeck process is given by

$$w_s(p,t) = \sqrt{\frac{\beta}{\pi D}} e^{-\beta p^2/D} \tag{2.91}$$

and a general solution can be written as

$$w(p,t) = \sum_{n=0}^{\infty} \sqrt{\beta/2^n n! \pi D} e^{-\beta p^2/D} H_n(p\sqrt{\beta/D}) e^{-n\beta t} A_n. \tag{2.92}$$

Here H_n are the Hermite polynomials, and

$$A_n = \int_{-\infty}^{\infty} \mathrm{d}p \; w(p,0) H_n(p\sqrt{\beta/D}) (2^n n!)^{-1/2}. \tag{2.93}$$

In the stationary solution (2.91) the diffusion and drift coefficients of (2.90) only enter as D/β which determines the width of the stationary distribution and can be interpreted as equilibrium temperature of this diffusion process.

The general solution (2.92) approaches the steady state on the timescale β. Here β is the rate constant for deterministic relaxation, and it thus determines the slowest timescale in the relaxation. Thus if the momentum distribution of the system is disturbed, the friction coefficient β determines the rate at which the system approaches its steady state.

Chapter 3

Numerical Simulation

Numerical simulations of the atom-cavity-trap system can be done on various levels of approximation, the most general are wavefunction Monte Carlo simulations (Carmichael, 1991; Mølmer *et al.*, 1993) of an atomic wavepacket in the cavity. If the position spread of the atomic wavepacket is small compared to the wavelength of the light and the momentum spread is small enough, the atomic wavepacket can be approximated by a point-like particle (Cohen-Tannoudji, 1992). In this case, the timescale of the internal dynamics is much faster than that of the external dynamics. This allows to solve for the internal dynamics of the atom-cavity system while keeping the position of the atom fixed. This solution can then be used to calculate the trajectory of a point-like particle.

The internal dynamics of the atom-cavity-trap system can be solved numerically using the wavefunction Monte Carlo method or by direct integration of the master equation. In the regime of weak atomic excitation, the internal dynamics of the atom-cavity-trap system can be solved analytically as presented in chapter 2.4. The availability of analytical expressions for the radiative forces allows efficient calculation of the atomic trajectory in three dimensions. Fluctuations of the radiative forces are included via a diffusion mechanism in momentum space.

As the atomic excitation is kept very low in the experiment, this is the method of choice and is used for the simulations presented in this chapter. The analytical solutions for the transmission of the cavity, the atomic excitation and more generally all expectation values of system operators strongly depend on the position of the atom with respect to the two standing waves. A comparison of these theoretical predictions of measured quantities with the experiment can be done by calculating trajectories of single point-like atoms and comparing the simulated transmission for these trajectories with the transmission measured in the experiment.

In order to obtain a good agreement between experiment and simulation, the experiment is modelled in detail: The trajectories of single atoms

injected from below into the cavity are calculated in three dimensions. Analogous to the experiment, the intensity of the far-detuned trapping field is increased upon detection of an atom by a drop in transmission of the near-resonant probe field. The trajectory of the atom is calculated until the atom leaves the cavity.

An overview of the algorithm used for the simulation is given in section 3.1. Section 3.1.1 describes the implementation of the forces calculated analytically for the atom-cavity-trap system, while section 3.1.2 describes the implementation of parametric heating induced by technical intensity fluctuations of the trapping field. The consideration of initial and boundary conditions, as well as detection and capture of an atom in the trap is presented in section 3.1.3.

Results of the numerical algorithm are used in section 3.2 to investigate the dominating loss mechanisms of atoms from the trap for the cooling parameters used in the experiment. The simulation of the measurement of the normal-mode spectrum of the bound atom-cavity system is described in section 3.3. In section 3.3.1 the qualification scheme used to select "strongly coupled" probe intervals is investigated. The spectra of the cavity transmission and inverse storage time calculated with these methods are compared with the measurements in chapter 7.

3.1 Algorithm

In the simulation, the trajectory of a single atom is calculated in three dimensions by integration of the Newtonian equation of motion for a point-like particle. The trajectory is determined by the geometry, the detunings and the intensities of the standing-wave trapping and probe fields.

In order to model the experiment in detail, atoms are injected into the cavity mode from below. The trapping field is used to guide the atoms entering the mode in the region of high intensity of the trapping field. In the centre of the cavity, where the nodes and antinodes of the trapping and probe fields coincide, the atoms are thus guided into the regions of strong coupling. For the parameters chosen in the experiment, the presence of an atom leads to a distinct drop of cavity transmission. This drop allows to detect an atom in the cavity with high signal to noise ratio within a short time. When the transmission drops below an adjustable threshold, the intensity of the trap field is increased to capture the atom in the trap. After trapping the atom, the probe frequency and power is adjusted to model the experiment. The trajectory of the atom is recorded until the atom leaves the cavity mode.

3.1.1 Langevin equation for the atomic motion

In the regime of low saturation of the atomic transition, analytical expressions for the expectation values of dipole force, velocity-dependent force and momentum diffusion coefficient in the combined atom-cavity-trap system were calculated in section 2.4. Using the expectation values of these forces, the Newtonian dynamical equations for a point-like particle can be used to integrate the trajectory of an atom. The differential equations for the atomic position, $\mathbf{r}(t)$, and the momentum $\mathbf{p}(t)$ are

$$\begin{aligned} \dot{\mathbf{r}}(t) &= \frac{\mathbf{p}(t)}{m_{\mathrm{Rb}}} \\ \dot{\mathbf{p}}(t) &= \langle \mathbf{F}_{dp}(\mathbf{r}(t)) \rangle + \langle \mathbf{F}_{v}(\mathbf{r}(t)) \rangle + \dot{\mathbf{p}}_{dp}(\mathbf{r}(t)) + \dot{\mathbf{p}}_{se}(\mathbf{r}(t)). \end{aligned} \tag{3.1}$$

Here $\dot{\mathbf{p}}_{dp}(\mathbf{r}(t))$ and $\dot{\mathbf{p}}_{se}(\mathbf{r}(t))$ are momentum kicks modelling the effects of fluctuations of the forces on the atomic trajectory and will be discussed in the following paragraphs.

Fluctuations of the dipole force lead to a spreading of the momentum distribution and can be quantified by the diffusion coefficient

$$D = \frac{1}{2}\frac{\mathrm{d}}{\mathrm{d}t}\left(\langle \mathbf{p}^2 \rangle - \langle \mathbf{p} \rangle^2\right), \tag{3.2}$$

which is a measure of the increase of the variance of the momentum distribution. The expectation value of the diffusion coefficient can also be calculated analytically in the regime of low saturation and lowest order of the atomic velocity (chapter 2.2.7) and is included in the dynamic equation 3.1 using a stochastic force with zero expectation value, i.e. $\langle \dot{\mathbf{p}}_{dp} \rangle = \langle \dot{\mathbf{p}}_{se} \rangle = 0$. The momentum diffusion in the atom-cavity system originates from fluctuations of the dipole force $\dot{\mathbf{p}}_{dp}$ and from photons scattered by the atom $\dot{\mathbf{p}}_{se}$. These two contributions also differ in their spatial properties.

The dipole force is proportional to the square of the gradient of the atom-cavity coupling strength, which is about ten times larger in axial direction. Thus, the dipole force is mainly directed along the cavity axis. The momentum diffusion generated by fluctuations of this force is also mainly acting in axial direction. In the simulation, the axial momentum of the atom is changed in each time step by $\dot{p}_{dp}$, chosen randomly from the interval $[-p_{\mathrm{max,dp}}, p_{\mathrm{max,dp}}]$ with equal probability. The maximal change of the momentum $p_{\mathrm{max,dp}}$, in one time step of length δt, is given by

$$D_{dp}\delta t = \frac{1}{2}(\langle \delta p^2 \rangle - \langle \delta p \rangle^2) = \frac{1}{2}\frac{1}{2p_{\mathrm{max,dp}}}\int_{-p_{\mathrm{max,dp}}}^{p_{\mathrm{max,dp}}} p^2 \mathrm{d}p\,, \tag{3.3}$$

which results in

$$p_{\mathrm{max,dp}} = \sqrt{6 D_{dp}\delta t}. \tag{3.4}$$

The emission of a photon from the atom imprints the photon recoil of $\delta p = \hbar k$ on the motion of the atom. The spatial distribution of scattered

photons and thus also of photon recoils is given by the emission characteristics of the polarised excited state of the atom. For ^{85}Rb atoms which are optically pumped to the $F = 4, m_F = 4$ excited state, 2/5 of the momentum diffusion acts in direction of the quantisation axis and 3/10 points along each of the two orthogonal radial directions. This diffusion mechanism is included in the simulation by applying a momentum kick randomly chosen from the solid ellipsoid with the main axes given by

$$p_{\max,z} = \sqrt{4D_{se}\delta t}, \quad \text{and } p_{\max,x} = p_{\max,y} = \sqrt{3D_{se}\delta t}, \tag{3.5}$$

where the z-axis points in direction of the cavity axis.

The momentum kicks which are used to generate the stochastic force reproduce the first moment of the spreading of the spreading of the momentum distribution, the diffusion coefficient. For the numerical integration of the differential equation a Runge-Kutta algorithm with adjustable step size is used (Schwarz, 1997). For stochastic processes, the "Mersenne Twister" pseudorandom number generator is used, which is a highly equidistributed uniform pseudorandom number generator (Matsumoto and Nishimura, 1998).

3.1.2 Parametric heating in the dipole trap

In the experiment, the storage time in the bare trap without probe light is found to be limited by parametric heating. This heating is caused by technical fluctuations of the relative frequency difference between the trapping laser and the cavity resonance, resulting in intensity fluctuations of the intracavity field. A theoretical investigation (Savard *et al.*, 1997) shows that the heating rate is proportional to the spectral noise power density of the intracavity intensity at the second harmonic of the trap frequency. In the simulation, this heating mechanism is modelled by randomly changing the intensity of the trapping field in each time step δt. This leads to a white spectrum of the noise power density for frequencies up to $1/2\delta t$. The white noise spectrum used in the simulation is a reasonable approximation to the real noise spectrum of the intracavity intensity. The intensity in each time step is chosen according to a Gaussian distribution, where its mean is the average trapping field intensity. The width of the distribution is adjusted to reproduce the experimentally observed storage time of an atom in the dark trap. Figure 3.1 shows the simulated storage time of an atom in the fluctuating dipole trap. The storage time is inversely proportional to the noise power and a fit is used to select the noise power used to simulate the experiment.

3.1.3 Boundary conditions and triggering

The integration of an atomic trajectory is started with an atom located at $x_0 = 2w_0$ below the cavity axis (a definition of the coordinate system

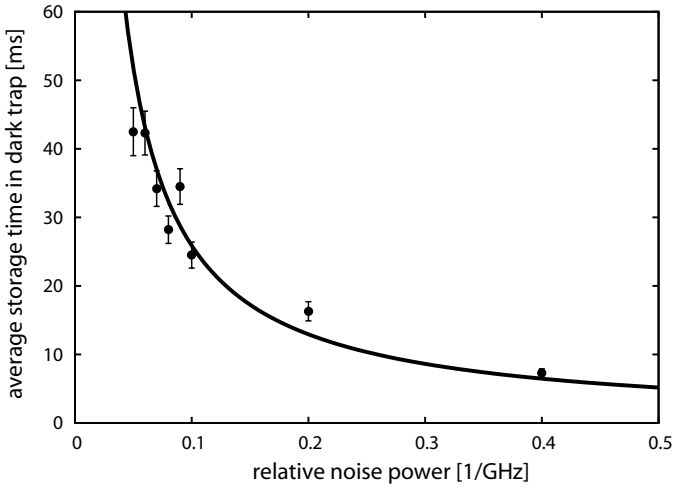

Figure 3.1: Simulated storage time of an atom in the dark trap as a function of the relative noise power of the trapping laser intensity. A trap depth of $400\,\mu$K is used to guide the atoms. Upon detection of an atom, the trap depth is increased to 2 mK. The heating rate is proportional to the noise power density as expected theoretically. The storage time of an atom in the trap is therefore inversely proportional to the noise power, as indicated by a fit (solid line). The parameters of the probe beam which is applied prior to capturing the atom are $\Delta_a = 2\pi \times 35\,\mathrm{MHz}$, $\Delta_c = 0$ and one photon in the empty resonant cavity, $n_e = 1$. The detuning of the trapping laser is $2\pi \times 2.46\,\mathrm{THz}$ and the intracavity photon number of the trapping laser n_{trap} is increased from 80×10^3 to 180×10^3 corresponding to trap depths of $400\,\mu$K and 1.4 mK, respectively.

used for the simulations can be found in figure 2.1). For larger distances, the interaction of the atom with the cavity mode is very weak and can be neglected. The position along the cavity axis z_0 is selected randomly from the interval $[-20\lambda, 20\lambda]$ axially centred around the cavity centre. The start position in $y-$direction y_0, is also randomly chosen from the interval $[-w_0, w_0]$. An analysis of the trigger probability presented below will show that the chosen intervals cover the interesting region. The initial velocity is $v_0 = (0.1, 0, 0.01)\,\mathrm{m/s}$. The injection velocity of 0.1 m/s in x-direction is the mean velocity of atoms entering the mode in the experiment. Due to geometric filtering the axial velocity of an atom reaching the cavity mode is below about 0.01 m/s. Using these initial conditions, the atomic trajectory is integrated using equations (3.1). To simulate the trigger mechanism, which detects the presence of a strongly coupled atom in the cavity, the following procedure is used: The intracavity photon number, which is proportional to the transmitted intensity of the cavity, is sent through a low-pass filter to obtain the smoothed intracavity photon number. In each time step, the smoothed intracavity photon number is compared with the photon number

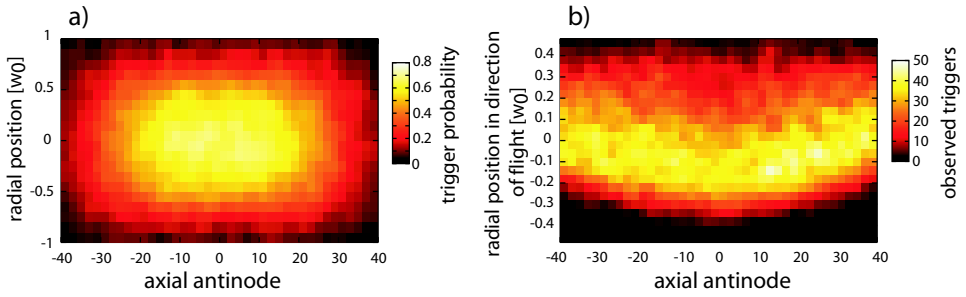

Figure 3.2: Analysis of the trigger mechanism as realised and evaluated in simulated trajectories. a) probability for an atom injected at a given axial antinode and radial position to activate a trigger. Only atoms entering the cavity axially and radially close to the mode centre have a high probability to activate a trigger. b) axial and radial distribution of the positions at which an atom is detected. The radial position at which the trigger is activated depends on the axial antinode in which the atom is detected. An atom channelling around an antinode near the centre is detected at a larger radial distance than an atom entering at an antinode away from the cavity centre. The parameters of the probe light prior to atom capture are $\Delta_a = 2\pi \times 35\,\mathrm{MHz}$, $\Delta_c = 0$ and $n_e = 1$ and the trap has a depth of $400\,\mu\mathrm{K}$ ($n_{\mathrm{trap}} = 80 \times 10^3$). The data includes the trigger events from more than 150000 simulated trajectories.

of the cavity without an atom. If the smoothed photon number drops below the threshold of 9%, the atom is detected and the trigger is activated. This leads to an instantaneous increase of the trapping power. After the atom is captured, the probe detuning and intensity can be adjusted in order to model the experimental probing scheme.

The threshold of 9% of the empty-cavity intensity ensures that only atoms which are strongly coupled to the cavity mode are detected. In order to localise the atoms in the regions of strong coupling, the trapping laser is used with a moderate trap depth of $400\,\mu\mathrm{K}$. Strong coupling of an atom is only reached if an atom is localised at one of the antinodes of the trapping field which has a significant overlap with an antinode of the probe field. The trigger probability for an atom, injected at a given axial and radial position is depicted in figure 3.2 a). It reaches its highest value of about 80% for an atom injected right in the centre of the cavity. Radially the trigger probability drops to about 40% at a distance of $w_0/2$ while it vanishes for atoms with a radial distance larger than w_0. Axially, the trigger probability is highest if the antinodes of both light fields coincide in the centre. For a distance of about 10λ, the trigger probability drops to about 40% and vanishes for a distance larger than 20λ. This shows that the initial conditions of atoms in the simulations cover the range in which an atom activates the trigger, since an antinode of the trapping field matches a node of the probe field at 20λ.

Figure 3.2 b) shows the position of the atom at the moment the trigger is activated. In the centre of the cavity, the trigger is activated if the atom is still below the cavity axis, while for an atom at a larger axial distance, the trigger is activated if the atom has reached the smallest radial distance to the cavity axis. Choosing a threshold which activates the trigger at the optimal position for all atoms is not possible in the simulation and thus also in the experiment.

The trajectory of the atom is recorded until the atom reaches a radial distance of more than $2w_0$. In this case, the atom is defined to have left the cavity radially at the time when it reached a distance of $1.5w_0$ for the last time. This procedure is chosen to match the evaluation of experimental traces, described in section 4.5. An atom which reaches a distance of $2w_0$ is unlikely to return to the cavity centre within a short time and therefore will not be judged as the same atom in the experiment. When the atom reaches a distance of $1.5w_0$, it cannot be observed any more, therefore this distance defines the exit time.

An atom which reaches an axial distance from the cavity centre of more than 80λ hits one of the cavity mirrors and is therefore defined to have left the cavity axially.

3.2 Simulation of cavity cooling

For interpretation of the experiments on cavity cooling that will be presented in chapter 6, it is a prerequisite to identify the loss mechanism which limits the storage time depending on the probe power. Using the distinction between axial and radial loss defined above, the loss channel can be determined from the simulation. As in the experiment, the power of the probe field is adjusted after an atom is captured in the trap. For each atom the total storage time and the type of the loss channel (axial or radial) is recorded.

3.2.1 Cooling as a function of probe power

The friction force and momentum diffusion generated by a weak near-resonant light field are proportional to the incident probe power if the atomic excitation is kept low. In contrast, parametric heating is independent of the probe power. Parametric heating, friction force and momentum diffusion generated by fluctuations of the dipole force act mainly in axial direction. In radial direction, only heating caused by scattered photons is significant.

The simulated storage time and the type of the loss channel are shown in figure 3.3 for the parameters, $\Delta_c = 0$ and $\Delta_a = 2\pi \times 35\,\mathrm{MHz}$, which are also used in the experiment. Without probe light, the storage time is limited by parametric heating and the atoms leave the trap in axial direction. If probe light is applied, the axial parametric heating is compensated by the

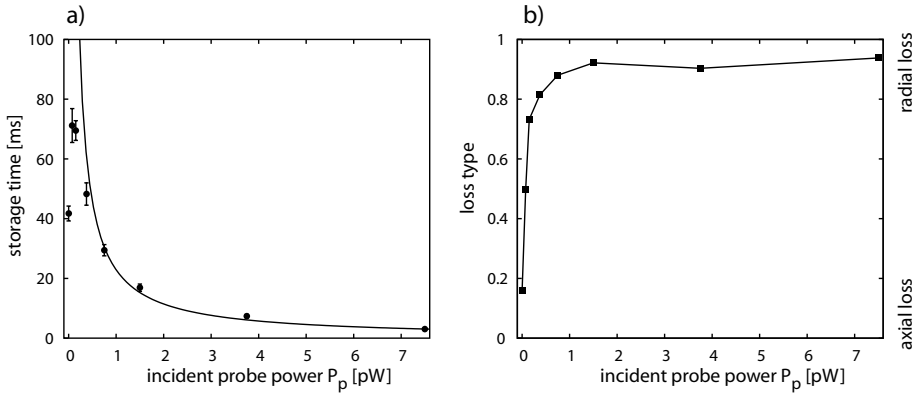

Figure 3.3: a) Simulated storage time, and b) loss channel of atoms as a function of the incident probe power P_p. The solid line in a) is a $1/P_p$-fit of the storage time to the points $P_p > 0.5\,\mathrm{pW}$. The loss type is defined as the fraction of atoms leaving the cavity radially. For very weak probe power, about 85% of the atoms leave the cavity axially. For probe powers above 1 pW, 90% of the atoms leave the cavity radially. The simulation was done for the detunings $\Delta_a = 2\pi \times 35\,\mathrm{MHz}$, $\Delta_c = 0$ and $n_{\mathrm{trap}} = 180 \times 10^3$. An incident probe power of 6.8 pW corresponds to one photon in the empty resonant cavity ($n_e = 1$).

friction force generated by the probe light. Therefore the storage time is increased from about 40 ms without probe light to about 70 ms for 0.1 pW incident probe power. Yet, the atomic excitation is increased simultaneously. This leads to radial heating of the atom. Since the friction force in radial direction is very weak, the atoms are mainly lost radially for a probe power above 0.5 pW.

For a probe power of more than 0.5 pW about 10% of the atoms leave the cavity axially independent of the probe power. This behaviour can be explained using the Fokker-Planck equation for atomic momentum distribution (see section 2.5): As momentum diffusion and friction force are both proportional to the probe power, the equilibrium temperature, which is the ratio of momentum diffusion and friction coefficient, stays constant. However, the diffusion in momentum space takes place on a faster timescale. Thus the probability for the atom to escape the potential increases linearly and the storage time becomes inversely proportional to the probe power. If axial heating induced by probing dominates parametric heating, both axial and radial loss mechanisms are proportional to the applied probe power. Therefore the ratio between axial and radial loss is independent of the probe power in this regime.

3.3 Simulation of normal-mode spectra

The main challenges in measuring a well-resolved normal-mode spectrum of the bound atom-cavity system, are to localise an atom in the trap strongly coupled to the mode and to compensate heating which arises while the atom is probed. To meet these challenges, an alternating cooling and probing scheme is used. This scheme is explained in detail in chapter 7 and applies probe intervals of 100 μs duration which are sandwiched between 500 μs cooling intervals. The cooling intervals are used to compensate for heating and thereby prepare the atom to be strongly coupled for the next probe interval. Furthermore, the transmission during cooling can be used to measure the coupling of the atom to the field independently of the probing. This allows to qualify the "strongly coupled" probe intervals.

To model this cooling and probing scheme, the same protocol is used in the simulations. The numerical data is then evaluated in the same way as the experimental data. The simulated transmission and storage times are compared with the experimental data in section 7.3. The simulations also allow to investigate the qualification of strongly coupled probe intervals in more detail, which is the subject of the following section.

3.3.1 Qualification of strongly coupled probe intervals

The maximum coupling of an atom to the light field is only reached for an atom which is located radially close to the cavity axis and axially at the position of an antinode of the probe field. For increasing radial distance, the coupling of an atom drops. Therefore, the atom has to be close to the cavity axis in order to ensure strong coupling during the probe interval. Figure 3.4 shows the distribution of radial positions of the atoms as a function of the transmission of the preceding cooling interval. For a large cooling transmission, the radial distribution is broad and atoms are found up to a distance of $1.4\,w_0$. For decreasing cooling transmission, the radial localisation during probing improves and only few atoms have a radial distance of more than $0.5\,w_0$ if the transmission during cooling is below 2% of the empty cavity transmission. Note that the probability to find an atom at a given radius is considered. Since the differential area increases linearly with the radius, the probability to find an atom, distributed uniformly is also proportional to the radius. This analysis shows that the qualification of probe intervals according to the transmission during the preceding cooling interval selects probe intervals during which the atom is localised near the cavity axis.

Even more important than the radial distribution is the distribution of the coupling of an atom to the cavity field. Figure 3.5 shows the distribution of the coupling strength as a function of the transmission of the preceding cooling interval. While the probability distribution is broad for a cooling transmission above 10% of the empty cavity transmission, the distribution

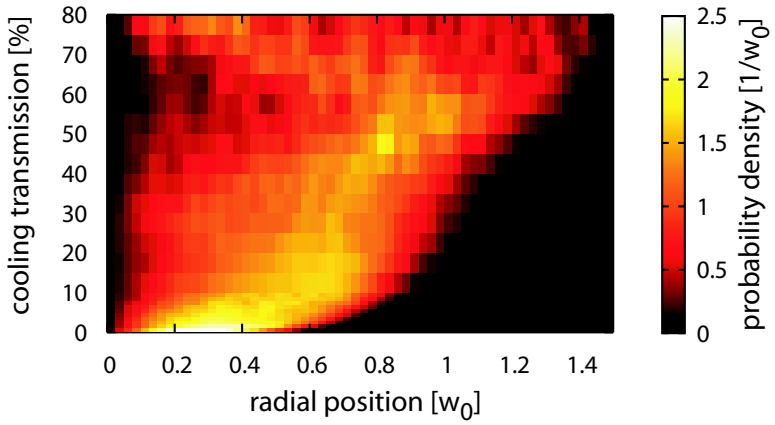

Figure 3.4: Simulated radial distribution of atomic positions during probe intervals. Each row of the density plot shows the probability distribution of the radial distance of an atom from the cavity centre for which the intracavity photon number during the preceding cooling interval is in the range given on the left axis in units of the empty cavity transmission. This plot contains all data simulated for spectrum a) presented in figure 7.6 ($n_{\mathrm{trap}} = 180 \times 10^3$).

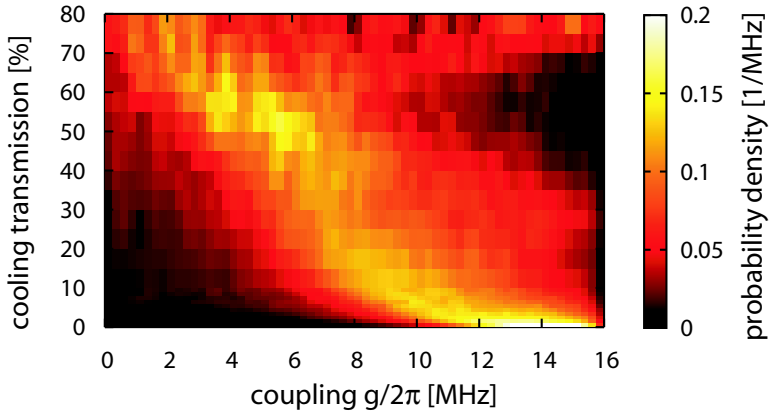

Figure 3.5: Distribution of couplings as a function of the transmission during the preceding cooling interval. Each row of the density plot shows the probability distribution of the coupling of an atom for which the intracavity photon number during the preceding cooling interval is in the range given on the left axis in units of the empty cavity transmission. This plot contains all data simulated for spectrum a) presented in figure 7.6 ($n_{\mathrm{trap}} = 180 \times 10^3$).

shows a pronounced maximum at about 13 MHz for a low cooling transmission. This proves that the independent qualification scheme is capable of selecting the strongly coupled intervals.

3.3.2 Axial energy of trapped atoms

In the last section we have seen that the qualification scheme allows to select strongly coupled probe intervals. This is achieved partly by excluding intervals during which the atom has a large radial distance and hence a weak coupling. However, an atom can also be weakly coupled due to axial oscillations with a high amplitude. The following analysis shows, that qualification also excludes intervals with a high axial oscillation amplitude. Figure 3.6 shows the average axial energy of an atom during probing as a

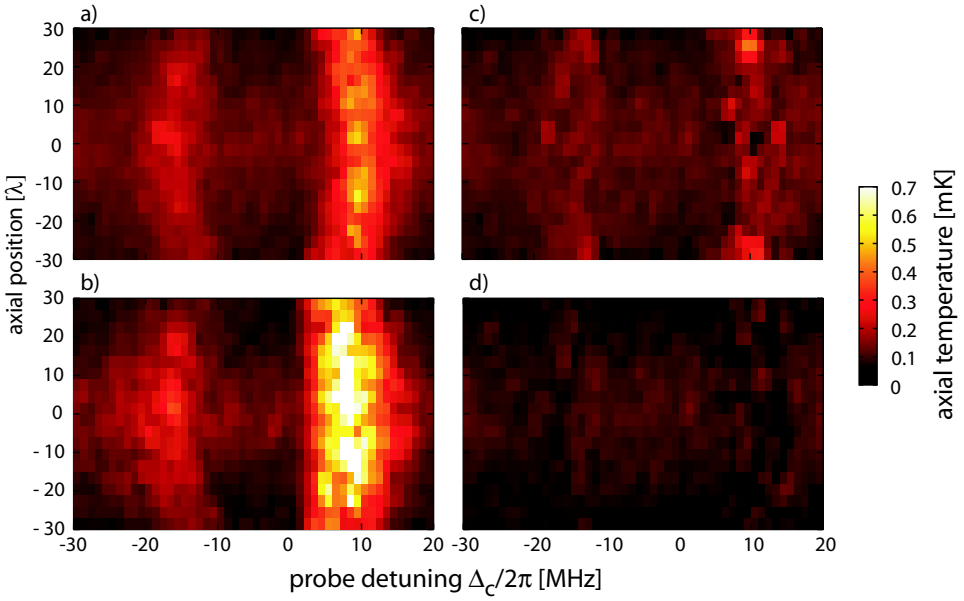

Figure 3.6: Mean axial (kinetic plus potential) energy of an atom during probing for different qualifications. Each density plot shows the average axial energy as a function of probe detuning and axial antinode. The simulation uses an intracavity photon number of 180×10^3 for the trapping field and the atom-cavity detuning $\Delta = 2\pi \times 35\,\mathrm{MHz}$. The incident probe power is 1.5 pW which is applied during the 500 μs cooling intervals with detuning $\Delta_c = 0$. The probe intervals have a duration of 100 μs. The data shown in a) includes all probe intervals while plot b) shows the subensemble of probe intervals for which the preceding cooling interval showed a transmission of more than 10% of the empty cavity transmission and which are removed by the qualification scheme. Plots c) and d) include all intervals for which the cooling light transmission is below 5% and 2%, respectively. All plots are based on the data simulated for spectrum a) presented in figure 7.6 ($n_{\mathrm{trap}} = 180 \times 10^3$).

function of probe detuning and axial position. At the position of the normal modes, $\Delta_c = 2\pi \times -15\,\mathrm{MHz}$ and $\Delta_c = 2\pi \times 10\,\mathrm{MHz}$, the atom is heated axially which results in an increased axial energy. This can be seen in plot (a) which includes all probe intervals. If qualification is used (plots (c) and (d)), the average axial kinetic energy of atoms in the remaining subensemble of probe intervals is clearly reduced. For 2% qualification by about a factor of 7. During the probing intervals which are removed by qualification (b), the average axial energy is highest.

In conclusion, the qualification scheme used in this work selects intervals during which the atom is radially near the cavity axis and at the same time has a low axial energy. During these intervals, the atom is localised at a region of strong coupling. The agreement between simulation and experimental results also allows to estimate the axial localisation of an atom in the experiment, which will be discussed in section 7.5.

Chapter 4

The atom-cavity apparatus

The textbook example of atom-light interaction is a single two-level atom interacting with a single mode of an optical cavity. The realisation of this system in the laboratory necessitates an extremely good cavity and the ability to control the motion of a single atom. The technological progress in manufacturing dielectric coatings for high-quality mirrors, made the first steps towards the realisation of this idealised textbook example in the laboratory possible (Rempe *et al.*, 1992). At room temperature, atoms are moving with a velocity of about 300 m/s on average and are too fast to be observed one by one within an optical cavity. To achieve a sufficiently long interaction time, laser cooled atoms are injected into the cavity using an atomic fountain. They reach the cavity with a velocity smaller than 0.1 m/s. The cavity is pumped with a weak near-resonant laser used to observe the atom and a far-detuned laser which provides an intracavity dipole trap. An atom entering the cavity shifts the system out of resonance with the incident laser, hence the transmitted power drops. The distinct drop allows to detect the arrival of an atom and thereupon increase the depth of the dipole trap. This compensates for the kinetic energy of the atom and leads to trapping. Subsequently the atom can be observed and manipulated.

In this chapter, the experimental set-up which allows to capture, trap, investigate and manipulate a single atom strongly coupled to the mode of the cavity is described. While this work gives an overview on the complete set-up and describes recent advances in detail, more detailed information on the basic set-up can be found in Münstermann (1999) and in Fischer (2002).

Section 4.1 describes the preparation and transfer of cold atoms into the cavity. The high-finesse cavity and its stabilisation scheme as well as the detection of light transmitted by the cavity are discussed in section 4.2. Section 4.3 presents the set-up of the far-detuned dipole trap, which is the basis for the measurements presented in this thesis. The measurement sequence and the evaluation of the results are explained in section 4.4.

4.1 The atomic fountain

A schematic overview of the experimental set-up to deliver laser cooled atoms into the cavity is shown in figure 4.1 and a technical drawing and a photograph of the vacuum chamber are shown in figure 4.2. Rubidium-85 atoms emitted by an electrically heated dispenser (SAES Getter) are collected in a magneto-optical trap (MOT) (Raab *et al.*, 1987; Metcalf and van der Straten, 1999). The atomic cloud is further cooled to about 5 μK using polarisation gradient cooling (Lett *et al.*, 1988; Dalibard and Cohen-Tannoudji, 1989). Subsequently the atoms are accelerated towards the high-finesse cavity by cooling them in a moving frame of reference, a technique also known as "moving molasses".

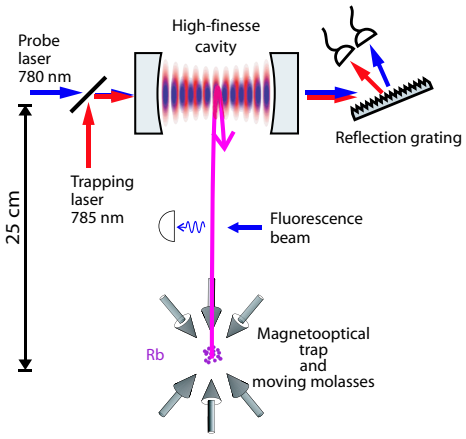

Figure 4.1: Schematic of the experimental set-up. ^{85}Rb atoms are collected in a magneto-optical trap and cooled by an optical molasses. By cooling the atoms within a moving frame of reference, the cold atom cloud is launched towards the cavity. The high-finesse cavity has a length of 122 μm and a finesse of 4.3×10^5. It is pumped by a near-resonant probe laser and a far-red detuned trapping laser. The transmitted light is separated by a grating and detected by independent detectors.

The light field used for the magneto-optical trap, polarisation gradient cooling and the moving molasses is composed of six independent, circularly polarised laser beams in a face centred cubic set-up. The laser light has a wavelength of $\lambda \approx 780.243\,\text{nm}$ and is slightly red detuned from the $5S_{1/2}F = 3 \leftrightarrow 5P_{3/2}F = 4$ transition of ^{85}Rb (figures 4.4 and A.1). The light is generated by a Titanium-Sapphire (Ti:Sa) laser which is stabilised at a frequency of $2\pi \times 260\,\text{MHz}$ below the trap transition of ^{85}Rb using Doppler-free saturation spectroscopy. The linewidth of this laser is 30 kHz (r.m.s). The quadrupole magnetic field used for the MOT has a magnetic field gradient of about 15 Gauss/cm. During polarisation gradient cooling and moving molasses, the quadrupole magnetic field is switched off. The residual magnetic field is permanently compensated for. For the MOT and polarisation gradient cooling, all six light beams are tuned to the same frequency. For trapping, a detuning of $2\pi \times -15\,\text{MHz}$ from the trap transition is used with a light intensity of about $1\,\text{mW/cm}^2$ in each of the beams. For polarisation gradient cooling, the detuning is increased to $2\pi \times -45\,\text{MHz}$ and the intensity is reduced to $0.3\,\text{mW/cm}^2$. Polarisation gradient cooling is ap-

plied for 2.5 ms. To accelerate and cool the atoms in the moving frame, the three lower beams are slowly blue detuned with respect to the upper beams with a rate of 1 MHz/ms until the selected maximal detuning between the upper and lower beams is reached. After 5.5 ms the light is switched off and the atoms follow a ballistic trajectory. By adjusting the maximal detuning between the upper and lower beams the vertical velocity of the launched atoms can be tuned. About 4 cm below the cavity, a laser beam can be used to illuminate the atomic cloud for the adjustment of the atomic fountain.

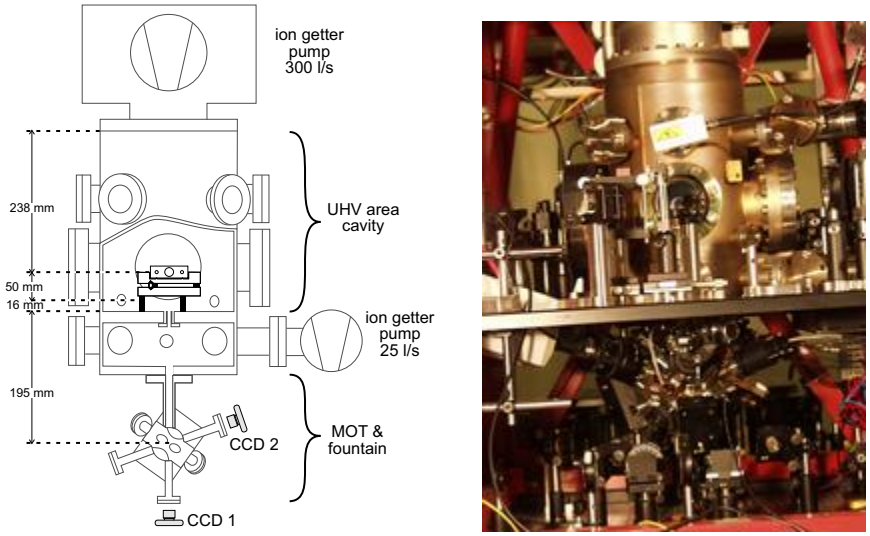

Figure 4.2: Vacuum chamber. *Left:* technical drawing of the vacuum chamber. The cavity is mounted on a two-stage vibration isolation mounting in the ultra high vacuum part of the chamber. The MOT cube is connected through a small hole to allow for differential pumping. *Right:* Photograph of the vacuum chamber.

4.1.1 Characterisation of the atomic fountain

The maximal detuning of the lower beams with respect to the upper beams of the moving molasses allows to adjust the velocity of atoms entering the cavity between 4 m/s and about 0 m/s. The ability to control the velocity of atoms traversing the cavity was demonstrated in earlier experiments (Münstermann *et al.*, 1999b) by measuring the transit time of single atoms as a function of the atomic velocity. In order to capture and store atoms in an intracavity trap it is important to inject slow atoms into the cavity. Therefore the number of atoms collected in the MOT and the detuning of the atomic fountain are adjusted to ensure that only single atoms with very small velocities arrive at the cavity. For a maximal molasses detuning of $2\pi \times 3.2$ MHz, the turning point of the atomic fountain is found to be within

the cavity mode. Figure 4.3 shows the probability to detect an atom in the cavity as a function of the time after the launch of the atomic cloud. The number of atoms detected per time interval is proportional to the atom

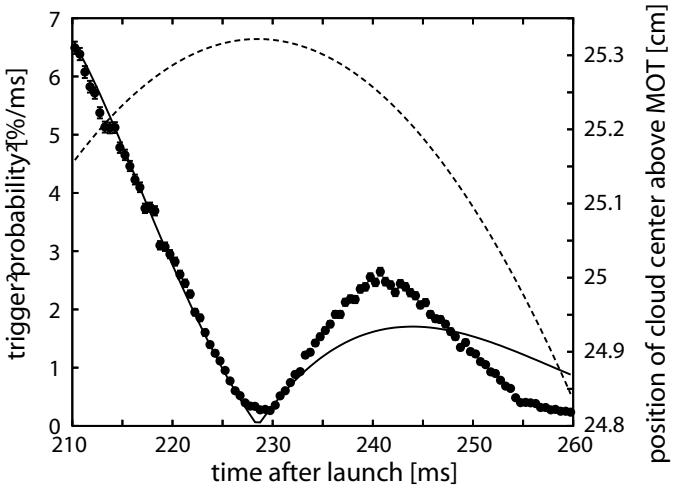

Figure 4.3: Arrival time of atoms in the cavity. The experimentally observed probability density to detect an atom is plotted as a function of the time after launch (points). The maximal detuning of the lower molasses beams is 3.2 MHz for all points. This plot contains the arrival times of more than 150000 trigger events. The solid line represents the expected probability for the parameters of the experiment calculated with a simple model described in the text. The dashed line shows the vertical position of the cloud centre within the model on the right scale.

flux, that is entering into the cavity mode. Since the atomic flux vanishes near the turning point of the atomic cloud, the number of detected atoms also vanishes close to the turning point near 230 ms. The atoms which are detected earlier are on their way upwards, while the atoms detected later enter the cavity mode from above. The measured probability to detect an atom can be qualitatively explained by a simple model. A point like atomic cloud with a temperature of about 5 μK is launched at $t = 0$ and expands due to its finite temperature. The cloud is geometrically filtered by the cavity mirrors about 25 ms before reaching the cavity mode. The atoms which enter between the two mirrors and which approach the cavity mode have a nonzero axial velocity. Thus before reaching the cavity mode, their density drops as some of the atoms hit one of the cavity mirrors. Oversimplified, this loss of atoms is treated as an exponential decay of the atom density. The number of atoms reaching the cavity mode according to this model is depicted by the solid line in figure 4.3. Prior to the turning point of the atomic cloud at 230 ms, the measured trigger probability agrees well with the simple model, while the distribution after the turning point differs. This could be due to light forces that the atoms experience on their way up. An-

other possibility is, that the model, which assumes an exponential decay of the number of atoms within the cavity as mentioned above, is not detailed enough.

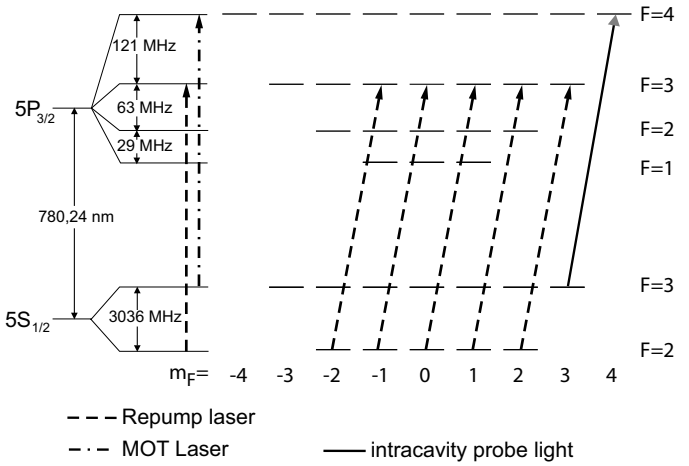

Figure 4.4: Rubidium-85 D_2 level scheme: The MOT operates on the $5S_{1/2}, F = 3 \leftrightarrow 5P_{3/2}, F = 4$ transition. A re-pumper returns atoms to the cooling cycle of the MOT by exciting them from the $5S_{1/2}, F = 2$ level to the $5P_{3/2}, F = 3$ level. For the detection and the manipulation of the atom in the cavity, the $5S_{1/2}, F = 3, m_F = 3 \leftrightarrow 5P_{3/2}, F = 4, m_F = 4$ transition is used since it forms a closed two level system with the highest transition strength of the ^{85}Rb D_2 lines.

4.2 The high-finesse cavity

The high-finesse cavity is the core part of the whole experimental set-up. It determines the spectral mode density of the electromagnetic field and therefore influences the interaction of an atom with the radiation field. The aim of this experiment is to realise the regime of strong coupling where the interaction strength, g, between a single mode of the radiation field and a single atom dominates the coupling of the atom to the modes of the electromagnetic vacuum, γ, and the coupling of the cavity mode to the vacuum, κ. The maximal coupling of an atom to a single TEM_{00} mode of the cavity at an anti-node of the standing wave field, g_0, is proportional to $V^{-\frac{1}{2}}$, where V is the mode volume of the cavity. For a near planar cavity the mode volume is given by

$$V = \frac{\pi}{4} w_0^2 l, \tag{4.1}$$

where w_0 is the beam waist and l the cavity length.

4.2.1 Cavity set-up

The cavity consists of two dielectric mirrors (Research Electro-Optics) with losses of $\mathcal{T}+\mathcal{L} = 7.1\,\text{ppm}$ and a transmission of $\mathcal{T} = 2.6\,\text{ppm}$. The radius of curvature is 200 mm and the diameter of the mirror substrates is 7.75 mm. As shown in figure 4.5, the mirrors are glued onto aluminium mounts which are separated by a piezo ceramic tube. By applying a highly stable voltage to the piezo tube, the length of the cavity can be tuned very precisely. The piezo tube has 4 holes allowing access of atoms and vacuum to the cavity mode.

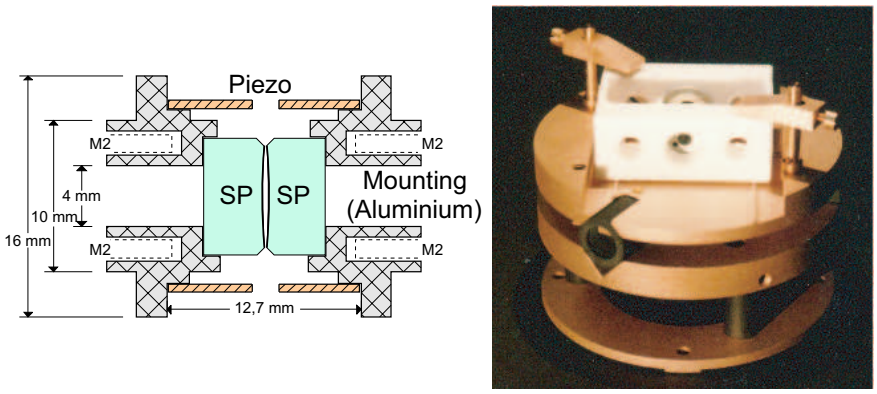

Figure 4.5: *Left:* Sketch of the cavity set-up. The two mirror substrates are glued to aluminium holders, which are separated by a piezo ceramic tube. *Right:* Photograph of the cavity set-up. The cavity is mounted in a Teflon holder and the whole set-up is mounted onto a vibration-isolation stage.

Two laser beams are independently mode matched to the cavity mode (see figure 4.6): A very weak probe beam near resonant to the atomic transition with a typical maximal mode-matched input power of $P_p = 7.5\,\text{pW}$. And a second laser beam resonantly pumps the TEM_{00} mode of the cavity which is two free spectral ranges ($2\pi \times 2.46\,\text{THz}$) red-detuned from the atomic transition. This laser beam is used for the dipole trap and serves at the same time to continuously stabilise the length of the cavity.

4.2.2 Length stabilisation of the cavity

The high finesse of the cavity $\mathcal{F} = 4.4 \times 10^5$ affords a tremendous absolute stability of the mirror distance. A change of the cavity length of about 1 pm tunes the cavity out of resonance with the incident laser beam. To compensate for thermal drifts and mechanical vibrations of the mirror separation, the length of the cavity has to be continuously stabilised. The laser used for the stabilisation of the cavity length serves at the same time as an intracavity dipole trap. In a dipole trap, modulations of the intracavity

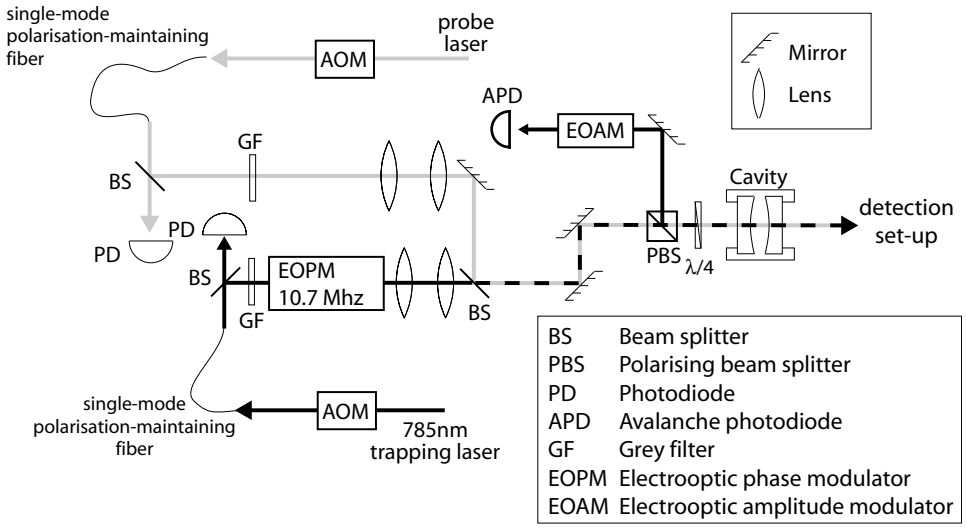

Figure 4.6: Coupling of the two laser beams to the cavity: The frequency of the light in each of the two beams can be adjusted with an acoustooptical modulator (AOM) which is used in double pass configuration. By adjusting the radio-frequency power used to drive the AOM, the power of the beams can be regulated. In order to get a clean TEM_{00} mode, each of the beams passes through a polarisation-maintaining single-mode fibre. A part of the light transmitted through each fibre is directed onto a photo diode which is used for the power stabilisation. Each beam is independently mode matched to the cavity with a telescope and a periscope before they are superimposed on a beam splitter. Together they pass through a polarising beam splitter and a quarter wave plate. Therefore both beams impinging on the cavity are σ^+ polarised. The light reflected from the cavity again passes through the $\lambda/4$ plate and is reflected from the PBS onto an avalanche photo diode used for the length stabilisation of the cavity.

intensity at frequencies near the first harmonics of the trap frequencies must be avoided to keep parametric heating low. Therefore a radio-frequency stabilisation scheme following Drever *et al.* (1983) with a modulation frequency of 10.7 MHz is used (see figure 4.7). The modulation frequency is large compared to the projected axial trap frequency of about 1 MHz. Since it is necessary to switch the depth of the trap while simultaneously stabilising the cavity, the error signal for the stabilisation is required to be independent of the laser power impinging on the cavity. This is achieved by dividing the generated error signal by the power of the incident laser beam. In order to compensate for nonlinearities of the used rf-photodiode, the beam reflected by the cavity is attenuated by an electro-optic amplitude modulator before it is detected. Using this scheme the power in the trapping beam can be switched by a factor of about 10 without influencing the cavity frequency stabilisation.

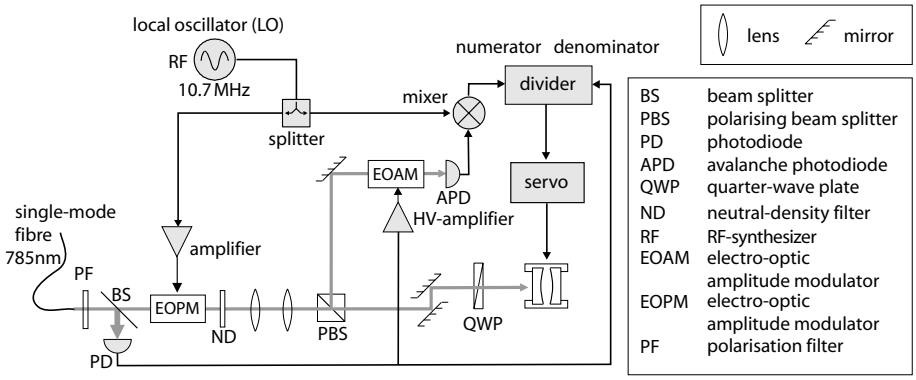

Figure 4.7: Cavity stabilisation. For simplicity, the part of the set-up used to couple the probe laser into the cavity is omitted here (see figure 4.6). The stabilisation light is mode cleaned with a single mode fibre. A power stabilisation is used to reduce intensity fluctuations. An electro-optic phase modulator is used to modulate the phase of the light with a frequency of 10.7 MHz. The light reflected from the cavity is attenuated by an electro-optic amplitude modulator and is then directed onto a rf-coupled avalanche photodiode. Multiplying the photodiode signal with the local oscillator yealds the error signal. Since the error signal is approximately proportional to the power of the laser beam, the error signal is divided by the power of the laser beam. To account for nonlinearities of the photodiode used, a voltage proportional to the power in the beam is applied to the amplitude modulator. With this set-up, the power of the stabilisation light can be switched by a factor of 10 without affecting the cavity length stabilisation.

4.2.3 Detection set-up

The atom-cavity system is observed via photons transmitted through the cavity. For one photon in the cavity on average, the transmitted power is 0.9 pW, corresponding to a rate of single photons of only 3.5 MHz. Therefore it is indispensable to detect these photons with a high efficiency at a low dark count rate. However the light transmitted through the cavity contains in addition to the weak probe light (1 fW to 1 pW) the trapping light with a power between 50 nW and 1 μW. Therefore the detection set-up must allow the efficient separation of the two light fields which share the same spatial mode and polarisation and have a wavelength difference of only 5 nm. In addition, birefringence of the cavity causes variations in the polarisation of the transmitted light. Therefore the separation efficiency must be polarisation independent.

These challenges are met with the following set-up. A holographic reflection grating (American Holographics) with 2300 lines/mm and an efficiency of more than 90% for vertically polarised light is used to spatially separate the two light frequencies. The efficiency of the grating for horizontally polarised light is much lower. Therefore the transmitted light is split using

a polarising beam splitter. The horizontally polarised part is rotated by a $\lambda/2$-plate and impinges onto the grating with vertical polarisation as well (see figure 4.8). Behind the grating, the originally vertically polarised beam passes through a $\lambda/2$-plate and the two beams are recombined, each rotated in polarisation by 90°, with their original polarisation relation. The deflection of the grating angularly separates the two wavelengths and allows to reflect the trapping light onto a photo multiplier tube (Hamamatsu R8396) using a sharp edged mirror. The signal coming from the photomultiplier is amplified by a transimpedance amplifier (Femto) with a transimpedance of 500 kΩ and a bandwidth of 4 MHz and is recorded with a transient recorder.

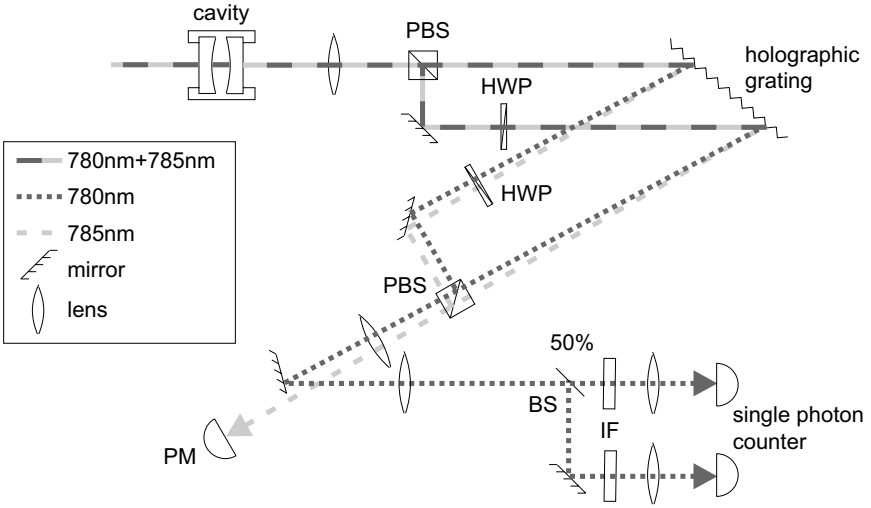

Figure 4.8: Optical paths from the cavity to the detectors: Probe light at 780 nm as well as trapping light at 785 nm are transmitted through the cavity. Both share the same spatial mode and polarisation. They are separated with a high efficiency using a holographic grating. To achieve independence of the efficiency of the polarisation, the light is separated by a polarising beam splitter. The polarisation of the horizontally polarised part is rotated by a $\lambda/2$-plate. Behind the reflection grating, the beams are recombined with their original polarisation relation. In the focal plane of a lens ($f = 150$ mm), the trapping light and probe light have spatially separated foci. The trapping light is directed onto a photomultiplier (PM) while the probe light is further filtered with an interference filter (IF) and is detected by two single-photon counting modules. (PBS polarising beam splitter, HWP half wave plate, BS nonpolarising beam splitter).

The intensity of the trapping light within the spatial mode of the probe light behind the grating is attenuated by 50 dB. Since the dipole light is in the extreme case 80 dB brighter than the transmitted probe light (300 nW trapping light, 3 fW probe light), the probe light additionally passes through a narrow band interference filter (NanoLayers) with a peak transmission of above 80% and a spectral width below 1 nm. Thereby trapping light

is attenuated additionally by at least 33 dB. The rest contributes to the dark count rate of about 2.5 kHz corresponding to about 2.5 fW observed in the experiment. The probe light is then split by a polarisation independent beam splitter and directed onto two single photon counting modules (SPCM AQR-13 PerkinElmer). These detectors have a quantum efficiency of about 50% and a dead time of about 50 ns. The whole set-up achieves a quantum efficiency of about $\xi = 30\%$ for photons transmitted through the cavity.

The photon clicks from the detectors are time stamped with a resolution of 1 ns and stored for later evaluation. Additionally a home made count rate to voltage converter generates an analog signal with an update rate of 100 kHz. The analog signal is further low pass filtered and used for the real-time detection of an atom entering the cavity.

4.2.4 Cavity characterisation

The free spectral range (FSR) of the cavity is measured by determining half the frequency difference of the trapping and probe fields which are resonant with two TEM_{00} modes two free spectral ranges apart. From the result $\mathrm{FSR} = \pi c/l = 1.232\,\mathrm{THz}$ a cavity length of $l = 156\,\lambda_{780} \approx 121.7\,\mu\mathrm{m}$ is obtained. The linewidth of the cavity is measured by stabilising the cavity to the trapping light and slowly scanning the frequency of the probe light. With this measurement scheme a linewidth (HWHM) of $\kappa = 2\pi \times 1.4\,\mathrm{MHz}$ and hence a finesse of

$$\mathcal{F} = \frac{2\pi\,\mathrm{FSR}}{2\kappa} = 4.4 \times 10^5. \tag{4.2}$$

is obtained. The transmission and losses of the two mirrors are determined as described in Hood *et al.* (2001) by measuring the absolute power of light transmitted through and reflected by the cavity. Without exact knowledge of the mode matching factor, it is necessary to assume that both mirrors have the same transmission. For the cavity a transmission of 2.6 ppm and an absorption of 4.5 ppm per mirror was obtained. From the cavity length and the mirror curvature ($R = 200\,\mathrm{mm}$) the maximal coupling of the $5S_{1/2}, F = 3, m_F = 3 \leftrightarrow 5P_{3/2}, F = 4, m_F = 4$ transition of an ^{85}Rb atom to the light mode at an anti-node, $g_0 = 2\pi \times 16\,\mathrm{MHz}$, can be calculated. The mirror transmission and absorption also determines the maximum transmission of the cavity. On the resonance a mode-matched incident power of 6.8 pW is needed to obtain one photon on average in the cavity $n_e = 1$, which leads to a transmission of 0.9 pW.

At the wavelength of the trapping laser, the cavity has the same finesse. Thus an intracavity photon number of $n_{\mathrm{trap}} = 1$ of the trapping field corresponds also to a transmission of 0.9 pW.

4.3 The dipole trap

The near-resonant light field used to observe the atom can also be used to capture and store an atom in the cavity (Pinkse *et al.*, 2000; Hood *et al.*, 2000). However using an independent far-detuned light field as first realised by Ye *et al.* (1999), allows to achieve significantly longer storage times. This also allows to optimise the detuning and the intensity of the near-resonant light field for the observation and manipulation of the atom.

4.3.1 Laser frequency

The dipole force exerted by a far-detuned light field drops linearly with increasing detuning from the atomic resonance, $F \propto 1/\Delta_a$, while the atomic excitation drops quadratically, $\langle \sigma^+ \sigma \rangle \propto 1/\Delta_a^2$. Therefore a trap with a large detuning introduces less atomic excitation and a lower momentum diffusion for the same trap depth. To achieve the same depth at large detuning the power has to be increased linearly. However, for very high laser intensities, the energy dissipation in the coating of the cavity mirrors becomes large enough to significantly heat the coating and self locking or self anti locking effects emerge. For the cavity the critical transmission is about $2\,\mu$W corresponding to an intracavity power of about 0.8 W. In the experiment a detuning of two free spectral ranges is chosen. Therefore the trapping laser is also in resonance with the cavity. This results in a wavelength of $\lambda_{\text{trap}} = 785.28\,\text{nm}$.

4.3.2 Trap depth

The intracavity photon number in the dipole field $n_{\text{trap}} = P/0.9\,\text{pW}$ can be obtained from the transmitted power P and the mirror properties. The Stark shift $\Delta_S = n_{\text{trap}} \times 100\,\text{Hz}$ can then be calculated using equation (2.65). The resulting trap depth is $U_{\text{trap}} = n_{\text{trap}} \times 5\,\text{nK}$. Hence, the maximal transmission of $2\,\mu$W corresponds to a maximal trap depth of 11 mK. Unfortunately it was not possible to measure the trap depth in an independent way as discussed in section 5.2.3.

4.3.3 Trapping laser set-up

The trapping laser is a commercial external cavity diode laser (DL100 XL, Toptica Photonics with extended cavity) with a grating in Littrow configuration. It is running at a wavelength of 785.28 nm. The non-stabilised linewidth is a few MHz and the output power is approximately 25 mW.

The light of the trapping laser is used to generate an intracavity dipole trap. Frequency fluctuations of the trapping laser are converted into amplitude fluctuations in the cavity. This leads to a fluctuating potential depth and thus to parametric heating of the stored atom. In order to reduce this

heating effect, the linewidth of the trapping laser must be small compared to the linewidth of the cavity.

The trapping laser is stabilised to a transfer cavity (Ernst, 1995). The stabilisation set-up is explained in detail in figure 4.9. This near planar Fabry-Perot cavity has a free spectral range (FSR) of 310 MHz and a linewidth of about 100 kHz. On timescales below 1 s, the cavity is very stable. To prevent drifts of the resonance frequency on the timescale of several seconds, the cavity is itself stabilised to the Ti:Sa.

The small linewidth of the transfer cavity allows to generate an error signal with a steep slope which in turn allows to achieve a narrow linewidth of the trapping laser. The error signal is generated using a radio frequency technique (Drever *et al.*, 1983) with a phase modulation frequency of 18.5 MHz. The resulting error signal has a bandwidth of about 4 MHz and allows to achieve a laser linewidth of 13 kHz r.m.s. The light from the Ti:Sa used for the stabilisation of the transfer cavity is phase modulates with a frequency of 2.5 MHz. The bandwidth of the error signal is reduced to about 100 Hz using an RC low pass filter. Both light fields impinging on the transfer cavity have the same polarisation. They are separated using a reflection grating (Edmund Scientific, 2400 lines/mm, $\approx 50\%$ efficiency) and are directed onto two independent rf-photodiodes. The grating allows to completely spatially separate the two beams with a wavelength difference of 5 nm. This scheme allows to stabilise several lasers to the cavity provided their wavelength differs by more than about 2 nm.

4.3.4 Trapping laser characterisation

The power density spectrum of the frequency noise (figure 4.10) characterises the frequency excursions of the trapping laser. The heating rate of a dipole trap is proportional to the noise power density at the harmonic of the trap frequency and the square of the trap frequency (Savard *et al.*, 1997). In our case, the axial and radial trap frequencies are about 300 kHz and 2 kHz, respectively. Thus the reduction of intensity noise at about 300 kHz is most important to reduce parametric heating. As frequency fluctuations of the laser are converted to intracavity intensity fluctuations at twice the frequency, the noise power density at a frequency of 300 kHz dominates the strength of parametric heating of an atom in the trap. Therefore the stabilisation is tuned to achieve a low noise power below about 500 kHz (figure 4.10).

The r.m.s. linewidth of the trapping laser can be calculated from the discrete spectral noise power density as

$$\Delta\nu_{\mathrm{rms}} = \sqrt{\sum_k S_\nu(\nu_k)\Delta_\nu}. \tag{4.3}$$

Here $S_\nu(\nu_k)$ is the noise power density at frequency ν_k measured with a

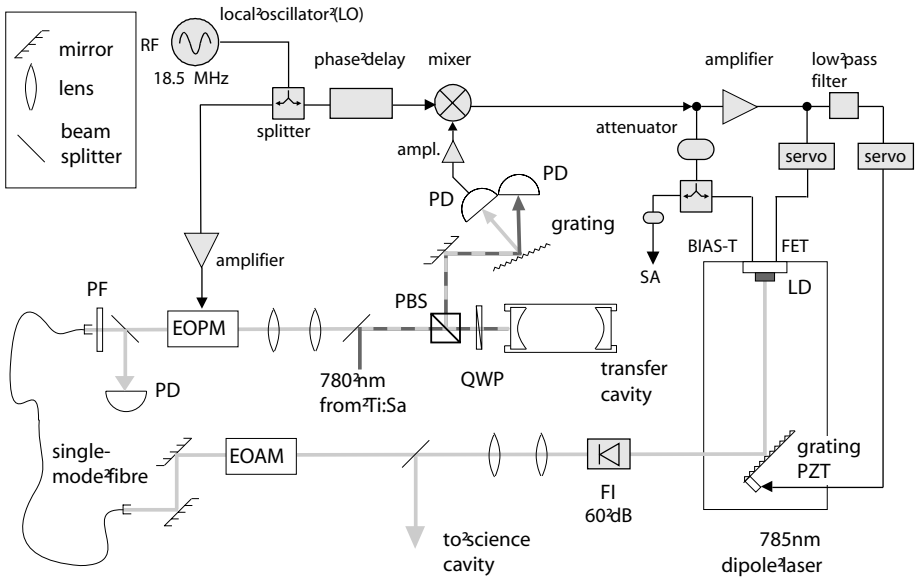

Figure 4.9: Trapping laser set-up and stabilisation: The light from the diode laser is mode cleaned using a single mode polarisation maintaining fibre. A power stabilisation is realised by measuring the power transmitted through the fibre and adjusting the power with an electro-optic amplitude modulator (EOAM). The phase of the light is modulated with a frequency of 18.5 MHz using an electro-optic phase modulator (EOPM). The diode laser beam is superimposed with the light from the Ti:Sa and is mode-matched to the cavity mode with a telescope and a periscope. The light reflected from the cavity is separated from the Ti:Sa using a reflection grating and detected by a rf-photodiode. The error signal is obtained by multiplying the photodiode signal with the phase-delayed local oscillator signal. The error signal is then split in three branches. A low pass filtered part is used to control the grating position to compensate drifts and fluctuations below 10 Hz. A second branch with a bandwidth of 100 kHz adjusts the laser diode current via a FET bypass. The third branch capacitively couples (using a bias-T) the error signal onto the diode current, a power splitter allows to measure the error signal with a spectrum analyser (SA). (PD photodiode, EOPM electro-optic phase modulator, EOAM electro-optic amplitude modulator, QWP quarter-wave plate, PF polariser, PBS polarising beam splitter, LD laser diode, PZT piezo stack, FI Faraday isolator)

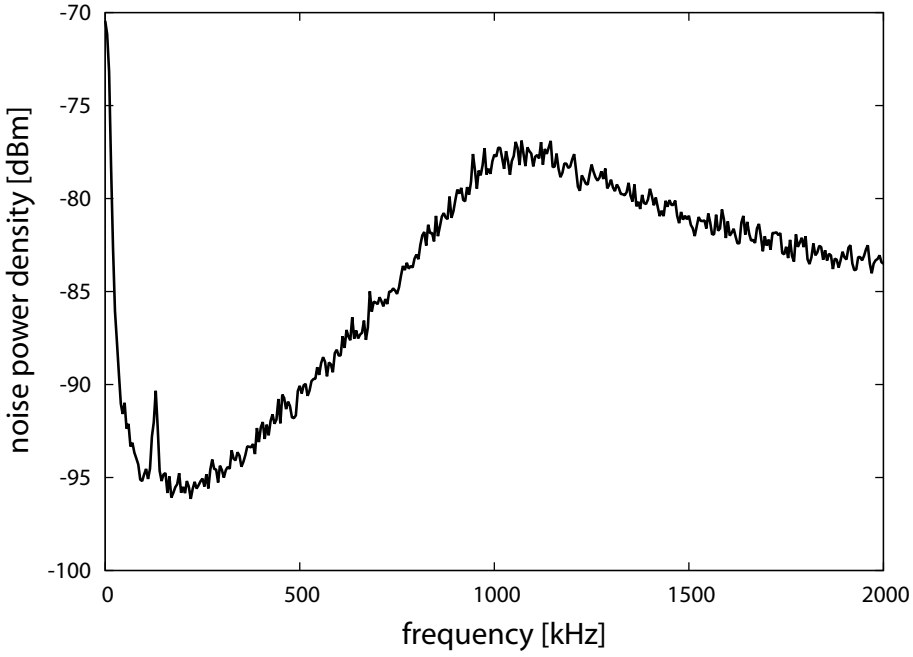

Figure 4.10: Power density spectrum of the frequency of the trapping laser. The error signal was measured with a spectrum analyser using a resolution bandwidth of 5 kHz.

resolution bandwidth of Δ_ν. Summing over all $S_\nu(\nu_k)$ with $\nu_k < 4\,\mathrm{MHz}$, the r.m.s. linewidth is calculated from the measured noise power density spectrum to give

$$\Delta\nu = 12.6 \pm 0.5\,\mathrm{kHz}. \tag{4.4}$$

4.4 Experimental sequence

The whole measurement sequence is generated by a computer which also stores all parameters of the measurement in a relational database. The sequence starts with the loading of the magneto-optical trap. While loading, a current of 7.5 A heats the rubidium dispenser to release rubidium atoms. These atoms are collected in the MOT. The number of atoms in the MOT is determined by measuring its fluorescence using a photodiode. When the fluorescence exceeds an adjustable threshold, the heating of the dispenser is stopped. Since the current through the dispenser changes the magnetic quadrupole field, the MOT is loaded for additional 200 ms to allow the cloud to reach the minimum of the magnetic field without contributions of the dispenser current. Subsequently polarisation gradient cooling is applied for 2.5 ms. Thereupon the lower molasses beams are detuned with respect to the upper beams to accelerate the atomic cloud. The start of this time interval

is defined as the begin of the launch and serves as the time reference for each experimental cycle. The current in the compensation coils for the magnetic field is switched 50 ms after launch to generate a magnetic field of about 1 Gauss in direction of the cavity axis and thereby determine the quantisation axis. At the same time the probe light impinging on the cavity is tuned to the cavity resonance and an incident (mode-matched) power of 7.5 pW. Cavity and probe laser are detuned by $\Delta_a = 2\pi \times 35\,\mathrm{MHz}$ above the atomic resonance and the trap is adjusted to a depth of $400\,\mu\mathrm{K}$. The trigger circuit is armed 210 ms after launch when the fastest atoms of the cloud which cannot be captured in the trap have already passed the cavity. The trigger circuit stays armed for an interval of 50 ms. As the probe laser is resonant with the empty cavity, an atom entering the cavity tunes the system out of resonance. The distinctive drop in transmission is used to detect the arrival of an atom in the cavity. The transmitted probe light is detected by two single photon counting modules. The voltage pulses generated from these modules are time stamped and stored in the computer. The same pulses are also counted and converted to a voltage signal with an update rate of 100 kHz. This signal is further fed through an RC low pass filter with a 3 dB frequency of 25 kHz. A drop of the resulting signal below 9% of the empty cavity signal activates the trigger. The time of this trigger after the launch of the atomic cloud is defined as the arrival time of the atom in the cavity. Upon this trigger, the depth of the trap is increased by switching up the incident power of the trapping beam. Now the atom is captured in the trap and is available for the measurements described in chapters 5, 6 and 7.

The number of atoms collected in the MOT before launch is adjusted so that only single atoms reach the cavity mode. During the measurements on average one atom is detected every fifth launch of the MOT. The probability that an atom is detected in the cavity is below 7 %/ms (figure 4.3). The transit time of an atom through the cavity mode is below 1 ms. Therefore the probability to find two atoms in the cavity within the same 1 ms interval is below 0.5%.

4.5 Evaluation of single experimental traces

The photon arrival times recorded for each captured atom are evaluated later. To cope with the huge number of single traces for which the storage time of an atom has to be evaluated (in total more than 150000) and to exclude human bias, the evaluation is done using a computer algorithm. The results of this evaluation are stored in a relational database. The use of a database allows the extraction of the data for the plots. Furthermore it allows sophisticated checks for experimental drifts and allows to exclude systematics.

For the measurements of the normal-mode spectra which will be pre-

sented in chapter 7, the transmission of each cooling interval and each probe interval is stored in the database. This allows to extract the data of the spectra using the qualification on the transmission of the preceding and proceeding cooling intervals.

Chapter 5

Trapping and observing the motion of single atoms

In the strong coupling regime of cavity QED, the drastic influence of a single atom in the cavity on the transmission of the cavity allows to detect single atoms passing through the cavity with high signal to noise and bandwidth (Mabuchi *et al.*, 1996; Münstermann *et al.*, 1999b). The light force an atom experiences in the cavity can be large, even for a cavity field containing only single photons on average (Hood *et al.*, 1998; Münstermann *et al.*, 1999a). Using these forces, a single atom can be captured and stored in the same near-resonant light field used for simultaneous observation of the atom (Hood *et al.*, 2000; Pinkse *et al.*, 2000). In these experiments, the depth of the trap is rapidly increased when a single atom is detected in the cavity, in order to compensate for radial kinetic energy of an atom entering the mode. On the other hand, the near-resonant trapping laser leads to strong heating of the atom. This strong heating limits the observed average storage times to a few hundred microseconds or equivalently a few radial oscillation periods.

The use of the near-resonant light field to simultaneously observe and trap the atom implies a compromise in the detunings from the atomic and cavity resonance and the laser powers which can be chosen in the experiment: Since the dipole force drops linearly with increasing detuning of the laser from the atomic resonance and the atomic excitation and heating rates drop quadratically, using a far-red-detuned light field for the trap strongly suppresses heating of the atom, thus leading to a drastic rise in the storage times. The drawback of a large detuning is that it is more difficult to observe the atom. To satisfy both needs, a near-resonant laser field is used for observation and a far-detuned field is employed for trapping.

Section 5.1 describes the detection and capturing of a single atom in the far-detuned dipole trap. Section 5.2 focuses on the motion of a single atom in the trap as observed using the photon autocorrelation function of the

cavity transmission. Even a single stored atom yields enough information to observe its characteristic axial and radial oscillation. The lifetime of the trap without near-resonant probe light, the "dark dipole trap", is analysed in section 5.3.

5.1 Capturing an atom

In this experiment, single atoms are captured and stored in the far-red-detuned dipole trap. Since the influence of a single atom on the power of a far-detuned light field is negligible, the atom cannot be detected by measuring the transmission of this field. Instead, a second, independent, near-resonant light field is used for observation of the atom. This allows to tailor the detuning and the power of the near-resonant light, to enable the observation of the atom while heating is kept small.

The far-detuned light field used for the trap is resonant with a TEM_{00} mode of the cavity two free spectral ranges ($2\pi \times 2.46\,\mathrm{THz}$) red detuned with respect to the near-resonant light and the atomic transition. Hence, the trapping field has two antinodes less than the near-resonant cavity mode and the antinodes of the two fields only coincide in the centre of the cavity and at the mirrors. To select atoms which enter near the centre of the cavity, a trap depth of 0.25 mK is employed to localise the atom at an antinode of the trapping field. The threshold for triggering on the arrival of an atom is chosen low enough that the trigger is only activated by atoms which are strongly coupled to the near-resonant cavity mode. Therefore only atoms guided in an antinode near the cavity centre are strongly coupled to the probe field, cause a trigger and are trapped.

If an atom is detected within the cavity mode, the power of the trapping light is increased within about $10\,\mu\mathrm{s}$, a timescale which is fast compared to the radial motion. Therefore, the kinetic energy of the atom does not suffice to leave the trap and the atom is trapped. Atom detection as well as the increase of the trap depth are slow compared to the axial motion. Hence, the axial position of the atom cannot be resolved and its axial energy is on average high. An example of a single trapping event is shown in figure 5.1. In this example, the atom stays in the cavity for about 20 ms.

5.2 Real-time observation of the motion of a single atom

The cavity transmission is determined by the coupling strength of the atom to the cavity mode, the oscillatory motion of an atom hence leads to an oscillation of the power of the transmitted light.

The radial oscillation of a single atom in the trap is sufficiently slow to be observed in real time as demonstrated by Hood *et al.* (2000) and Pinkse *et al.*

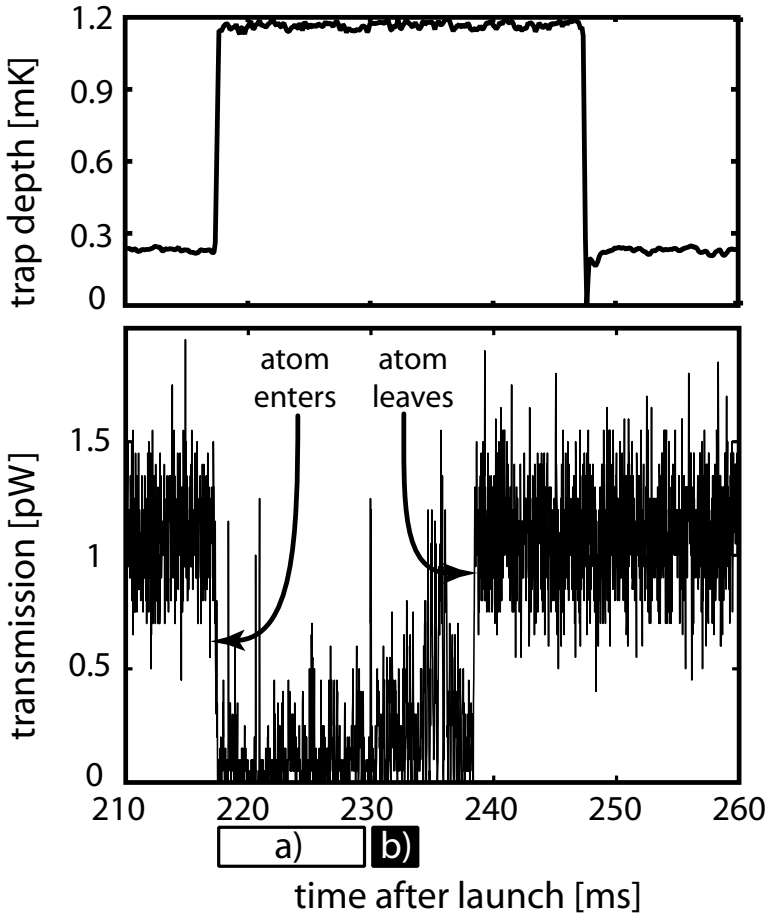

Figure 5.1: Single trapping event. The upper graph shows the trap depth as measured from the transmitted light of the far-detuned light field as a function of the time after launch of the atomic cloud. In the lower graph, the transmission of the cavity is shown. The cavity is excited on resonance with an incident probe power of 7.5 pW which is blue detuned with respect to the atomic resonance ($\Delta_a = 2\pi \times 35\,\mathrm{MHz}$, $\Delta_c = 0$). Upon detection of a single atom in the cavity mode (218 ms after launch of the atomic cloud), the trap depth is increased. The signature of the stored atom is then visible for about 20 ms before the atom leaves the trap. The transmission during two time intervals a) and b), is further analysed in figure 5.2. The noise which can be seen in the transmission signal of the empty cavity (for example $240 - 260\,\mathrm{ms}$) is dominated by shot noise in the photon detection rate.

(2000). The axial oscillation of an ensemble of single atoms in the cavity has already been observed by Münstermann *et al.* (1999b). The long storage time which is achieved for an atom in the far-detuned trap combined with near-resonant probe light allows to observe and analyse the axial motion of one individual atom within a few milliseconds.

5.2.1 Motion of an individual atom

The radial oscillation of the atom can be observed in real time in the cavity transmission. This is not possible for the axial motion, as during a period of the axial oscillation of about 3 μs, only 0.3 photons are detected on average. However, the oscillation can be observed in the autocorrelation function of the transmitted photons

$$g^{(2)}(\tau) = \frac{\langle p(t)p(t+\tau)\rangle}{\langle p(t)\rangle^2}. \tag{5.1}$$

It gives the joint probability to observe a photon at time $t+\tau$ if a photon was observed at time t, normalised to the average probability to detect two photons at the same time. The photon autocorrelation function for two distinct intervals of the trapping event in figure 5.1 is depicted in figure 5.2. The two intervals differ in the average transmission. The first interval, a), has a lower average transmission, corresponding to stronger average coupling of the atom to the mode. Almost no oscillation is visible on the timescale of the radial oscillation (panel a2): During this interval, the atom has a low radial oscillation amplitude. The axial oscillation leads to an oscillation in the correlation function which is clearly visible in panel a1. The oscillation period of 2.5 μs corresponds to a frequency of 400 kHz, which is in the frequency range expected for the axial oscillation. Thus during this interval the atom oscillates mainly along the cavity axis. During the second interval, b), the radial oscillation is clearly visible and has a frequency of about 4 kHz. Since the radial oscillation amplitude is larger than during interval a), the average coupling of the atom is lower, which leads to a lower average transmission.

The trap depth in axial direction depends on the radial position of the atom. For an atom which is near the cavity axis, the axial trap depth is maximal while it drops with increasing radial displacement of the atom. An atom with large radial oscillation amplitude therefore experiences different axial trap depths. As the width of the trap is constant, the restoring forces vary radially, causing a radial dependency of the axial trap frequency. This leads to a de-phasing of the axial oscillation and a lower oscillation frequency on average, which can both be observed in the autocorrelation signal of interval b).

Similar signatures of the atomic motion are found in the example trace presented in figure 5.3. Furthermore this example trace allows to observe

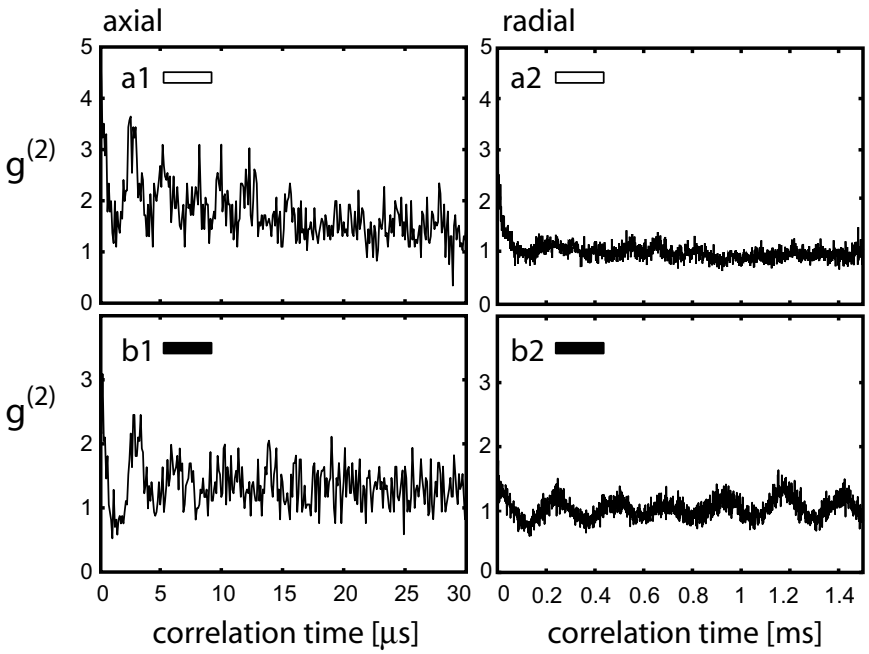

Figure 5.2: Photon autocorrelation function calculated from the transmission of two intervals of the single trapping event shown in figure 5.1. For each interval, the first 30 μs (left), and the first 1.5 ms (right) are plotted, where the atomic oscillation in axial and radial direction can be observed, respectively.

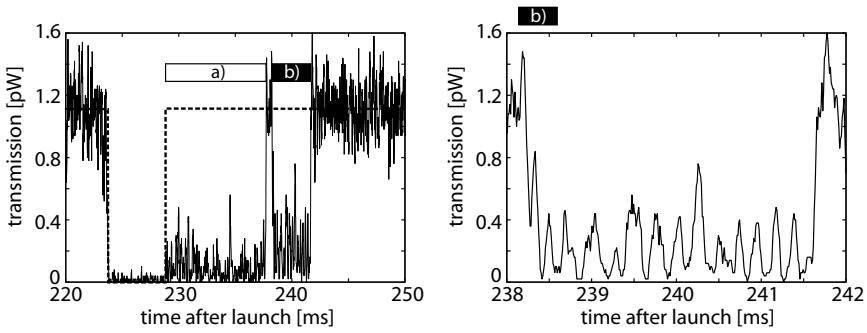

Figure 5.3: *left:* Upon detection of an atom in the trap, the probe light was switched off for 5 ms. The transmission expected without an atom is depicted by the dashed line. After the light is switched on, the motion of the atom in the trap can be observed for about 11 ms. *right:* A zoom of the left trace between 238 and 242 ms (interval b)) clearly shows the radial oscillation of the atom in real time. An axial and radial autocorrelation function of interval a) of this event can be found in figure 5.4. In figure 5.5 the axial oscillation is analysed in more detail. The parameters of the probe beam are $\Delta_a = 2\pi \times 35\,\mathrm{MHz}$, $\Delta_c = 0$ and $n_e \approx 1.1$. The transmission of the dipole trap is 250 nW.

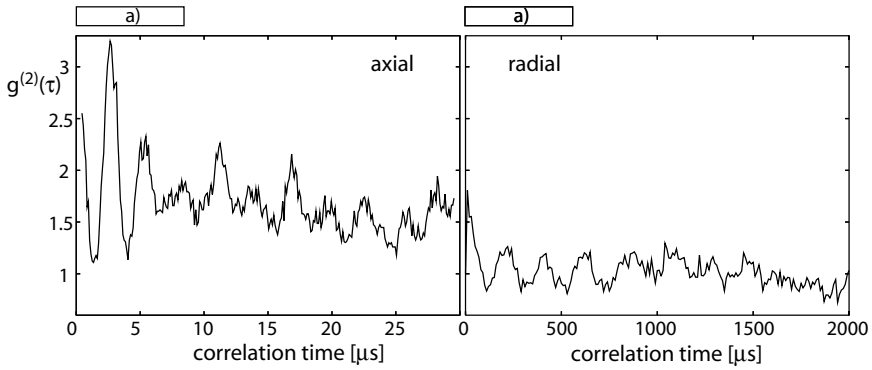

Figure 5.4: Photon autocorrelation function of the interval a) $(229 - 237\,\mathrm{ms})$ from the trapping event shown in figure 5.3. The radial oscillation has a period of about $220\,\mu\mathrm{s}$ and is clearly visible in the right panel. The axial oscillation with a period of $2.8\,\mu\mathrm{s}$ as seen in the left panel, is damped due to the radial oscillation as explained in the text.

the different axial trap frequencies for an atom close to the cavity axis and near the turning point of the radial oscillation. In this measurement, the probe light was switched off for 5 ms after capturing the atom in the trap. When the probe light is switched on again, the atomic motion is observed for 13 ms before the atom leaves the trap. From the transmission, two intervals can be distinguished: During the first interval, a), $(229 - 237\,\mathrm{ms})$ the transmission is low on average while during interval b) $(238 - 242\,\mathrm{ms})$ the average transmission is larger than during interval a). In interval b), the radial oscillation can be directly observed in the transmission. The autocorrelation function of the transmission during interval a) is depicted in figure 5.4. The autocorrelation function clearly shows the radial oscillation with a period of $220\,\mu\mathrm{s}$. The axial oscillation with a period of $2.8\,\mu\mathrm{s}$ only leads to two well resolved peaks in the autocorrelation function. The third peak expected around $8.4\,\mu\mathrm{s}$ is very shallow. Peaks hat even larger correlation times seem to be more pronounced. This "revival" is investigated next.

The radial oscillation can be observed directly as depicted in the left graph of figure 5.5. The cavity transmission is low for an atom in the centre of the trap and high if the atom is away from the centre. The quarter periods during which the atom is near the cavity centre (central) and near one of the turning points (peripheral) can be determined. This allows to calculate the photon autocorrelation function for the central and peripheral parts of the trajectory separately. The result is shown in the right panels of figure 5.5. Two different oscillation frequencies are found for the central ($\nu_c = 410\,\mathrm{kHz}$) and peripheral ($\nu_p = 360\,\mathrm{kHz}$) parts of the trajectory. The autocorrelation function of each part shows less dephasing than the autocorrelation of the whole interval.

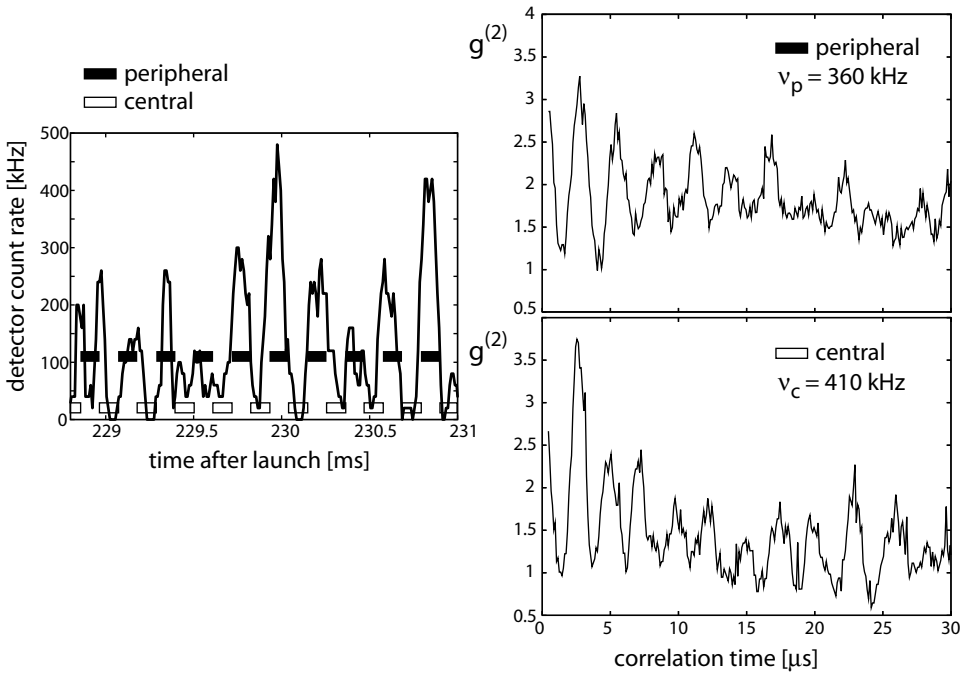

Figure 5.5: *left:* Zoom of the trapping event shown in figure 5.3. The quarter periods of the radial oscillation during which the atom is near the cavity centre and near the point of largest radial elongation are marked by open and closed rectangles, respectively. *right:* The photon autocorrelation calculated for the central and peripheral parts of the trajectory separately.

5.2.2 Intracavity intensity of the trapping light

The intracavity intensity of the trapping light field can be calculated from the transmitted power of the trapping light and the measured transmission of the output mirror (see section 4.2.4). For the measurement of the mirror transmission and absorption, it is necessary to assume equal transmission of both cavity mirrors (Hood *et al.*, 2001). This can lead to a systematic error in the calibration of the intracavity intensity. Therefore it would be advantageous to have an independent and more direct calibration of the intracavity intensity of the trap light.

On first sight, it should be possible to calibrate the trap depth by measuring the oscillation frequency of an atom oscillating in the trap. The evaluation of several single traces for different trap depths allows to analyse the observed axial and radial oscillation frequencies as a function of the trap depth. Figure 5.6 shows the square of the oscillation frequency as a function of the trap depth. For the axial as well as the radial oscillation, the data can be described by a linear fit. However, the oscillation frequency expected from a harmonic approximation near the trap centre is by a factor 3 larger

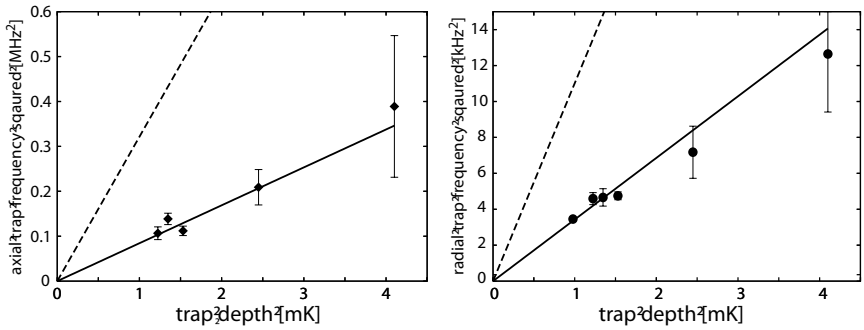

Figure 5.6: Oscillation frequency squared of an atom in the trap, as observed in the autocorrelation function of a set of selected traces. The trap depth is calculated from the transmitted power of the trapping field and the transmission of the cavity mirrors. A transmitted power of 0.9 pW corresponds to one intracavity photon $n_{\mathrm{trap}} = 1$ and a trap depth of 5 nK. *Left:* for the axial oscillation and *right:* for the radial oscillation. The data shows a linear dependence as expected (solid line). However the oscillation frequency calculated for the harmonic approximation of the trap is three times higher (dashed line).

than the observed oscillation frequency.

This discrepancy can be explained by the nonlinear relation between atomic position and cavity transmission: An atom oscillating radially must reach an amplitude of about w_0 in order to appreciable change the transmission. For this oscillation amplitude, the harmonic approximation is not valid any more and the oscillation frequency is only about half the frequency expected within the harmonic approximation.

In radial direction, the trap has a Gaussian profile. Differing from a harmonic trap, for which the oscillation frequency is independent of the amplitude, the oscillation frequency decreases with increasing amplitude. In figure 5.7, the square of the radial oscillation frequency divided by the trap depth is shown as a function of the average cavity transmission. The average transmission increases for a distant atom and is therefore a measure of the oscillation amplitude. For a harmonic trap no dependency of the oscillation frequency on the oscillation amplitude is expected. Despite the limited signal to noise ratio, a decrease of the oscillation frequency is observed for increasing average transmission.

For the axial oscillation, figure 5.8 displays the relative transmission as a function of the axial position of an atom for various radial positions of the atom. An atom which is localised near the cavity axis needs a large oscillation amplitude in order to modulate the transmission distinctly. For large oscillation amplitudes however, the harmonic approximation around the trap centre loses its validity and the oscillation frequency is significantly lower than expected. For an atom at a larger radial distance, oscillations

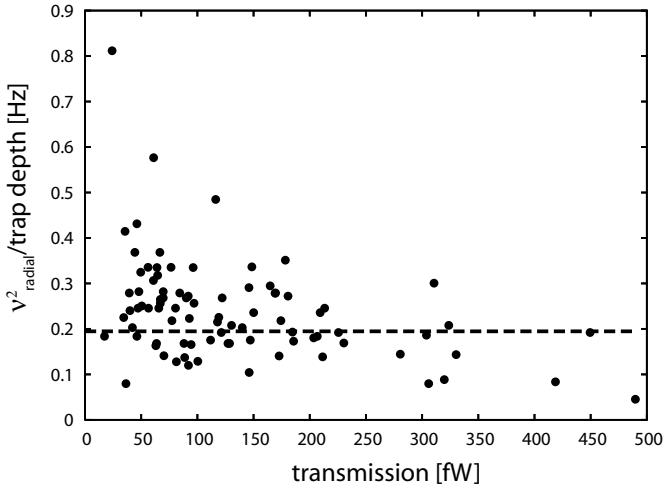

Figure 5.7: Oscillation frequency squared divided by trap depth as a function of the average cavity transmission. Each point is evaluated from a short (few ms) interval of the transmission of a single atom trapped in the cavity. In a harmonic trap, the oscillation frequency is independent of the amplitude and therefore from the transmission (dashed line). The measured data shows that for an increased average transmission which corresponds to a large oscillation amplitude the oscillation frequency drops.

with a low amplitude should also be visible. In this case the trap is shallower and therefore the oscillation frequency is also lower.

Another misinterpretation can occur if the atom is not trapped in the central antinode. In this case the antinode of the probe field does not coincide with the antinode of the trapping field. As an example, figure 5.8 b) depicts the dependence of the cavity transmission on the atomic position for a shift between the two antinodes of $\lambda/8$. Since in this case the transmission is not symmetric with respect to the trap centre, the light is only switched on once during one oscillation period. Therefore in this case the modulation frequency of the transmitted light directly gives the oscillation frequency of the atom. According to the numerical simulation, this scenario is very likely.

In conclusion, the observed oscillation frequency of an atom in the trap does not reveal the trap frequency nor the trap depth. This is caused by the fact that only large radial oscillations can be observed and thus the anharmonicity of the trap is important. Also, the visibility of the axial and the radial oscillation is affected by the Stark shift and is thus also biased by the trap depth.

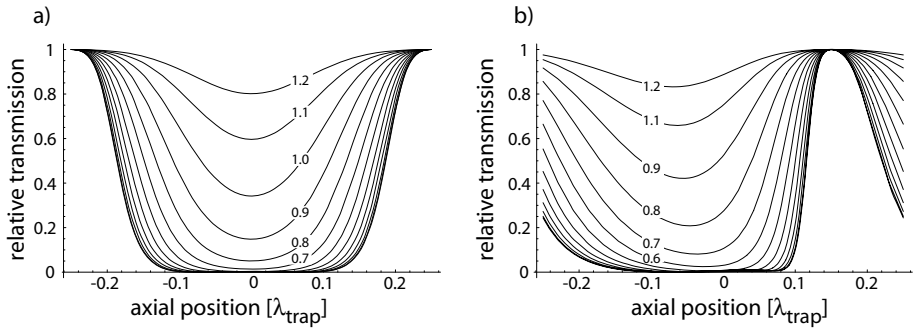

Figure 5.8: Cavity transmission as a function of the axial position of a single atom relative to the transmission of the empty cavity. a) in the centre of the cavity and b) for trap and probe fields shifted by $0.1\lambda_{\mathrm{trap}}$ (an antinode of the probe field is located at $0.15\lambda_{\mathrm{trap}}$). The radial position is varied between $1.2w_0$ and 0 and is marked on the curves. For a radial distance of less than $0.5w_0$, the transmission shows a pronounced switching behaviour which plays a crucial role in the visibility of the oscillation of an atom. The parameters used are $\Delta_a = 2\pi \times 35\,\mathrm{MHz}$, $\Delta_c = 0$, $2\Delta_S = 2\pi \times 45\,\mathrm{MHz}$.

5.2.3 Photon autocorrelation averaged over many atoms

The photon autocorrelation function can be averaged over many atoms in order to improve the signal and to focus on the average motion in contrast to the example of the individual motion of a single atom. In this section, the photon autocorrelation function is calculated from data taken to measure the normal-mode spectrum (chapter 7). For this measurement the transmission of trap light was varied between 250 nW and 340 nW. The average photon autocorrelation function on the timescale of the axial oscillation is shown in figure 5.9. The nonlinear relationship between transmission and axial position (figure 5.8) leads to a very low transmission for an atom in the centre while the transmission is suddenly switched on if the atom reaches a threshold distance. This behaviour leads to the characteristic triangular shape of the autocorrelation function, which resembles the autocorrelation of a square signal.

The oscillation frequency calculated from these autocorrelation functions is shown in figure 5.10 as a function of the depth of the trap. The square of the oscillation frequency can be described by a straight line which, in contrast to first expectations does not pass through the origin.

The reason for this behaviour is again the nonlinearity of the transmission function and the light shift caused by the trap. For a transmission of the trap light of about 280 nW, the Stark shift caused by the trap light compensates the initial atom-cavity detuning. If the trap depth is increased, the oscillation frequency increases. However, the position-transmission dependence also changes and atoms oscillating at a larger radial distance are better

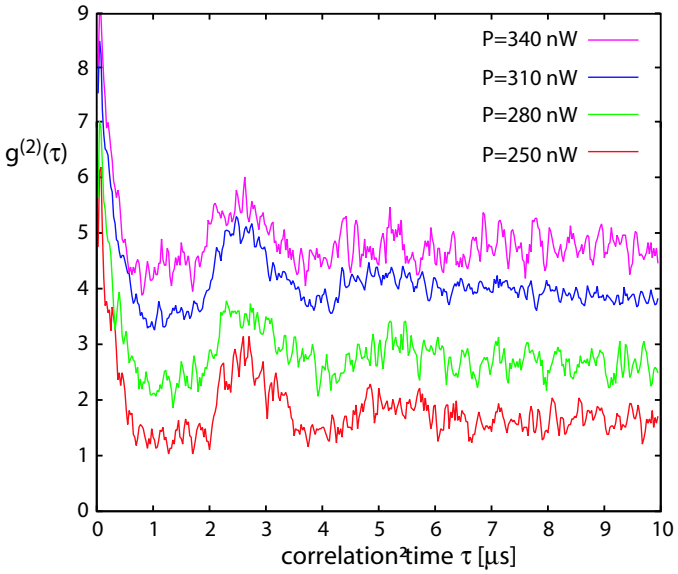

Figure 5.9: Averaged photon autocorrelation. Four autocorrelation functions for different depth of the dipole trap expressed in terms of the transmitted dipole power P are shown. The graphs for $P = 280$, 310, and 340 nW are offset by 1, 2, and 3, respectively.

visible in the autocorrelation function. This effect reduces the dependence of the observed oscillation on the trap depth.

In conclusion, due to the nonlinear dependence of the transmission on the atomic position, the anharmonicity of the trap and the Stark shift of the atomic resonance, the oscillation frequencies deduced from $g^{(2)}(\tau)$ for different trap depth do not give a conclusive answer on the intracavity power of the trap light.

5.3 Lifetime in the trap

Another characteristic quantity of the trap is the storage time of atoms. To measure the storage time of the far-detuned trap, the near-resonant light used to detect the atom is switched off completely as soon as an atom is detected. After an adjustable time Δt, the probe light is switched on again to determine whether the atom is still stored in the trap. An example trace of such a measurement is shown in figure 5.11.

The data obtained for the storage time of atoms in the trap before and after improvement of the frequency stability of the trapping laser is shown in figure 5.12. Before improving the frequency stability of the trapping laser a storage time of 10 ms was obtained whereas with the revised laser stabilisation a more than threefold extension to 35 ms was achieved. In both mea-

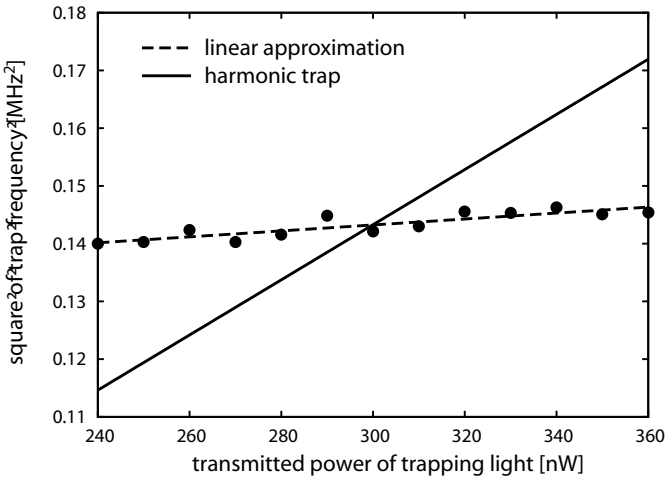

Figure 5.10: Observed oscillation frequencies as evaluated from averaged photon autocorrelation functions (circles). The data can be approximated by a straight line (dashed line) but deviates significantly from expected linear dependence (solid line) on the trap depth which also crosses the origin.

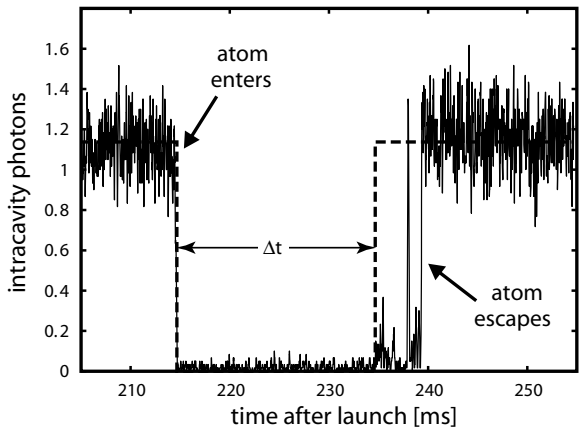

Figure 5.11: Measurement of the storage time of the dipole trap: Upon detection of an atom, the trap depth is increased from 400 μK to 1.2 mK and the probe light is switched off completely. After an adjustable time Δt, the probe light is switched on again (dashed line) to detect if the atom is still in the trap.

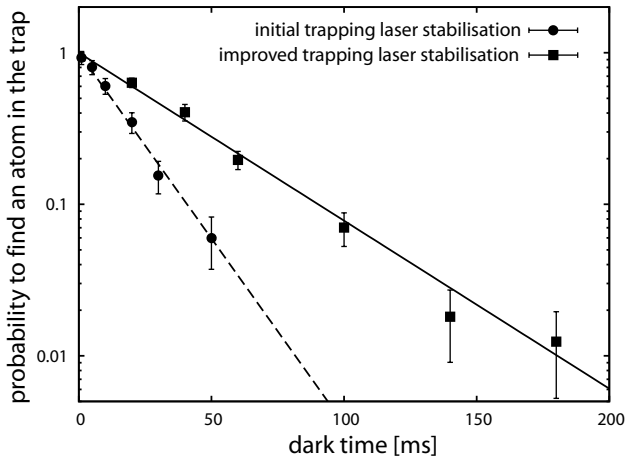

Figure 5.12: Storage time in the dark trap: Probability to find an atom in the trap as a function of the time Δt during which the probe light was switched off after the atom was captured in the trap. The two measurements presented here show the storage time before (dots, dashed line) and after (squares, solid line) the frequency stability of the trapping laser was improved. In both cases the decay is very well modelled by an exponential decay with a storage time of 18 ms and 35 ms, respectively. For capturing, the trap depth is increased from 400 μK to 1.2 mK in each case.

surements, the probability to find an atom in the trap drops exponentially as a function of the time the atom stayed in the dark trap. An exponential decay means that the probability to lose the atom from the trap in a time interval is constant. Note that this also means that no significant ageing of an atom in the trap is observed in this measurement.

The first data points as well as the exponential approximation show a probability of about unity to find an atom in the trap after triggering. This proves that if an atom is coupled strongly enough to activate the trigger it is captured in the trap in nearly every case.

In all the following measurements including near resonant probe light the storage time of an atom in the dark trap was measured concurrently. The storage time in the dark trap measured at the same performance of the laser and cavity stabilisation serves as reference for the performance of the experiment.

5.3.1 Loss mechanisms of the dark trap

Compared to free space dipole traps for neutral atoms (Grimm *et al.*, 2000) the storage time obtained in this experiment with an intracavity dipole trap is rather limited.

The heating rate induced by scattering of far-detuned photons is 12 μK/s

corresponding to an expected storage time of about 40 s for a trap depth of 1 mK[(i.)]. Due to the orientation of the atomic dipole, $\frac{2}{5}$ of the heating is in axial direction, while each of the two orthogonal transverse directions is subject to $\frac{3}{10}$ of the calculated heating rate.

Fluctuations of the dipole force heat the atom in the direction of the dipole force. Since the forces are much stronger axially than radially, heating due to dipole fluctuations mainly heats the atom in axial direction. In the strong coupling regime of cavity QED, the heating due to dipole fluctuations is unfortunately strongly enhanced. The expression of the dipole diffusion (2.54) can be approximated for $\Delta_c = 0$ and large detuning (2.61) as

$$D_{\mathrm{dp,cav}} = \hbar^2 (\nabla g)^2 \frac{\eta^2}{\kappa^2} \frac{\gamma}{\Delta_a^2} \left(1 + \frac{4g^2}{\gamma\kappa}\right) = D_{\mathrm{dp,free}} \left(1 + \frac{4g^2}{\gamma\kappa}\right). \tag{5.2}$$

For the parameters of this experiment, heating due to dipole fluctuations of the dipole force is increased by a factor of 240 over the comparable case in free space and leads to a heating rate of 2 mK/s corresponding to a storage time of about 250 ms. Even though this heating mechanism is much larger than in free space, it cannot explain the observed limited storage times.

Relative fluctuations of the trapping laser frequency and the cavity frequency lead to a fluctuating intracavity intensity of the trap light and therefore to a fluctuating trap depth. As described in Savard *et al.* (1997), this leads to a diffusion in momentum space and to heating of the atom in the trap. The time derivative of the motional energy of the atom is

$$\langle \dot{E} \rangle = \frac{\pi}{2} \omega_{\mathrm{trap}}^2 S_\nu(2\omega_{\mathrm{trap}}) \langle E \rangle .$$

Here ω_{trap} denotes the trap frequency and S_ϵ the spectral noise power density. Since the heating rate depends on the spectral noise power density at the first harmonic of the trap frequency, intensity fluctuations at this frequency must be controlled carefully. Because the trap frequency enters quadratically in the heating rate, the atom is heated mainly in axial direction where the trap frequency is about $\omega_{\mathrm{axial}} \approx 2\pi \times 300\,\mathrm{kHz}$, as compared to the radial trap frequency of $\omega_{\mathrm{radial}} \approx 2\pi \times 3\,\mathrm{kHz}$. The atoms will therefore leave an antinode of the standing wave field and will ultimately hit one of the mirrors.

Further improvement of the stabilisation of the trapping laser can enhance the storage time, as technical heating is reduced. Horak *et al.* (1997) postulated a cavity cooling mechanism which also relies on strong coupling between atom and light field. The measurements presented in the next chapter will show that this cooling mechanism can be used to compensate for axial heating.

[(i.)] For the implemented trapping scheme, the minimal kinetic energy of the atom after switching up the trap depth is given by the depth of the shallow guiding trap. Hence, after increasing the trap depth from 400 μK to 1 mK atoms entering with an average velocity of 0.1 m/s are lost from the cavity after a energy gain of about 500 μK.

Chapter 6

Observation of cavity cooling

All conventional methods to cool atoms employing lasers rely on repeated cycles of optical pumping and spontaneous emission of a photon by the atom. Spontaneous emission in a random direction is the dissipative mechanism required to remove entropy from the atom. However, alternative cooling methods have been proposed for a single atom strongly coupled to a high-finesse cavity (Horak *et al.*, 1997; Vuletić and Chu, 2000). In these schemes the role of spontaneous emission is replaced by the escape of a photon from the cavity. Application of such cooling schemes would improve the performance of atom-cavity systems for quantum information processing (Kuhn *et al.*, 2002; Monroe, 2002). Furthermore, as cavity cooling does not rely on spontaneous emission, it can be applied to systems that cannot be laser-cooled by conventional methods. These include molecules (which lack closed transitions) and collective excitations of Bose condensates (Horak *et al.*, 2000), which are destroyed by randomly directed recoil kicks. Furthermore even cooling of an atom carrying a quantum bit was proposed (Griessner *et al.*, 2004).

In this chapter, cavity cooling of single rubidium atoms stored in an intracavity dipole trap is demonstrated (Maunz *et al.*, 2004). The cooling mechanism results in extended storage times and improved localisation of atoms. An estimate shows that the observed cooling rate is at least five times larger than the cooling rate which can be achieved by free-space cooling methods for comparable excitation of the atom.

6.1 Cavity cooling

The basic idea behind cavity cooling can be understood from a simple classical picture based on the notion of a refractive index. Consider a standing-wave optical cavity, resonantly excited by a weak probe laser, blue detuned from the atomic resonance. For strong atom-cavity coupling, even one atom can significantly influence the optical path length between the cavity mir-

rors. Consequently, the intracavity intensity is strongly affected by the atom (Mabuchi *et al.*, 1996; Münstermann *et al.*, 1999b; Sauer *et al.*, 2004). For example, at a node of the standing wave, the atom is not coupled to the cavity, thus the intracavity intensity is large. At an antinode of a blue-detuned light field, in contrast, an atom shifts the cavity to a higher resonance frequency because the atom's refractive index is smaller than unity above its resonance. This tunes the cavity out of resonance from the probe laser and leads to a strongly reduced intracavity intensity. However, in a high-finesse cavity the intensity cannot drop instantaneously when the atom moves away from a node. Instead, the blue shift of the cavity frequency leads to an increase of the energy stored in the field. The photons finally escaping from the cavity are therefore blue-shifted from the photons of the probe laser. This occurs at the expense of the atom's kinetic energy. The reverse effect, namely the acceleration of an atom approaching an antinode, is much smaller since the cavity is initially out of resonance with the probe laser and consequently the intracavity intensity is small.

Note that the cooling process does not rely on atomic excitation. Indeed, the atomic excitation is low at all times as the atom is not coupled to the light near a node while the intracavity intensity is very low for an atom near an antinode. It follows that the lowest attainable temperature is not limited by the atomic linewidth, as for free-space Doppler cooling, but by the linewidth of the cavity, which can be much smaller. Therefore temperatures below the Doppler limit are feasible (Hechenblaikner *et al.*, 1998). An upper limit on the velocity of the atom, for which the cooling force is proportional to the velocity, is given by the requirement that the atom must not move further than about one-quarter of a wavelength during the lifetime of a photon in the cavity. In our experiment, this corresponds to a velocity of about 3 m/s. We emphasise that cavity cooling is applied to a single two-level atom and differs from the mechanical effects observed for an atomic ensemble (Chan *et al.*, 2003; Nagorny *et al.*, 2003; Kruse *et al.*, 2003). A description of cavity cooling in terms of dressed-states pictures of the strongly coupled atom-cavity-trap system can be found in section 2.4.6.

A treatment of cavity cooling combined with trapping by means of an auxiliary far-red detuned dipole laser is quantitatively different from the situation without trapping laser. The dynamic Stark shift renders the atomic resonance frequency position dependent, making it larger for an atom at an antinode. This effect even enhances the cooling force by effectively increasing the refractive index variations for a moving atom. The combined system can be investigated numerically (van Enk *et al.*, 2001). Moreover, in the limit of low atomic excitation, analytic expressions for all relevant forces including the cooling force are derived in section 2.4. The expressions are lengthy but valuable for parameter optimisation and straightforward trajectory calculation.

6.2 The cooling force

As discussed in chapter 5.3, the average storage time of the atom in the dark intracavity trap is measured by switching off the probe light for an adjustable time interval, Δt, after the atom is captured. As a function of this dark time, Δt, the fraction of atoms still trapped drops exponentially with a decay constant of 18 ms, defining the storage time of the atoms in the trap. The theoretical limits imposed by light scattering (40 s) and cavity QED dipole fluctuations (250 ms) (Horak *et al.*, 1997) cannot explain this rather short time (Ye *et al.*, 1999; McKeever *et al.*, 2003). Instead, the observed loss of the atom is attributed to parametric heating, due to fluctuations of the intracavity intensity. These are mainly caused by frequency fluctuations of the dipole laser. This technical noise critically depends on the performance of the laser stabilisation. Indeed, the storage time in the dark dipole trap has been increased from 18 ms to 31 ms by improving the frequency stability of the dipole laser. As this stability and other sources of noise are hard to control, a concurrent measurement of the storage time of the dark dipole trap serves as a reference in each of the following experiments.

Parametric heating is proportional to the square of the trap frequency (Savard *et al.*, 1997). As the axial trap frequency is about 100 times larger than the radial trap frequency the atom is mainly heated in axial direction. Since axial and radial motion are only weakly coupled, the heated atom usually escapes the antinode of the standing wave dipole field along the axis, thereby hitting one of the mirrors. This conjecture is supported by numerical simulations of the experiment, as further discussed in section 3.2.

To demonstrate that cavity cooling can be used to compensate for the axial heating caused by the dipole trap, the probe beam is not switched off completely after capturing an atom. Instead, the probe power is strongly reduced. In figure 6.1 a single trapping event is shown. At 215 ms after launch, the observed transmission of the cavity drops below 9% of the empty cavity transmission and actuates atom detection. Upon detection of the atom in the cavity mode, the trap depth of the dipole trap is increased. At the same time, the incident probe power is reduced from 7.5 pW to 0.37 pW for 250 ms. The intracavity photon number is below 0.005 for about 217 ms. At this moment the atom leaves the trap and the intracavity photon number increases to about 0.05, the value expected without an atom for the incident probe power of 0.37 pW. For these parameters ($\Delta_c = 0$; $\Delta_a = 2\pi \times 35\,\mathrm{MHz}$; $n_e = 0.05$) the storage time is larger than in the case without any near-resonant light. At the same time, these detunings allow to continuously observe the presence and the escape of the atom in the trap. The possibility to determine the storage time of each atom reduces the measurement time needed to determine the average storage time compared to the case of the dark trap, where the probe light must be switched on to determine whether the atom is still present in the trap.

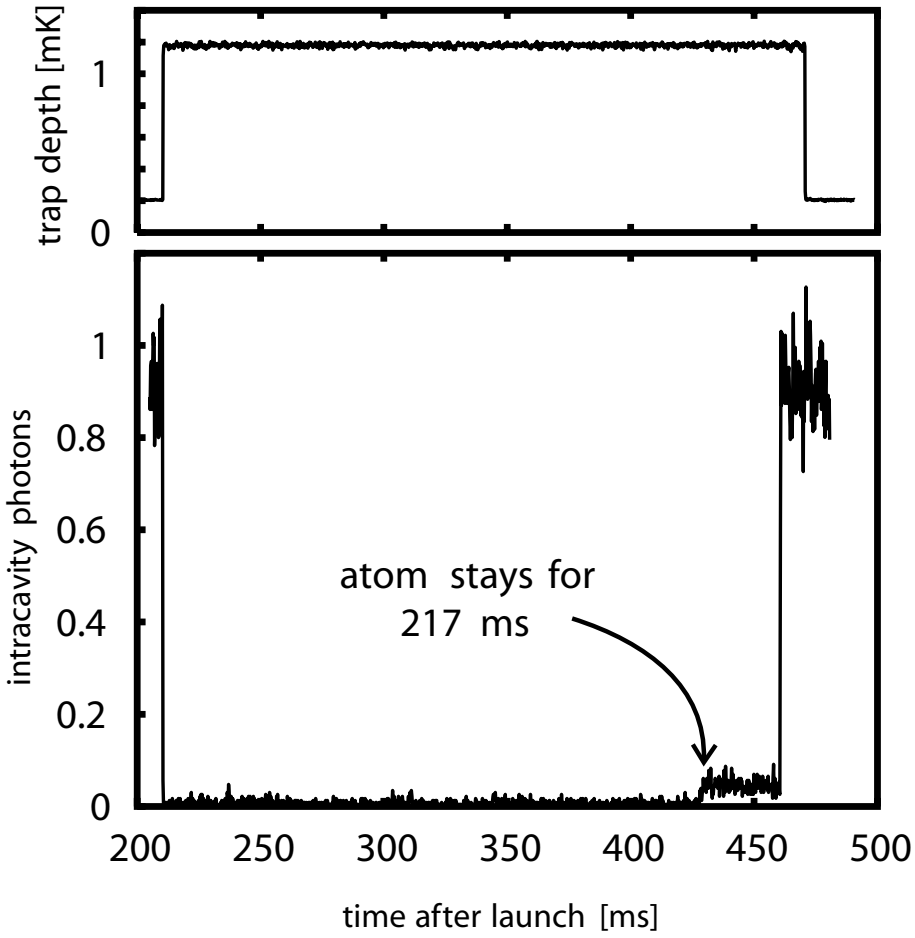

Figure 6.1: Experimental trace for cooling parameters. Upon detection of the atom by a drop of the cavity transmission below 9% of the empty cavity transmission, the trap depth of the far-detuned trap is increased from about 0.2 mK to about 1.2 mK to capture the atom in the trap. At the same time the incident probe power is switched from 7.5 pW (corresponding to approximatively one intracavity photon in the cavity without an atom) to 0.37 pW. 250 ms later, the incident probe power is switched back to the detection power of 7.5 pW. The probe light is on resonance with the empty cavity ($\Delta_c = 0$) and the detuning from the atomic resonance excluding the light shift is $\Delta_a = 2\pi \times 35$ MHz. Therefore the presence of an atom in the cavity leads to a strong reduction of the transmission. About 217 ms after capturing, the atom left the cavity as indicated by an increase of the transmission to the expected transmission without an atom.

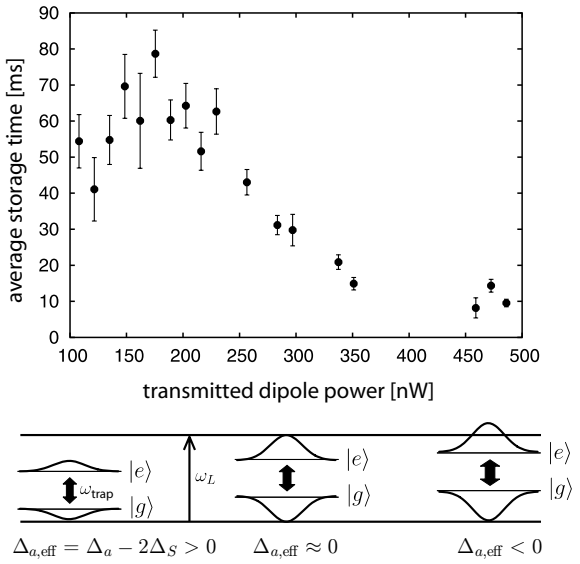

Figure 6.2: Storage time as a function of the trap depth (measured in the experiment as the transmitted dipole power). For the parameters $\Delta_c = 0$; $\Delta_a = 2\pi \times 35\,\text{MHz}$, the average storage time of an atom in the trap is determined as a function of the depth of the trap after capturing the atom. The trap depth before capturing the atom is kept fix for all measured data points and corresponds to a transmitted power of 80 nW. The three lower plots indicate the effect of the trapping laser on the atomic transition frequency. In the case $\Delta_{a,\text{eff}} = \Delta_a - 2\Delta_s > 0$ the probe laser is blue detuned for an atom at an antinode of the probe field, while in case of $\Delta_{a,\text{eff}} \approx 0$ the Stark shift tunes the atom in resonance with the probe laser and even tunes it across the resonance for the case of a deep trap ($\Delta_{a,\text{eff}} < 0$).

6.2.1 Trap depth dependence of the storage time

The depth of the trap influences the storage time through two major mechanisms. The difference between the trap depth just before and after capturing the atom determines the maximal energy an atom must gain in order to radially leave the trap. This effect favours an initially shallow trap which is strongly increased upon detection of an atom. Secondly, the Stark shift $2\Delta_S$ of the atomic resonance generated by the trap light effectively changes the detuning $\Delta_{a,\text{eff}} = \Delta_a - 2\Delta_S$ of the probe light to the atomic resonance. For a detuning of $\Delta_a = 2\pi \times 35\,\text{MHz}$, the effective detuning in the trap is positive (blue detuned) for a shallow trap. For larger trap depth the detuning is reduced and eventually becomes negative (red detuned). The velocity-dependent forces only cool the atom in the case of the blue-detuned probe light, while the atom is heated for a red-detuned light field. The storage time should therefore decrease again in the case of a deep trap.

Figure 6.2 shows the storage time as a function of the trap depth after capturing the atom. The trap depth prior to capturing is fixed at a trans-

mission of 80 nW in order to ensure equal start conditions. For a larger trap depth, the storage time increases and reaches a maximum of about 70 ms for a trap light transmission of about 180 nW. If the trap depth is further increased, the effective detuning for a maximally coupled atom changes from blue-detuned to red-detuned. Therefore the average storage time drops. For a transmission above 250 nW the storage time drops below the storage time of the dark trap.

We emphasise that in contrast to Doppler cooling, cavity cooling extends the storage time for a probe field which is blue detuned from the atom. If the detuning is changed from blue to red, by adjusting the atom-cavity detuning, while keeping the dipole power constant and the probe laser resonant with the cavity, the average storage time decreases and drops below the storage time of the dark trap. This clearly demonstrates that the extension of the storage time cannot be attributed to Doppler cooling.

6.2.2 Influence of the probe intensity on the storage time

To investigate the influence of the probe power on the storage time of an atom, the incident probe power is reduced to a fixed value after the atom is captured. Figure 6.3 shows the storage time as a function of the incident probe power, P_p. For large probe power, the storage time is shorter than in the dark trap. However, the storage time increases with decreasing power.

This effect is attributed to the reduction of spontaneous emission, which heats the atom in all directions and which cannot be compensated for in the radial direction, since cavity cooling acts mainly axially. As the atomic transition is still far from being saturated, the radial heating is proportional to the probe power, even for the highest considered level of $P_p = 7.5\,\mathrm{pW}$. Hence, as long as the probe power is large enough to compensate for axial heating, the storage time τ increases with decreasing probe power as $\tau \propto P_p^{-1}$ (solid line). For weak probe power, the storage time exceeds the result in the dark trap — a signature of cavity cooling which compensates for axial heating.

In the axial direction, parametric heating is antagonised by cavity cooling. However with increasing probe power, momentum diffusion generated by fluctuations of the dipole force introduces heating which is proportional to the probe power. If the probe power is sufficiently large for the probe-induced diffusion to dominate parametric heating, a further linear increase of probe power leads to a linear reduction of the timescale on which an atom is lost. This can be explained using the Fokker-Planck equation for the atomic probability distribution (Gardiner, 1985) and is discussed in more detail in sections 2.5.2 and 3.2.1. As a consequence, the axial loss mechanism also leads to $\tau \propto P_p^{-1}$.

In summary, the atom is expected to leave the cavity axially for vanishing probe power, while in case of larger power, radial losses dominate.

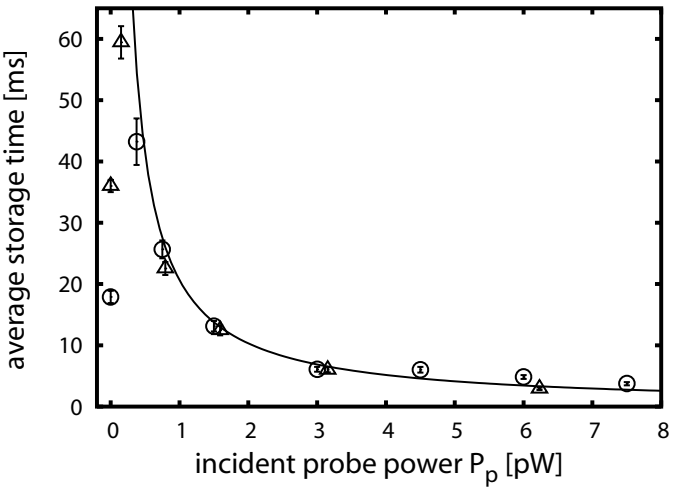

Figure 6.3: Storage time. The storage time of a trapped atom as a function of the incident probe power P_p. Two sets of data taken before (circles) and after (triangles) improving the laser stabilisation are shown. The corresponding storage times in the dark trap ($P_p = 0$) are 18 ms and 36 ms, respectively. For an incident probe power exceeding about 0.5 pW, the storage time is limited by radial escape due to spontaneous emission. In this range, the measured storage time (in ms) can be approximated by $20/P_p$ (where P_p is in units of pW; solid line). The storage time of 18 ms obtained for the dark trap increases by more than a factor of two by applying 0.37 pW of probe light. After the stabilisation of the dipole laser was improved, the storage time was increased from 36 ms to 60 ms at a probe power of $P_p = 0.11$ pW. The probe powers correspond to an average intracavity photon number of 0.005 and 0.0015 for 0.37 pW and 0.11 pW, respectively.

The interpretation given here is confirmed by a Monte Carlo simulation of a point-like atom moving in the trap under the influence of the forces and momentum diffusion calculated analytically. Parametric heating from the dipole trap is implemented in the simulation by a randomly changing potential depth (chapter 3). The storage times evaluated from the simulation agree well with the experiment (figure 3.3). Moreover, it can be concluded that for probe powers below 0.1 pW, more than 90% of the atoms leave the cavity mode by hitting a mirror, while for probe powers above 0.5 pW, 90% of the atoms leave radially.

6.3 Strength of the cooling force

In the following experiment cooling is demonstrated by directly observing the reduction of the kinetic energy of the atom. Furthermore, a direct measurement of the strength of the cooling force can be achieved. The experiment employs alternating heating and cooling intervals at a constant probe

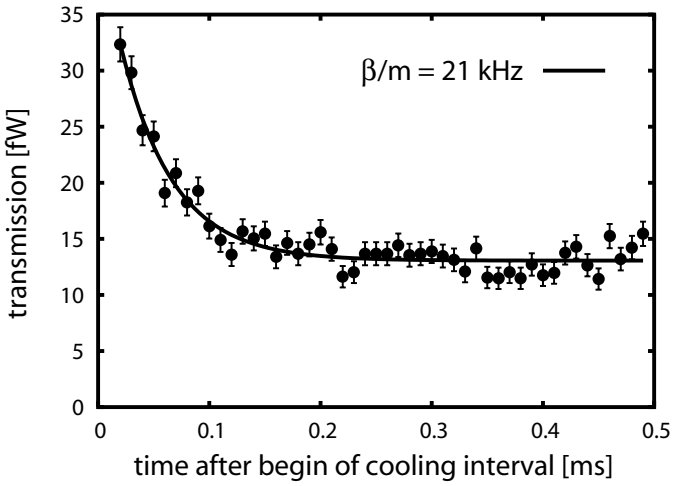

Figure 6.4: Average transmission during cooling intervals of length 0.5 ms after heating the atom for 0.1 ms (not shown). An incident power of $P_p = 2.25\,\mathrm{pW}$ is chosen for a good signal to noise ratio. Without an atom, the cavity transmission on resonance is 300 fW. The atoms are cooled during the first 0.1 ms. This leads to a stronger coupling to the cavity mode and, hence, to a smaller transmission. A cooling rate of $\beta/m = 21\,\mathrm{kHz}$ is estimated from an exponential fit. Radial heating occurs on a much longer timescale and is not visible here. The transmission of the trap light is 250 nW.

power of $P_p = 2.25\,\mathrm{pW}$. Axial heating is achieved by deliberately tuning the probe laser to a frequency of $2\pi \times 9\,\mathrm{MHz}$ above the cavity resonance ($\Delta_c = 2\pi \times 9\,\mathrm{MHz}$), where strong heating of the atom is expected from the theoretical analysis. This is done for a time interval of $100\,\mu\mathrm{s}$. In the following cooling interval of $500\,\mu\mathrm{s}$ duration, the probe laser is switched back to the cavity resonance ($\Delta_c = 0$). Figure 6.4 shows the cavity transmission averaged over many cooling intervals with an atom present in the cavity. The transmission drops by more than a factor of two during the first $100\,\mu\mathrm{s}$. This drop is a clear signature for the increasing atom-cavity coupling, and hence, a better localisation of the atom at the antinode of the probe field.

During the heating interval the motional state of the system is disturbed. The relaxation rate to the steady state at the beginning of the cooling intervals is directly given by the cooling rate. The exponential relaxation of the transmission allows to obtain an estimate of the mean cooling rate, $\beta/m = 21\,\mathrm{kHz}$, where β is the friction coefficient and m the atomic mass. This result is in good agreement with the Monte Carlo simulation, which also shows an exponential relaxation with about 20 kHz. In the simulation, both, the atomic localisation as well as the transmitted power show the same exponential dependence.

6.3.1 Comparison of cavity cooling with free-space cooling mechanisms

To compare the cavity cooling rate with free-space cooling rates of a two-level atom for a given rate of spontaneous emission events, knowledge about the atomic excitation is required. Here, an upper limit can be obtained by attributing the storage time of 9 ms (measured for a probe power of 2.25 pW; figure 6.3) solely to radial heating due to spontaneous emission. To leave the trap, an atom must have gained about 1 mK. This limits the atomic excitation to below 2.5%. At this excitation, free-space Sisyphus cooling (Aspect *et al.*, 1986; Dalibard and Cohen-Tannoudji, 1985) of a two-level atom in a blue-detuned standing wave with optimal detuning would achieve $\beta_S/m = 4\,\mathrm{kHz}$ while Doppler cooling would have $\beta_D/m = 1.5\,\mathrm{kHz}$ for optimal detuning. Thus introducing the cavity increases the cooling rate by at least a factor of 5 for constant atomic excitation.

The numerical simulations show that, on average, the atom spontaneously scatters one photon during the cooling time of 50 μs. This is a first step towards cooling without spontaneous emission. By improving the coupling of the atom to the cavity the atomic excitation and spontaneous emission can be reduced further.

6.4 Cooling down an atom in the trap

Cooling down an atom in the trap can also be demonstrated without additional heating intervals. For this purpose the atom is repeatedly left in the dark dipole trap without probe light for 2 ms time intervals. These intervals are short as compared to the average trapping time in the dark trap of 31 ms (with improved dipole laser). The atom always experiences parametric heating, also in the dark intervals. Between the dark intervals, 100 μs cooling intervals are applied using a probe beam with incident power $P_p = 1.5\,\mathrm{pW}$, on resonance with the cavity ($\Delta_c = 0$). The transmission of the probe light is also used to determine whether the atom is still present. An example of a single measurement trace is shown in figure 6.5. The total time an atom is stored in the dark trap under these conditions can be calculated by adding up all the 2 ms long dark intervals after which the atom is still found in the trap, but omitting the cooling intervals. The result is shown in figure 6.6: although the short cooling intervals have a duty cycle of only 5%, they increase the average trapping time by more than 50%. Obviously, heating the atom out of the trap requires more time in the presence of cooling. Therefore, the kinetic energy of the atom must have been reduced during the cooling interval.

In conclusion, strong coupling of a two-level atom to the cavity field was used to cool single atoms stored in an intracavity dipole trap. The storage time in the trap has been increased by a factor of two by exploiting the cool-

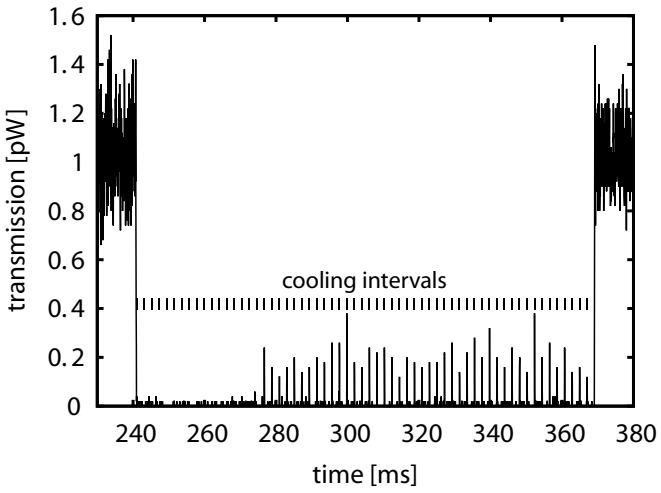

Figure 6.5: Measurement of cavity cooling. After capturing the atom in the trap, the near-resonant probe light is switched off. 100 μs cooling intervals with 1.5 pW of incident probe power are applied every 2.1 ms. The transmission during the cooling intervals is used to determine whether the atom is still stored in the trap. In this example, the atom is present in the first 16 cooling intervals corresponding to a storage time of 32 ms in the dark trap.

ing force generated by a near-resonant cavity field with an average photon number of only 0.005. In contrast to free-space laser cooling techniques, this cooling force acts mainly by exciting the cavity part of the coupled atom-cavity system. Thus strong cooling forces can be achieved while keeping the atomic excitation low. An estimate of the strength of the cooling force has shown to exceed the force expected for free-space Sisyphus cooling and Doppler cooling at comparable atomic excitation by at least a factor of 5 and 14, respectively. Avoidance of excitation could serve as a basis for cooling of molecules (Horak *et al.*, 1997; Vuletić and Chu, 2000) or collective excitations of a Bose condensate (Horak *et al.*, 2000). Another application might be to cool the motion of an atom with a stored quantum bit (Griessner *et al.*, 2004). If the two states forming the qubit have identical coupling to the cavity, the new cooling scheme would not disturb the superposition state. This advantage is not shared by any other cooling method.

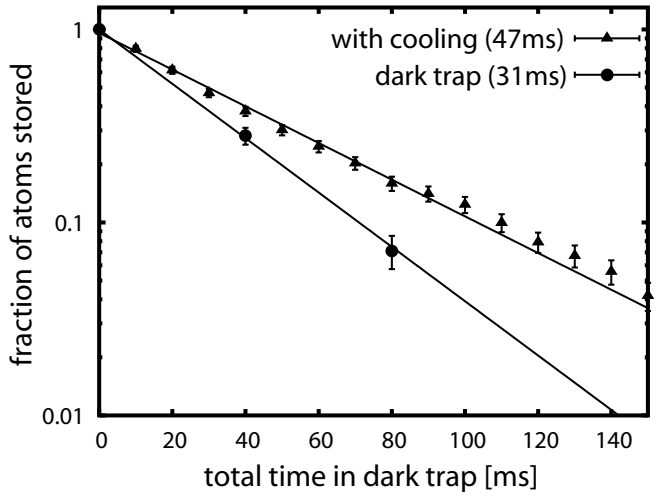

Figure 6.6: Cavity cooling. The fraction of atoms stored in the trap as a function of time after the dipole trap is switched on. The dark dipole trap has an average storage time of 31 ms (circles), as obtained from an exponential fit. If 100 μs long cooling intervals are applied every 2.1 ms, the average storage time without counting the cooling intervals is extended to 47 ms (triangles). The storage time in the dark trap varies slightly from day to day and is therefore measured concurrently with a few data points. Three data points (including the one at zero trapping time) are sufficient to obtain the storage time in the dark trap, because in several detailed measurements (figure 5.12) the remaining fraction of atoms found in the dark trap as a function of time was found to be very well described by an exponential decay.

Chapter 7

Normal-mode spectroscopy

Experimental research in quantum information science with atoms and ions (Monroe, 2002) is based on the ability to control individual particles in a truly deterministic manner. While spectacular advances have recently been achieved with trapped ions interacting via phonons (Riebe *et al.*, 2004; Barrett *et al.*, 2004), the precise control of the motion of neutral atoms exchanging photons inside an optical cavity (Münstermann *et al.*, 2000) or emitting single photons on demand (Kuhn *et al.*, 2002; McKeever *et al.*, 2004a) is still a challenge. Although very successful, experiments in cavity quantum electrodynamics with single laser-cooled atoms (Mabuchi *et al.*, 1996; Münstermann *et al.*, 1999b; Sauer *et al.*, 2004) are complicated by the motion of the atom in the standing-wave mode of the optical cavity (Pinkse *et al.*, 2000; Hood *et al.*, 2000). The lack of control over the atomic motion is mainly due to the heating effects of the various laser fields employed to trap and excite the atom inside the cavity in combination with the limited ability to cool the atom between two highly reflecting mirrors facing each other at a microscopic distance (Ye *et al.*, 1999; Fischer *et al.*, 2002). Only recently, good localisation of the atom at an antinode of the cavity mode has been achieved by applying optical molasses (McKeever *et al.*, 2003) or cavity cooling (chapter 6 and Maunz *et al.* (2004)) to a trapped atom.

The experiment described in this chapter goes one step further and employs cavity cooling to observe the distinctive normal-mode splitting of the energy spectrum of a single trapped atom, which is strongly coupled to a high-finesse resonator (Sanchez-Mondragon *et al.*, 1983; Agarwal, 1984). This experiment is the first in which the normal-mode (or vacuum-Rabi) splitting of an atom trapped at an antinode of the cavity field is observed. The results demonstrate that remarkably good control can be obtained over this fundamental quantum system.

Section 7.1 presents a short overview on previous experiments. The challenges which must be met in order to probe the strongly coupled system consisting of a single trapped atom and a single cavity mode, and the re-

sulting measurement sequence, are presented in section 7.2. In section 7.3, the measured transmission spectra are presented and compared with a numerical simulation. The storage time of the trap as a function of the probe frequency is analysed in section 7.4. The numerical simulations which are presented in section 7.5 can also be used to investigate the localisation and coupling of an atom. A short overview on the normal-mode theory and a comparison with the measured spectra is given in section 7.6.

7.1 History

The first experiments which investigated the normal-mode spectrum in the optical regime used atoms from a thermal beam passing through the cavity. Zhu *et al.* (1990) investigated the spectra for many atoms. Thompson *et al.* (1992) were able to measure the normal mode peaks for an average atom number of one. Childs *et al.* (1996) investigated the system by observing both, the transmission of the cavity and the light scattered from the atoms. The normal-mode spectrum was also measured using a cold atomic cloud transiting the cavity (Münstermann *et al.*, 2000). In each of these experiments, several atoms are required to realise an effective atom number of one and therefore these experiments were not in the single atom regime.

Hood *et al.* (1998) spectrally investigated single cold atoms transiting the cavity and observed a strong influence of radiative forces induced by probing. The localisation of a single atom in the cavity mode by means of an intracavity dipole trap and cooling now allows to measure a well-resolved normal-mode spectrum of a single atom strongly coupled to the cavity mode.

7.2 Measurement sequence

The storage time of a single atom in the far-detuned dipole trap without any near-resonant light is about 30 ms, as described in section 5.3. It is limited by axial parametric heating due to intensity fluctuations of the intracavity dipole trap. The dipole force of the probe light, which caused a shift and a distortion of the measured spectra in earlier experiments (Münstermann *et al.*, 2000; Hood *et al.*, 1998) can be neglected here because it is much weaker than the dipole force of the far-detuned light. However, depending on the relative frequencies of atomic transition, cavity resonance and probe laser, non-conservative forces can heat or cool the atom (Hechenblaikner *et al.*, 1998; Münstermann *et al.*, 1999b; Murr, 2003) mainly along the cavity axis. In order to measure the atom-cavity spectrum, it is necessary to probe the system at detunings for which these forces lead to strong heating. This quickly reduces the atomic localisation, and severely limits the available probe time by boiling the atom out of the trap.

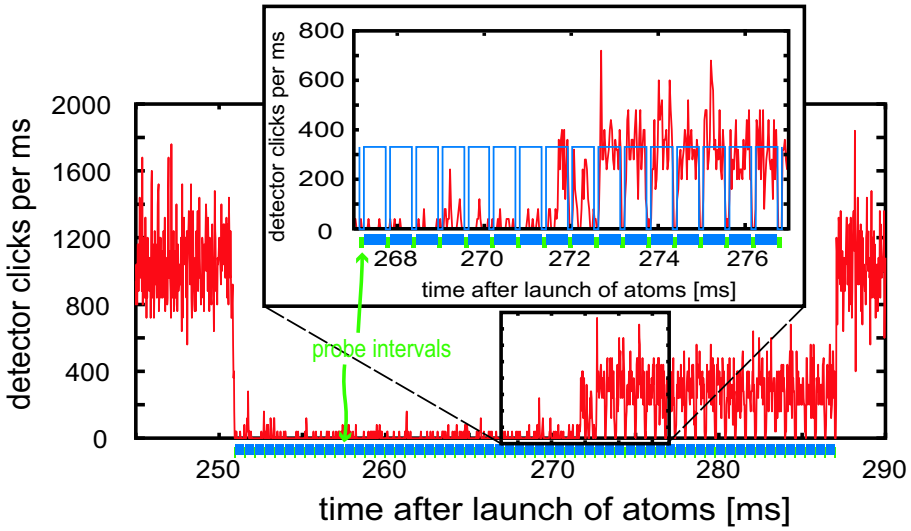

Figure 7.1: Example of an experimental trace. Upon detection of the atom 251 ms after the launch of the atomic cloud, the trap depth is increased and at the same time the alternating cooling and probing scheme is applied for 36 ms. The atom leaves the trap after 16 probe intervals about 272 ms after launch. The inset shows a zoom-in oo the trajectory. Here the expected transmission of the cavity without an atom during the cooling intervals is indicated by rectangles. During the last two cooling intervals, starting at 271.5 ms and 272 ms, the atom is only weakly coupled to the mode resulting in a larger cooling transmission. The transmission during the cooling intervals is used to qualify "strongly coupled" probe intervals.

To compensate the disastrous effect of heating, cooling intervals are applied to reestablish strong coupling of the atom to the cavity. This can be achieved by switching the probe laser to parameters for which the velocity-dependent forces lead to efficient cavity cooling (Maunz *et al.*, 2004). Of course, in the radial direction, the atom is heated by spontaneously scattering photons of the near-resonant probe light. Since there is no radial cooling mechanism, this heating mechanism contributes to the experimentally observed loss rate of atoms from the trap.

These considerations lead to the following protocol to perform the atom-cavity spectroscopy: After capturing the atom in the trap, a cooling interval of 500 μs duration is used to improve the localisation of the atom and to determine its coupling strength by pumping the cavity with a resonant probe laser ($\Delta_c = 0$). This is followed by a 100 μs probe interval, in which the frequency of the probe laser is changed to the desired detuning, Δ_c, which is kept fixed for all probe intervals applied for each atom. This sequence of cooling and probing intervals is then repeated. As long as the atom is stored in the trap, the transmission during the cooling intervals is low, while it is high if the atom has left (see figure 7.1). The end of the last cooling interval

in which the transmission is below 80% of the empty-cavity transmission, determines the exit time of the atom. The whole trapping scheme is repeated with many different atoms for different values of Δ_c. Within this sequence, each probe interval is enclosed by two cooling intervals in which the coupling strength before and after the probe interval can be determined independently of the probing. This allows to exclude probe intervals during which the atom is only weakly coupled to the cavity mode. The impact of this qualification scheme will be analysed in the next section.

7.2.1 Qualification of strongly coupled intervals

Weakly coupled atoms significantly modify the normal-mode spectra even if the atom is strongly coupled most of the time. This effect emerges since, for the parameters of this experiment, the transmission of the empty cavity is ten times larger than the transmission on the normal-mode resonances: The ratio between the transmission on resonance of the empty cavity and the normal-mode resonances of the atom-cavity system is determined by the ratio between the loss rate of the cavity excitation 2κ, and the loss of the atomic excitation 2γ. For weak saturation of the atomic transition, the probe transmittance is given by equation (2.42). In the regime of strong coupling ($g \gg \gamma, \kappa$), the ratio between the maximal transmittance of the cavity without an atom and the maximal transmittance on the normal-mode resonances of the coupled system is given by

$$\frac{T_{g=0}}{T_{g=g_0}} = \left(\frac{\kappa+\gamma}{\kappa}\right)^2 \overset{\text{this exp.}}{\approx} 10. \tag{7.1}$$

Hence, the contribution of weakly coupled intervals must be suppressed.

The effective detuning Δ_{eff} between the cavity resonance and the atomic resonance is modified by the Stark shift induced by the dipole trap. The Stark shift is proportional to the intensity of the trapping light field. Therefore the maximal Stark shift Δ_{S0} occurs at an antinode of the trapping field and the local shift shows the spatial dependence of its mode function $\phi_{\text{trap}}(\mathbf{r})$. The Stark shift is given by

$$\Delta_S(\mathbf{r}) = \Delta_{S0} \left|\phi_{\text{trap}}(\mathbf{r})\right|^2, \tag{7.2}$$

and the effective atom-cavity detuning at position $\mathbf{r}$ is

$$\Delta_{\text{eff}}(\mathbf{r}) = \Delta - 2\Delta_S(\mathbf{r}) = \omega_c - (\omega_a + 2\Delta_S(\mathbf{r})). \tag{7.3}$$

The coupling of the atomic transition to the probe field is proportional to the mode function of the probe field

$$g(\mathbf{r}) = g_0 \phi_p(\mathbf{r}). \tag{7.4}$$

In this system, the normal-mode spectrum for a point-like atom at a fixed position is not only a function of the local coupling $g(\mathbf{r})$, but also depends on $\Delta_S(\mathbf{r})$, since the energy of the dressed states depends on both, the local coupling and the effective detuning. This will be explained in more detail in section 7.6.

Figure 7.2 shows calculated transmission spectra for an atom fixed at various radial positions of the central antinode for which $\phi_{\mathrm{trap}}(\mathbf{r}) \approx \phi_p(\mathbf{r})$ ($\Delta = 2\pi \times 35\,\mathrm{MHz}$). Without an atom in the cavity, the transmission has

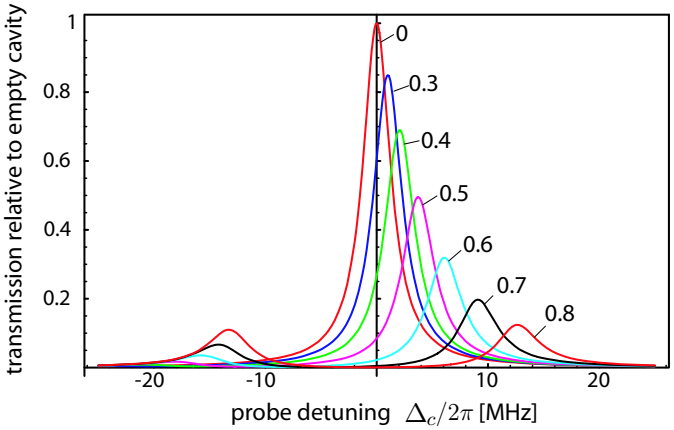

Figure 7.2: Calculated transmission of the cavity with a fixed atom experiencing various couplings to the probe and trapping fields $g = (0, 0.3, 0.4, 0.5, 0.6, 0.7, 0.8) \times g_0$ for the (red, blue, green, magenta, cyan, black, red) solid line, respectively. Without the light shift by the trapping field, cavity and atomic resonance are detuned by $\Delta = 2\pi \times 35\,\mathrm{MHz}$, the maximal Stark shift is $2\Delta_S = 43\,\mathrm{MHz}$.

a Lorentzian shape with a width of $2\pi \times 2.8\,\mathrm{MHz}$ (FWHM) centred around zero cavity detuning. If the atom is located at a large radial position, it experiences a small Stark shift. Therefore the cavity is still blue detuned ($\Delta_{\mathrm{eff}} > 0$) with respect to the atomic resonance. Since the coupling to the probe mode is also small, the transmission shows a high peak slightly shifted to positive detuning and a small peak at large negative detuning. While the radial distance of the atom from the cavity axis is reduced, the light shift increases. Therefore the effective detuning, Δ_{eff}, between cavity and atomic resonance drops. Additionally, the coupling to the probe mode increases, which further shifts the peaks to higher frequencies. The maximal transmission of the right peak drops whereas the transmission on the left peak increases.

In the evaluation of the experimental data, the two $500\,\mu\mathrm{s}$ cooling intervals which surround each probe interval allow to measure the coupling of the atom before and after each probe interval. Therefore it is possible to select the probe intervals for which the atom is with high probability strongly

coupled to the probe field.

The relative occurrence of cooling intervals with a certain average transmitted power is depicted in figure 7.3. This figure also shows the measured

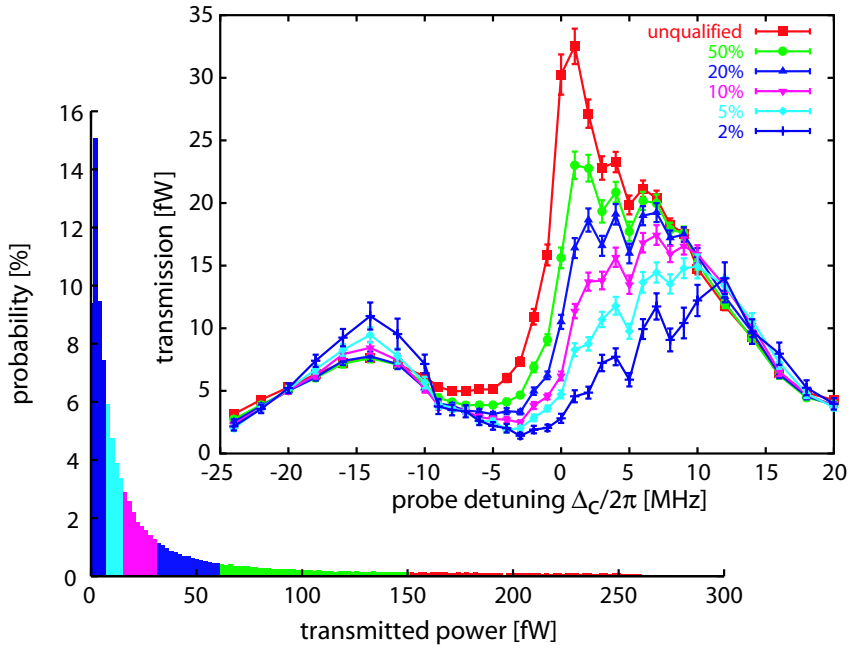

Figure 7.3: *Left:* Relative occurrence of measured average transmission during the cooling interval. The transmission of the empty cavity is 300 fW. For about 25% of the probe intervals the transmission is found to be below 2% = 6 fW. *Right:* Normal-mode spectra for different qualification of the probe intervals. The average transmission during all probe intervals for which both surrounding cooling intervals have a transmission below a certain threshold, is shown as a function of the probe detuning Δ_c. The peak near zero probe detuning is caused by the empty cavity transmission, which dominates the spectrum without qualification. It vanishes for the subensemble of the strongly coupled probe intervals.

transmission spectrum obtained from all probe intervals during which an atom was stored in the trap. A comparison with figure 7.2 shows that without qualification there is a significant contribution from intervals in which the atom is only weakly coupled to the cavity mode. If the transmission is only averaged over those probe intervals, where both surrounding cooling intervals have a transmission below 50% of the empty-cavity transmission, only few probe intervals are excluded. However, the additional peak near zero probe detuning is suppressed. If the average is further restricted, the peak provoked by intervals with weak coupling vanishes. Additionally, both normal-mode peaks are shifted to larger detunings, and the height of the left peak increases. These changes in the shape of the spectrum are in agreement with the elimination of contributions from atoms with weak coupling

as calculated in figure 7.2.

We find that for about 25% of the probe intervals in which an atom resides in the trap, both cooling intervals enclosing the probe interval have a transmission below 2% of the empty-cavity transmission. These probe intervals are defined as "strongly coupled" and are used for further analysis.

A comparison with numerical simulations of this measurement (see section 3.3.1) shows that exclusion by qualification occurs mainly in three different cases: First of all, atoms residing at a large radial distance from the cavity centre are excluded. Secondly, an atom trapped in one of the nodes where the coupling is low due to the displacement between the trapping and probe field antinodes, is excluded. Finally, atoms having a high axial temperature are excluded.

7.2.2 Influence of the probe power on the coupling

The analysis of the last section shows that the shape of the measured normal-mode spectrum depends critically on the localisation and axial temperature of the atom in the trap. Therefore it is important to investigate the influence of the incident probe power and the length of the probe intervals on the normal-mode spectrum. To this end, one spectrum measured using 2.25 pW incident probe power in 100 μs probe intervals is compared with a spectrum measured with 0.75 pW during 50 μs probe intervals (figure 7.4). The influence of probe induced forces should be six times less in the second spectrum. Without qualification, the empty cavity peak is much more prominent in the measurement with higher probe power as compared to the measurement using weaker probe power. This is a clear indication for stronger heating of the atom in the case of higher probe power. With qualification, the contribution of probe intervals with axially hot atoms is reduced, leading to equally well resolved normal-mode spectra. This comparison demonstrates that qualification of the strongly coupled probe intervals ensures a large coupling of the atom to the cavity mode and thereby strongly reduces the influence of heating on the spectra. Qualification also ensures that the coupling of the atom to the mode does not depend on the probe detuning. Therefore effects of near resonant forces on the shape of the spectrum are strongly reduced.

7.2.3 Localisation of an atom by cavity cooling

As described in section 6.3, the localisation of an atom in the trap can be improved by switching to parameters which allow efficient cooling. Figure 7.5 shows the average transmission of all cooling intervals as a function of the probe detuning during the preceding probe interval and the time after the beginning of the cooling interval. A high transmission corresponds to a poorly localised atom, while a low transmission indicates that the atom is tightly localised at an antinode of the probe field. Note that the (cool-

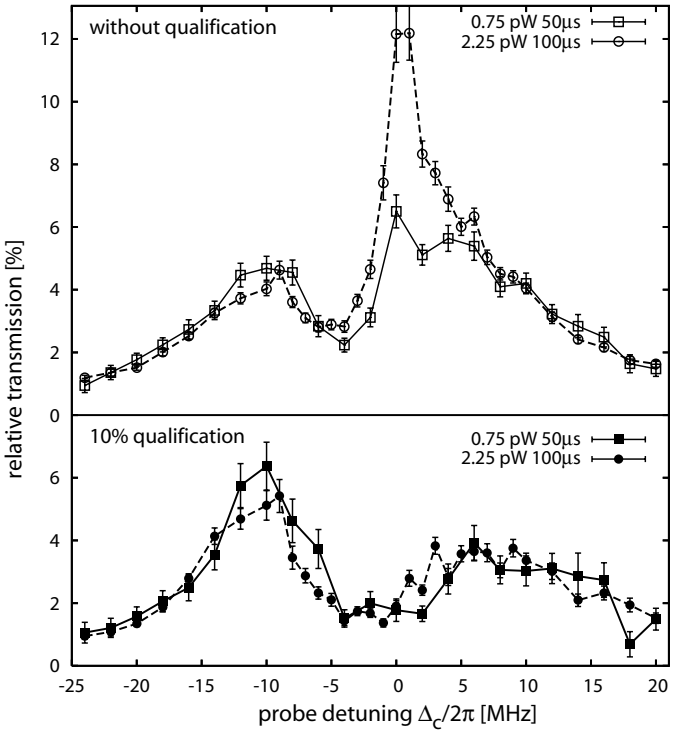

Figure 7.4: Measured transmission spectra for different powers of the incident probe laser. *Top* Without qualification. *Bottom:* Average transmission if both surrounding cooling intervals have a transmission below 5% of the empty cavity transmission. Without qualification, the heating effect due to probing is clearly visible as the additional empty cavity peak dominates the spectrum. If the weakly coupled intervals are eliminated, no significant difference of the spectra is observed.

ing) parameters are identical for all columns of figure 7.5, variations in the transmission are solely provoked by different atomic motion due to different probe detunings. The atomic motion at the start of the cooling interval is determined by the parameters during probing. If one of the normal modes of the system is excited, which is the case for probe detunings of about $\Delta_c = 2\pi \times -15\,\mathrm{MHz}$ and $\Delta_c = 2\pi \times 10\,\mathrm{MHz}$, the transmission at the start of the cooling interval is large and drops during the cooling interval. This shows that the atom is axially hot after the probe interval and its localisation is improved during the cooling interval. For zero and large detunings ($|\Delta_c| > 2\pi \times 16\,\mathrm{MHz}$) the transmission is low during the entire cooling interval, indicating that the atom is not heated significantly during probing. At the end of the cooling interval, the transmission and therefore the atomic localisation does not depend on the probe detuning. Therefore the atoms are well prepared for the next probe interval.

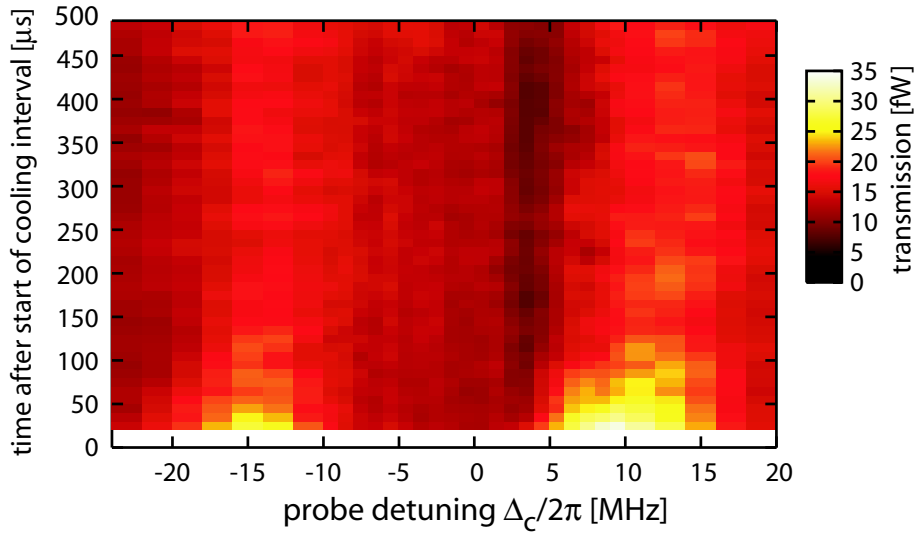

Figure 7.5: Improvement of atomic localisation during cooling intervals. Average transmission of all cooling intervals with an average transmission below 20% of the empty cavity transmission as a function of the probe detuning Δ_c during the preceding probe interval and the time after the beginning of the cooling interval.

7.3 Spectra of cavity transmission

The average cavity transmission during the strongly-coupled probe intervals as a function of the probe detuning is depicted in figure 7.6. The four spectra are obtained for different atom-cavity detunings and all show two well-resolved normal modes. Together, they display the avoided crossing between the atomic and the cavity resonance (Meystre and Sargent, 1999). The atom-cavity detuning is adjusted by tuning the atomic resonance via the dynamic Stark effect induced by the far-detuned trap light. The induced (position-dependent) shift, $\Delta_S(\mathbf{r})$, of the atomic resonance frequency is proportional to the trap depth. For a transmitted power of the trap light of about 280 nW, the dynamic Stark shift compensates the initial atom-cavity detuning of $2\pi \times 35$ MHz. The eigenstates of the atom-cavity system (dressed states) are superpositions of the atomic ground state with a cavity photon on the one hand and the atomic excited state without a cavity photon on the other hand. Since the probe laser only excites the cavity mode, the excitation of a dressed state is proportional to the contribution of the cavity state to the dressed state, which depends on the atom-cavity detuning. This explains why the height of the left normal-mode peak increases with increasing Stark shift, while that of the right peak decreases. For zero detuning between atom and cavity (about $P = 280$ nW), the contributions from the atomic and the cavity state are equal, so that the normal modes have the

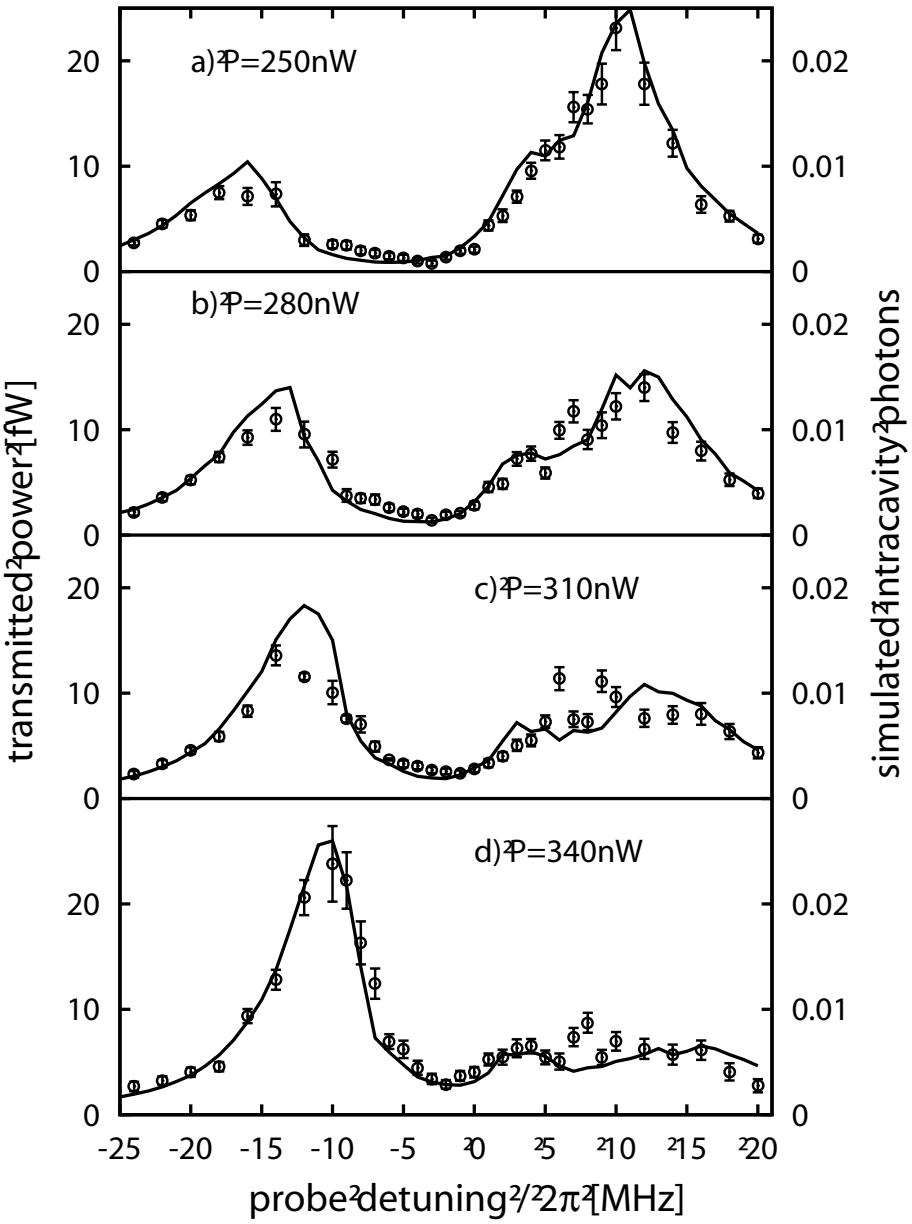

Figure 7.6: Average transmission of the atom-cavity system (circles). The four spectra are obtained for different depth of the trap, corresponding to a transmission of trap light between $P = 250\,\mathrm{nW}$ and $P = 340\,\mathrm{nW}$. The incident probe power is $P_p = 2.25\,\mathrm{pW}$ and the initial atom-cavity detuning without the light shift is $\Delta_a = 2\pi \times 35\,\mathrm{MHz}$. On average each point includes the data from about 350 probe intervals collected from between 35 and 1000 atoms. The solid line shows the results of a Monte Carlo simulation.

same height and reach a minimum splitting of $2g$. Here, the observed splitting of about $2 \times 2\pi \times 12\,\mathrm{MHz}$ is only slightly smaller than the maximal possible splitting of $2 \times 2\pi \times 16\,\mathrm{MHz}$, which is expected for a point-like atom at rest at an antinode. This proves that the atom is localised in the regime of strong coupling with $g \gg (\gamma, \kappa)$.

For a stationary atom, the widths of the two normal modes are given by a weighted mean of the atomic and cavity linewidth. Since the atom is not fixed at an antinode of the probe field, but oscillates in the trap, the atom-cavity coupling is time dependent. This leads to fluctuating eigenfrequencies of the normal modes and therefore to a broadening of the measured spectra.

The different widths of the normal modes of the spectra in figure 7.6 can be explained by taking into account the position-dependent Stark shift: An atom closer to an antinode of the trapping field experiences a larger Stark shift, which shifts both normal modes to larger probe detunings. Near the centre of the cavity, where the antinodes of both light fields overlap, this atom is also closer to an antinode of the probe field. Therefore its coupling to the cavity is also larger. This increases the splitting of the normal modes. Consequently, the frequency of the left normal mode is only weakly dependent on the atomic position while the two effects add up for the right normal mode. Therefore the motion of the atom broadens the right peak to a greater extent than the left.

The exact widths and line shapes of the measured normal modes are influenced by the details of the atomic motion in the trap. Cavity heating and cooling strongly depend on the atomic position and the frequency of the probe laser. These forces determine the atomic motion in a complex way. In order to obtain more information on the atomic motion, we compare the measured spectra with the results of a Monte Carlo simulation described in chapter 3. Results are shown in figure 7.6 and agree well with the experimental data if the power of the trapping field is reduced by 30% with respect to the intracavity power determined from the cavity transmission in the experiment. This could be explained by different transmissions of the two cavity mirrors, which lead to an error in the calibration of the intracavity light intensity. For consistency, the probe light power in the simulation is reduced by the same amount.

7.4 Spectra of observed storage time

Further characterisation of the normal modes can be obtained by investigating the average storage time of the atom in the trap as a function of the detuning during the probe intervals. While the atom is probed, additional heating can lead to a loss of the atom from the trap. The excess loss rate, defined as the surplus loss rate induced by probing the system, is shown in figure 7.7. These spectra also show two well-resolved peaks at detunings for

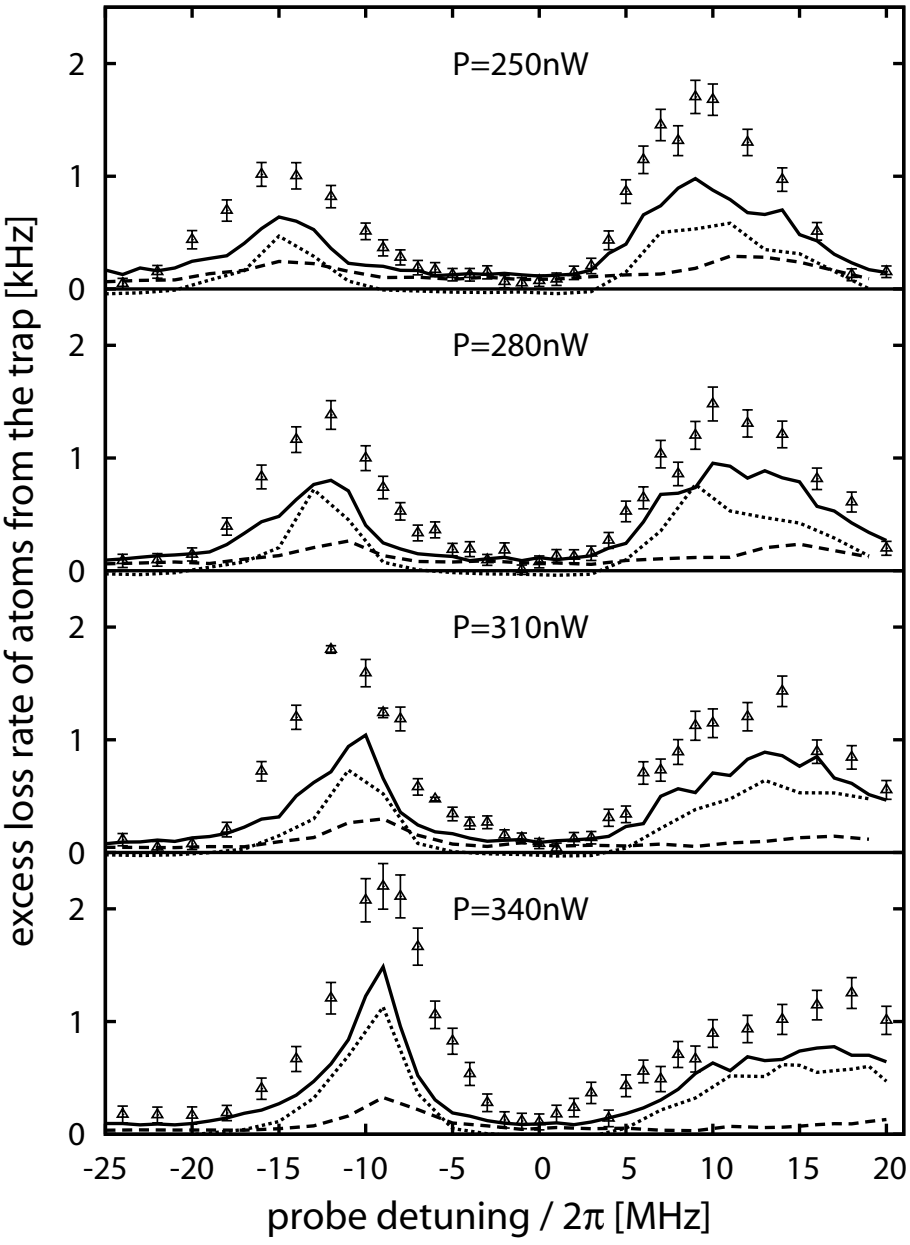

Figure 7.7: Observed excess loss rate of atoms from the trap as a function of the probe detuning (triangles). On average each point includes the data from between 35 and 1000 atoms. The lines show results of the Monte Carlo simulation including spontaneous emission only (dashed lines), diffusion due to dipole fluctuations only (dotted lines) and all diffusion mechanisms (solid lines).

which the excitation of the system is large. The experimentally observed excess loss rate is in qualitative agreement with the excess loss rate found in the Monte Carlo simulation. In figure 7.7 simulated loss spectra considering only heating from spontaneous emission are compared with simulations taking in account fluctuations of the dipole force only and a simulation including both diffusion mechanisms. The results show that for zero and large probe detunings, spontaneous emission accounts for about three quarters of the loss rate. If the probe light is resonant with one of the normal modes, momentum diffusion induced by the probe light dominates and causes more than four fifths of the loss rate. For the parameters of our experiment, the momentum diffusion introduced by the presence of the cavity is about 70 times larger than in free space for the same intensity of a standing wave light field (Hechenblaikner *et al.*, 1998; Murr, 2003). This remarkably large enhancement makes the normal modes clearly visible in the excess loss rate.

7.5 Atomic localisation

The Monte Carlo simulation presented in detail in chapter 3 accurately describes the observed transmission. The simulations can therefore be used to further analyse the localisation and coupling of an atom to the cavity mode. Figure 7.8 shows the axial distribution of atomic positions during the probe interval. Without qualification, the distribution has a width (FWHM) of $\lambda/7$. By qualification of the "strongly coupled" probe intervals, the width is reduced to $\lambda/10$. Qualification particularly removes probe intervals in which the atom has a distance of more than $\lambda/10$ from the trap centre.

For future experiments, the average coupling achieved during the probe intervals is important. Figure 7.9 shows the probability distribution of the coupling of the atom to the cavity mode. Inclusion of all probe intervals results in an average coupling of $2\pi \times 11\,\mathrm{MHz}$. If the evaluation is restricted to "strongly coupled" probe intervals the average coupling is increased and an average coupling of $2\pi \times 13\,\mathrm{MHz}$ is achieved. This agrees well with the experimentally achieved coupling of $2\pi \times 12\,\mathrm{MHz}$ extracted from the normal-mode spectra. Selection of those probe intervals for which the encompassing cooling intervals show a transmission below 2% of the empty cavity value effectively eliminates probe intervals with coupling below 6 MHz.

7.6 Avoided crossing

The closed system composed of a single atom and a single mode of the light field was first described by Jaynes and Cummings (1963) and can be solved analytically. The two eigenstates $|+\rangle$ and $|-\rangle$ of the first excited doublet of the combined atom-cavity system are superpositions of the atomic ground-state with one intracavity photon $|g, 1\rangle$ and the atomic excited state with

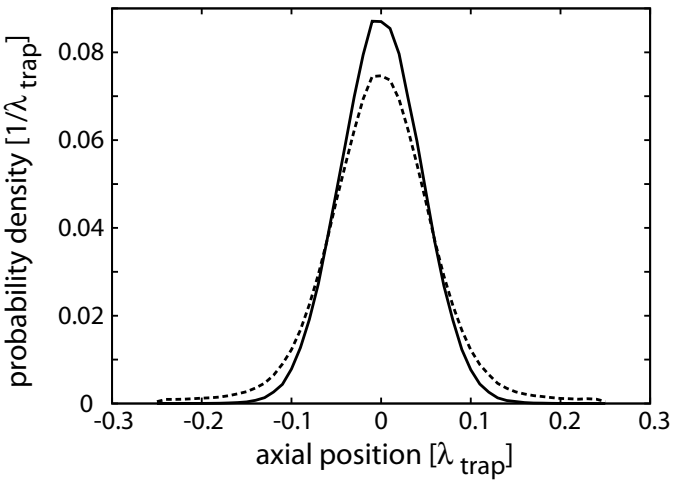

Figure 7.8: Axial localisation of an atom: Simulated probability to find an atom as a function of the axial position relative to the standing wave trap. The dashed line is obtained if all probe intervals are included. In this case the distribution has a width (FWHM) of $\lambda/7$. By selecting the "strongly coupled" probe intervals a width of $\lambda/10$ is achieved (solid line). Qualification particularly eliminates intervals during which the distance of the atom from the trap centre is larger than 0.1λ.

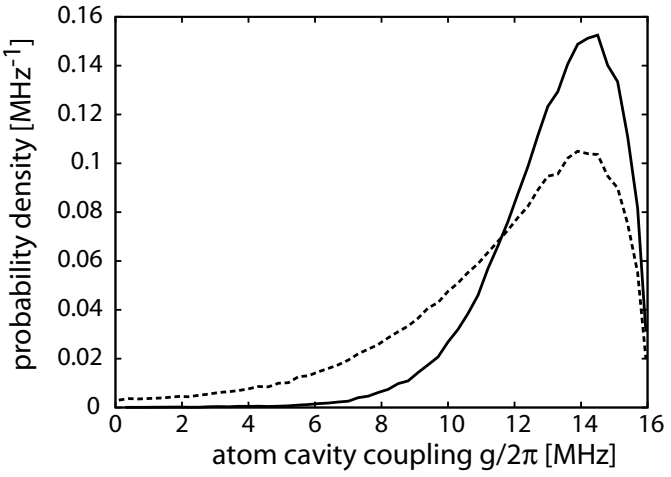

Figure 7.9: Simulated probability distribution of atomic coupling during the probe intervals. Without qualification, an average coupling of 11 MHz is reached. Selection of the strongly coupled probe intervals for which the encompassing cooling intervals show a transmission below 2% of the empty cavity value, effectively eliminates probe intervals with coupling below 6 MHz. The average coupling in this case is 13 MHz.

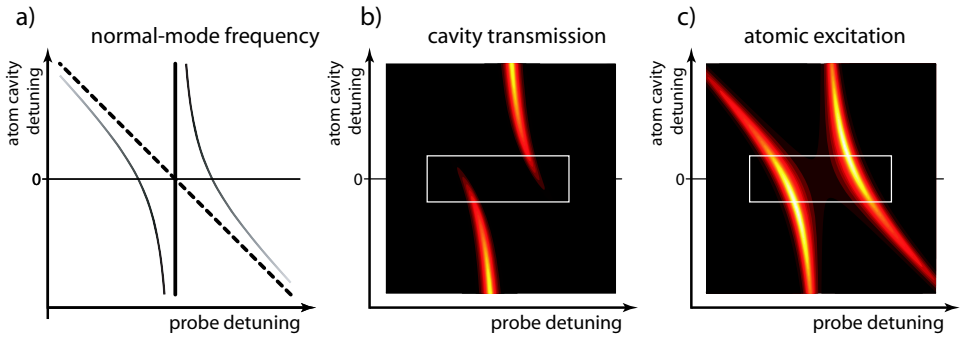

Figure 7.10: Normal modes as a function of trap depth and probe detuning. a) The coupling of atomic state (dashed line) and cavity state (solid line) generates new eigenstates which are superpositions of atomic and cavity state (red-blue lines). For vanishing detuning between atom and cavity the dressed states reach the minimal separation of $2g$. b) Cavity transmission as a function of probe detuning and atom-cavity detuning. c) Atomic excitation as a function of probe detuning and atom-cavity detuning. The different behaviour of the excitation with respect to the transmission is due to the fact that only the cavity part of the dressed state is pumped. In each of the plots the frequency range covered by the measurements is indicated by the white box.

zero photons $|e, 0\rangle$:

$$|+\rangle = \sin\theta|g, 1\rangle + \cos\theta|e, 0\rangle \tag{7.5}$$
$$|-\rangle = \cos\theta|g, 1\rangle - \sin\theta|e, 0\rangle. \tag{7.6}$$

They are also called "dressed states". The mixing angle $\theta = \frac{1}{2}\arctan(-2g/\Delta)$ depends on the detuning Δ between cavity and atomic resonance.

The open quantum system is subject to loss of photons from the cavity and spontaneously emitted photons from the atom and can be solved analytically in the limit of weak atomic excitation (Hechenblaikner *et al.*, 1998). To replenish lost photons, the system must be pumped by an incident light field. Since, in our case, only the cavity mode is excited by the impinging laser, the excitation of the dressed state is proportional to the contribution of the cavity state and the power of the impinging laser.

Figure 7.10 b) shows the calculated cavity transmission as a function of probe detuning and atom-cavity detuning. The transmission of the cavity is proportional to the number of photons in the cavity. Therefore the height of the two normal modes in the transmission spectrum is proportional to $\sin^2\theta$ and $\cos^2\theta$, respectively. For zero detuning of atom and cavity, the mixing angle is $\pi/4$ and the transmission at both normal-mode frequencies is equal. In this case, the distance between the two normal-mode frequencies reaches its minimum value of $2g$.

These effects are also visible in the measurement. In figure 7.11, the

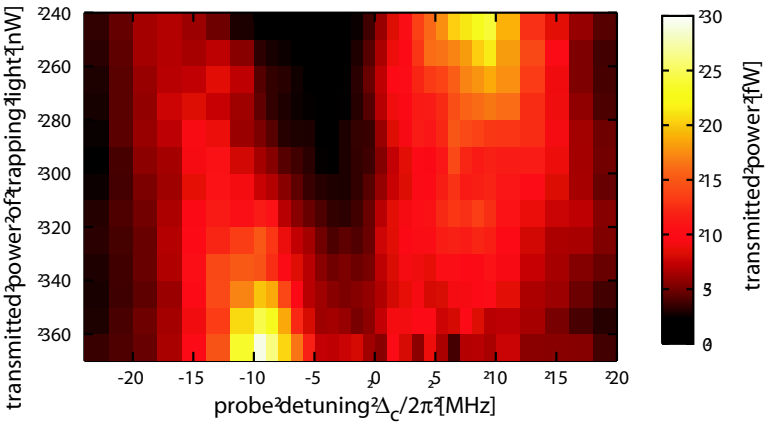

Figure 7.11: Cavity transmission as a function of trap depth and probe detuning. Tuning the trap depth changes the Stark shift induced by the trapping field and results in a change of the atom cavity detuning. The two normal modes are clearly visible in the transmission. They show the expected dependence on the atom cavity detuning which is proportional to the trap depth. The Stark shift which is not fixed but varies with the atomic position leads to a broadening of the right normal mode as described in the text in section 7.3.

transmission is plotted as a function of the probe detuning and the measured transmission of the trap laser. The data shown here is also included in figure 7.6. The avoided crossing and the strong dependence of the transmission on the atom-cavity detuning are clearly visible.

In contrast to the transmission, the calculated atomic excitation spectrum (figure 7.10 c)) shows a different dependency of the peak height on the mixing angle. As here again the cavity is excited while now the atomic excitation is observed, the height of both normal modes is proportional to $\sin\theta\cos\theta$ and hence only exhibits a weak dependency on the atom-cavity detuning. As a first approximation, one would expect the height of both normal modes to be equal for any given atom-cavity detuning. This symmetry is lifted due to the fact that the atomic decay rate γ, and the cavity decay rate κ, differ.

The atomic excitation cannot be measured directly in the experiment. The loss rate from the trap which is shown in figure 7.12 is dominated by heating generated by fluctuations of the dipole force. Nonetheless the large enhancement of dipole heating on the normal-modes resonances makes the normal modes clearly visible in the excess loss rate.

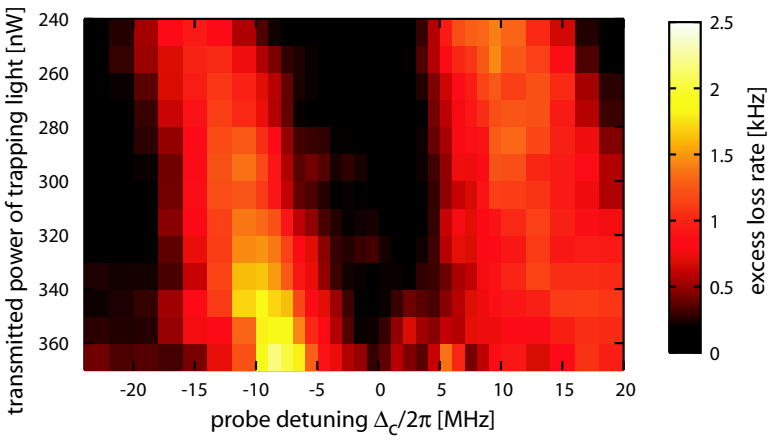

Figure 7.12: Observed excess loss rate from the trap as a function of trap depth and probe detuning. Tuning the trap depth changes the Stark shift induced by the trapping field and results in a change of the atom cavity detuning. The two normal modes are clearly visible. As expected from the theory and in contrast to the normal modes seen in the cavity transmission, the height of the normal modes measured via the trap loss rate only changes slightly as a function of the atom cavity detuning. The broadening of the right normal-mode resonance due to the spatial variation of the Stark shift is also visible.

Chapter 8

Conclusion & outlook

At the end of this thesis I would like to give a more general view on the advancements achieved by the experiments of this work in section 8.1. Section 8.2 discusses the possibility to improve the control of the atomic motion with the current apparatus. Section 8.3 will shortly review advances in the design and manufacturing of microcavities which could be used to achieve strong coupling between an atom and a mode of the light field. In section 8.4 some interesting and feasible proposals for the investigation of the matter light interaction and other cavity-QED effects are presented. Finally section 8.5 gives a short overview on the multitude of ideas to apply the atom-cavity system in quantum information science.

8.1 Conclusion

Within the scope of this thesis, an intracavity dipole trap was implemented, which facilitates the control of the motion of a single atom within the mode of a high-finesse cavity. Compared to previously implemented near-resonant traps, which suffered from a diffusive motion of the atom, the storage time could be dramatically extended. The long storage time and the oscillatory motion of the atom in the conservative trap allowed to observe the radial and axial oscillations of an individual atom in real-time.

The most spectacular result of this work is the first observation of cavity cooling of a single atom. The observed cooling force allows to substantially extend the storage time of an atom in the trap. Furthermore, this cooling mechanism does not rely on spontaneous scattering of photons from the atom and allows in principle to laser cool other particles like molecules which do not have a closed transition or even an atom carrying a quantum bit. In this experiment it was demonstrated that the observed cooling force is at least five times stronger than the cooling force achievable for free-space laser cooling mechanisms for comparable excitation of a two-level atom.

Cavity cooling was applied in this thesis to measure the first well resolved

normal-mode spectrum of a single atom strongly coupled to the cavity mode. This measurement proves that strong coupling of an atom to the cavity mode is reliably achieved and demonstrates the distinctive control on the atomic motion.

The control of the motion of a single atom in a high-finesse cavity which was established by these experiments can serve as a basis for future experiments in cavity-QED, to investigate open quantum systems and for applications in quantum information science. Some possibilities for further improvements of the apparatus and proposed measurements are discussed in the remaining sections of this chapter.

8.2 Possible experimental improvements

The storage time in the dark trap is currently limited due to parametric heating from technical intensity fluctuations of the intracavity dipole trap. This heating mechanism could be reduced by further improving the stabilisation of the laser. A reduction of the noise power density at the harmonics of the trap frequencies by about 10 dB should allow to extend the storage time in the dark trap by a factor of ten without reaching the limit imposed by intrinsic fluctuations of the intracavity dipole trap. Even longer storage times seem possible by using a trapping laser which is detuned by about 50 nm. In this case the mirror transmission is larger, leading to a larger cavity linewidth and thus to lower intracavity intensity fluctuations. Furthermore, for increased mirror transmission, the atom is not strongly coupled to the cavity mode and hence the intrinsic heating mechanisms can be reduced by up to a factor of 200. The use of a "magic wavelength" for the trap, which is available for other atomic species, also allows to reach longer storage times (McKeever *et al.*, 2003, 2004b) and in addiation renders the atomic transition frequency independent of the position of the atom in the trap.

Cavity cooling allows to cool the axial motion of an atom in the trap. However, the lack of a radial cooling mechanism leads to radial loss of the atoms from the trap. Introducing a radial cooling mechanism could therefore be used to further enhance the storage time of an atom in the trap. Radial cooling could be achieved employing Doppler cooling or polarisation gradient cooling using two counter propagating beams orthogonal to the cavity axis. Another possibility is to use the information on the radial motion of the atom, which is provided by the transmitted light used for axial cooling, to realise feedback cooling of the radial motion. In the case of near resonant light the storage time of an atom could be increased by feedback (Fischer *et al.*, 2002), however feedback cooling was not demonstrated. The oscillatory motion of an atom in the far-detuned trap, which is more conservative than that in the near-resonant trap, and the demonstration of the

direct observation of the motion of and individual atom presented in this thesis makes this idea feasible.

The high-finesse cavity used in the current set-up could be improved by using coned mirrors. This would provide better optical access to the cavity mode in the plane perpendicular to the cavity axis, a prerequisite for the above mentioned transversal cooling possibilities. Furthermore, coned mirrors permit to reduce the cavity length and thereby increase the coupling of an atom to the cavity mode. Reducing the cavity length will reduce the critical photon number $n_0 = \frac{\gamma^2}{2g^2}$, however it will not reduce the critical atom number $N_0 = \frac{2\gamma\kappa}{g^2}$. Nevertheless more information on the quantum dynamics in the cavity revealed in this case by the increased cavity decay rate κ. Further reductions of the critical atom and photon numbers are possible using other types of microcavities discussed next.

8.3 Alternative microcavities

In addition to Fabry-Perot type cavities, there are other types of cavities which allow to insulate a single light mode from the environment. An overview on optical microcavities can be found in Vahala (2003). For instance in small fused silica microspheres, whispering gallery modes exist which are confined by total internal reflection. These allow to achieve a small mode volume and a high quality factor. However, in this system atoms can only be coupled to the evanescent field outside the microsphere and while the coupling of a dilute atomic vapour to the evanescent field was observed by Vernooy *et al.* (1998), localising a single atom near the surface of the microsphere is still a challenge. Promising candidates for the realisation of strong coupling are toroidal microcavities as realised by Spillane *et al.* (2005). In this system the realisation of a cavity with $(g, \kappa) = 2\pi \times (86, 1.3)\,\mathrm{MHz}$ is projected. The whispering gallery modes of these resonators are excited and probed using tapered optical fibres. These allow to tune the cavity decay rate, κ, by adjusting the separation of the fibre. Therefore the coupling of the system to the environment and thus the information which can be collected from the system can be adjusted. Lev *et al.* (2004) propose to couple an atom to photonic bandgap cavities (PBC). These should allow to achieve an extremely low mode volume and therefore a very high coupling. However, it is extremely challenging to also achieve a high resonator quality with PBCs.

8.4 Cavity quantum electrodynamics

The possibility to reliably localise an atom strongly coupled to the cavity mode, as demonstrated in this thesis, opens up new possibilities for measurements of cavity-QED effects: Conditional phase shifts measured using

an atomic beam (Turchette *et al.*, 1995) could be investigated in the true single atom regime. Third order correlations of the transmitted light field (Foster *et al.*, 2000) can be used to measure the relaxation of the intracavity light field, conditioned on the detection of a transmitted photon. These experiments can be used to observe the conditional time evolution in open quantum systems and are up to now not observed using a single atom. Reiner *et al.* (2003) proposed an experiment to directly observe the quantum jumps between the dressed states of the atom-cavity system. The localisation of an atom could also allow to perform non-linear spectroscopy on the combined atom-cavity system as described in Syassen (2003).

In current experiments investigating the motion of a single atom in the cavity the atom can be described by a point-like particle. If one succeeds to cool an atom in the cavity near the ground state of a trap, the size of the atomic wavepacket increases and can become comparable to the wavelength of the probe light. Vernooy and Kimble (1997) first studied the motion of an atomic wavepacket in the cavity field. Recently Leach and Rice (2004) theoretically investigated the autocorrelation function of the transmitted light including the quantisation of the centre of mass motion of the atom. They found that having a significant population outside the ground vibronic energy level prevents sub-Poissonian statistics and photon antibunching which is found for an atom in the ground state of the trap.

8.5 Quantum information processing

Investigation of applications of the strongly-coupled atom-cavity system for quantum information processing is a very interesting field of research. While spectacular advances have recently been achieved with trapped ions interacting via phonons (Riebe *et al.*, 2004; Barrett *et al.*, 2004; Chiaverini *et al.*, 2004), the realisation of quantum information processing schemes using the atom-cavity system is still a challenge. The advances on the control of the motion of an atom in the cavity achieved within the scope of this thesis and by Boca *et al.* (2004) should make some proposals experimentally feasible. An overview on quantum information processing schemes can be found in Monroe (2002). Different categories of proposals are discussed in the following four paragraphs. Some schemes use Raman-transitions and therefore require the atom to be near the motional ground state of the trapping potential. Cooling an atom to the ground state of the potential within an optical cavity currently cannot be realised. However in most schemes the Raman-transitions can be replaced by adiabatic passages and therefore could be realised with “hot” trapped atoms (Duan *et al.*, 2003).

8.5.1 Controllable single-photon and entangled-photon source

A single photon source allowing full control on all its properties, including spatial emission mode, emission time and pulse shape has important applications in quantum-information processing schemes (Knill *et al.*, 2001). These schemes are based on the interference of different single photon pulses. In order to interfere, the photon pulses must all have the same spatial and temporal mode. The generation of single photon pulses in a single spatial mode on demand employing an atom-cavity system was first realised by Hennrich *et al.* (2000) and Kuhn *et al.* (2002). In Legero *et al.* (2003) and Legero *et al.* (2004) the interference of single photon pulses which were generated independently was observed. These experiments can gain in efficiency by using a single atom trapped within the cavity as was realised recently using an atom (McKeever *et al.*, 2004a) and an ion stored in a cavity (Keller *et al.*, 2004). Furthermore it was proposed (Gheri *et al.*, 1998) to generate a pulse of entangled photons from a single atom in a cavity. Compared to parametric down conversion, this scheme allows to generate a stream of entangled photons in a single spatial mode and within a narrow frequency band.

8.5.2 Quantum communication between different cavities

Atoms are well suited to store quantum information and photons are ideal to transport quantum information. Cirac *et al.* (1997) proposed a scheme to utilise photons for transmission of quantum information between atoms located at single nodes of a future quantum network. This scheme uses atoms strongly coupled to high-finesse cavities and special laser pulses exciting an atom at the sending node so that its state is mapped into a time-symmetric photon wave packet that will enter the cavity at the receiving node and be absorbed by the atom stored there. Van Enk *et al.* (1998) discuss the more realistic situation of the transmission of quantum information through photonic channels in the presence of noise. Further possibilities to reduce the noise of the transmission channel by using few additional atoms are proposed. These schemes using single atoms compete with a scheme proposed by Lukin *et al.* (2000) which uses intracavity electromagnetically induced transparency to store a light pulse in an ensemble of Λ-type atoms stored in the cavity as recently realised in an atomic vapour (Julsgaard *et al.*, 2004).

8.5.3 Entanglement generation and atomic quantum teleportation

Entanglement is the key ingredient of quantum information and computing science. It stands at the origin of the mysteries of quantum teleportation as well as the speed-up expected by Shor's factoring algorithm (Shor, 1997). There is a whole variety of schemes to generate entanglement between atoms stored in the same or in different cavities. A very popular scheme uses

projective measurements to realise entanglement between different atoms (Cabrillo *et al.*, 1999; Bose *et al.*, 1999; Sørensen and Mølmer, 2003a,b; Duan and Kimble, 2003). Another scheme uses cascaded cavity-QED systems and quantum reservoir engineering to unconditionally entangle the two systems under steady state conditions (Clark *et al.*, 2003). Other schemes aim at the entanglement between an atom stored in a cavity and an emitted photon (Sun *et al.*, 2004). The entanglement of the internal state of an ion with the polarisation of an emitted photon was realised by Blinov *et al.* (2004) using a trapped ion. The efficiency of this experiment could be strongly increased by strongly coupling the ion to the mode of a cavity.

8.5.4 Quantum computation

Quantum computation schemes using atoms stored at fixed positions in an optical cavity were also proposed (Pellizzari *et al.*, 1995), where the strong long range interaction between atoms in a cavity is used to provide an interaction between different qubits. There are also ideas to realise a conditional quantum phase gate for atoms sharing the coupling to the same cavity mode (Yi *et al.*, 2003). Recently, the realisation of a controlled phase-flip gate between single photon pulses was proposed (Duan and Kimble, 2004). Here, the nonlinear interaction between single photon pulses is generated by successively reflecting them from an optical cavity with a single trapped atom.

In conclusion, there is a wealth of interesting and fundamental experiments in different areas of quantum optics, which could be based on the system realised experimentally in this work.

Appendix A

Rubidum energy levels

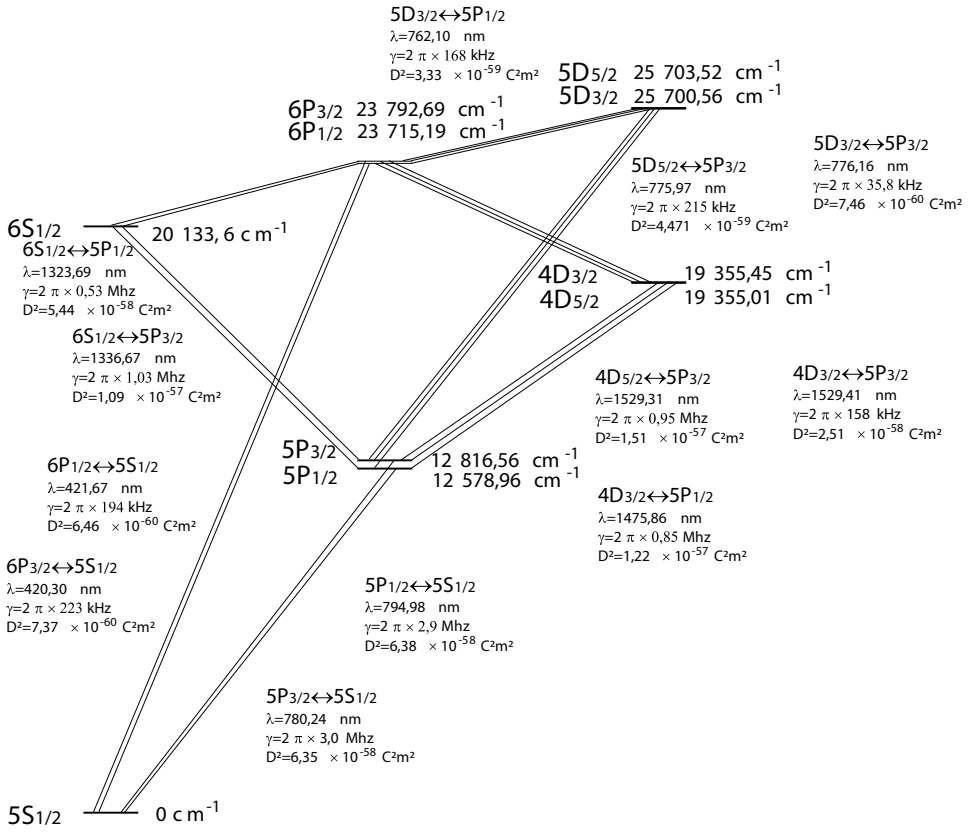

Figure A.1: Level scheme and transition strengths of Rubidium. The transition rate is $\gamma = \frac{1}{8\pi\epsilon_0}\frac{4(2\pi)^3}{3h\lambda^3}D^2$

Appendix B

Friction in the atom-cavity-trap system

The calculation of the friction coefficient is described in section 2.4.5. Using the definitions

$$\tilde{\Delta}_a := \Delta_a + i\gamma \tag{B.1}$$

$$\tilde{\Delta}_c := \Delta_c + i\kappa \tag{B.2}$$

$$A := g^2 - \tilde{\Delta}_a\tilde{\Delta}_c, \tag{B.3}$$

the friction coefficient for the atom-cavity-trap system reads

$$\begin{aligned} -\frac{2\hbar\eta^2}{|A|^6}\,\mathcal{I}m\,\Big(&\bar{A}^2\left(\tilde{\Delta}_a\bar{\tilde{\Delta}}_a\tilde{\Delta}_c^2 + g^2\tilde{\Delta}_a(2\tilde{\Delta}_a+\tilde{\Delta}_c) + g^4\right)(\nabla g)^2 \\ &- \bar{A}^2\left(g(\bar{\tilde{\Delta}}_a+\tilde{\Delta}_a)\tilde{\Delta}_c^2 + g^3\left((\tilde{\Delta}_a+\bar{\tilde{\Delta}}_a)+2(\tilde{\Delta}_a+\tilde{\Delta}_c)\right)\right)(\nabla\tilde{\Delta}_a)(\nabla g) \\ &+ \bar{A}^2g^2\left(g^2+\tilde{\Delta}_c^2\right)(\nabla\tilde{\Delta}_a)^2\Big). \end{aligned} \tag{B.4}$$

Here, $\bar{x}$ denotes the complex conjugate of x.

Bibliography

G. S. Agarwal. Vacuum-field Rabi splittings in microwave absorption by Rydberg atoms in a cavity. *Phys. Rev. Lett.*, **53**, 1732 (1984).

A. Aspect, J. Dalibard, A. Heidmann, C. Salomon, and C. Cohen-Tannoudji. Cooling atoms with stimulated emission. *Phys. Rev. Lett.*, **57**, 1688 (1986).

M. D. Barrett, J. Chiaverini, T. Schaetz, J. Britton, W. M. Itano, J. D. Jost, E. Knill, C. Langer, D. Leibfried, R. Ozeri, and D. J. Wineland. Deterministic quantum teleportation of atomic qubits. *Nature*, **429**, 737–739 (2004).

B. B. Blinov, D. L. Moehring, L. M. Duan, and C. Monroe. Observation of entanglement between a single trapped atom and a single photon. *Nature*, **428**, 153–157 (2004).

A. Boca, R. Miller, K. M. Birnbaum, A. D. Boozer, J. McKeever, and H. J. Kimble. Observation of the vacuum Rabi spectrum for one trapped atom. *Phys. Rev. Lett.*, **93**, 233603 (2004).

S. Bose, P. L. Knight, M. B. Plenio, and V. Vedral. Proposal for teleportation of an atomic state via cavity decay. *Phys. Rev. Lett.*, **83**, 5158–5161 (1999).

C. Cabrillo, J. I. Cirac, P. García-Fernández, and P. Zoller. Creation of entangled states of distant atoms by interference. *Phys. Rev. A*, **59**, 1025 (1999).

H. J. Carmichael. *An open Systems Approach to Quantum Optics*. Springer-Verlag (1991).

H. J. Carmichael. *Statistical Methods in Quantum Optics 1*. Springer-Verlag (1999).

H. J. Carmichael, H. M. Castro-Beltran, G. T. Foster, and L. A. Orozco. Giant violations of classical inequalities through conditional homodyne detection of the quadrature amplitudes of light. *Phys. Rev. Lett.*, **85**, 1855–1858 (2000).

H. W. Chan, A. T. Black, and V. Vuletić. Observation of collective-emission-induced cooling of atoms in an optical cavity. *Phys. Rev. Lett.*, **90**, 063003 (2003).

J. Chiaverini, D. Leibfried, T. Schaetz, M. D. Barrett, R. B. Blakestad, J. Britton, W. M. Itano, J. D. Jost, E. Knill, C. Langer, R Ozeri, and D. J. Wineland. Realization of quantum error correction. *Nature*, **432**, 602–605 (2004).

J. J. Childs, Kyungwon An, M. S. Otteson, R. R. Dasari, and M. S. Feld. Normal mode line shapes for atoms in standing-wave optical resonators. *Phys. Rev. Lett.*, **77**, 2901–2904 (1996).

I. Chiorescu, P. Bertet, K. Semba, Y. Nakamura, C. J. P. M. Harmans, and J. E. Mooij. Coherent dynamics of a flux qubit coupled to a harmonic oscillator. *Nature*, **431**, 159 (2004).

Steven Chu. Nobel lecture: The manipulation of neutral particles. *Rev. Mod. Phys.*, **70**, 685 (1998).

J. I. Cirac, P. Zoller, H. J. Kimble, and H. Mabuchi. Quantum state transfer and entanglement distribution among distant nodes in a quantum network. *Phys. Rev. Lett.*, **78**, 3221–3224 (1997).

Stephen Clark, Amy Peng, Mile Gu, and Scott Parkins. Unconditional preparation of entanglement between atoms in cascaded optical cavities. *Phys. Rev. Lett.*, **91**, 177901 (2003).

C. Cohen-Tannoudji. Atomic motion in laser light. In J. Dalibard, J.-M. Raimond, and J. Zinn-Justin, editors, *Fundamental systems in quantum optics*, number 53 in Les Houches Lectures, pages 1–164. Elsevier Science B.V. (1992).

Claude N. Cohen-Tannoudji. Nobel lecture: Manipulating atoms with photons. *Rev. Mod. Phys.*, **70**, 707 (1998).

J. Dalibard and C. Cohen-Tannoudji. Dressed-atom approach to atomic motion in laser light: the dipole force revisited. *J. Opt. Soc. Am. B*, **2**, 1707 (1985).

J. Dalibard and C. Cohen-Tannoudji. Laser cooling below the Doppler limit by polarization gradients: simple theoretical models. *J. Opt. Soc. Am. B*, **6**, 2023–2045 (1989).

A. C. Doherty, A. S. Parkins, S. M. Tan, and D. F. Walls. Motion of a two-level atom in an optical cavity. *Phys. Rev. A*, **56**, 833–844 (1997).

R. W. P Drever, J. L. Hall, F. V. Kowalski, J. Hough, G. M. Ford, A. J. Munley, and H. Ward. Laser phase and frequency stabilization using an optical resonator. *Appl. Phys. B*, **31**, 97 (1983).

L.-M. Duan and H. J. Kimble. Efficient engineering of multiatom entanglement through single-photon detections. *Phys. Rev. Lett.*, **90**, 253601 (2003).

L.-M. Duan and H. J. Kimble. Scalable photonic quantum computation through cavity-assisted interactions. *Phys. Rev. Lett.*, **92**, 127902 (2004).

L.-M. Duan, A. Kuzmich, and H. J. Kimble. Cavity QED and quantum-information processing with "hot" trapped atoms. *Phys. Rev. A*, **67**, 032305 (2003).

Urban Ernst. *Stabilisierung der Differenz zweier Laserfrequenzen mit Hilfe eines optischen Resonators*. Diplomarbeit, Universität Konstanz (1995).

T. Fischer, P. Maunz, P. W. H. Pinkse, T. Puppe, and G. Rempe. Feedback on the motion of a single atom in an optical cavity. *Phys. Rev. Lett.*, **88**, 1630002 (2002).

T. Fischer, P. Maunz, T. Puppe, P. W. H. Pinkse, and G. Rempe. Collective light forces on atoms in a high-finesse cavity. *New Journal of Physics*, **3**, 11.1–11.20 (2001).

Thomas Fischer. *Controlling the motion of an atom in an optical cavity*. Ph.d. thesis, Technische Universität München und Max-Planck-Institut für Quantenoptik (2002).

G. T. Foster, L. A. Orozco, H. M. Castro-Beltran, and H. J. Carmichael. Quantum state reduction and conditional time evolution of wave-particle correlations in cavity QED. *Phys. Rev. Lett.*, **85**, 3149–3152 (2000).

D. Frese, B. Ueberholz, S. Kuhr, W. Alt, D. Schrader, V. Gomer, and D. Meschede. Single atoms in an optical dipole trap: Towards a deterministic source of cold atoms. *Phys. Rev. Lett.*, **85**, 3777–3780 (2000).

Crispin W. Gardiner. *Handbook of Stochastic Methods*. Springer, second edition (1985).

K. M. Gheri, C. Saavedra, P. Törmä, J. I. Cirac, and P. Zoller. Entanglement engineering of one-photon wave packets using a single-atom source. *Phys. Rev. A*, **58**, R2627–2630 (1998).

A. Griessner, D. Jaksch, and P. Zoller. Cavity-assisted nondestructive laser cooling of atomic qubits. *J. Phys. B*, **37**, 1419–32 (2004).

R. Grimm, M. Weidemüller, and Y. B. Ovchinnikov. Optical dipole traps for neutral atoms. *Adv. At. Mol. Opt. Phys.*, **42** (2000).

G. R. Guthörlein, M. Keller, K. Hayasaka, W. Lange, and H. Walther. A single ion as a nanoscopic probe of an optical field. *Nature*, **414**, 49–51 (2001).

D. Haubrich, H. Schadwinkel, F. Strauch, B. Ueberholz, R. Wynands, and D. Meschede. Observation of individual neutral atoms in magnetic and magneto-optical traps. *Europhys. Lett.*, **34**, 663–668 (1996).

G. Hechenblaikner, M. Gangl, P. Horak, and H. Ritsch. Cooling an atom in a weakly driven high-Q cavity. *Phys. Rev. A*, **58**, 3030 (1998).

M. Hennrich, T. Legero, A. Kuhn, and G. Rempe. Vacuum-stimulated Raman scattering based on adiabatic passage in a high-finesse optical cavity. *Phys. Rev. Lett.*, **85**, 4872–4875 (2000).

Tetsuya Ido Hidetoshi Katori and Makoto Kuwata-Gonokami. Optimal design of dipole potentials for efficient loading of Sr atoms. *Journal of the Physical Society of Japan*, **68**, 2479–2482 (1999).

C. J. Hood, M. S. Chapman, T. W. Lynn, , and H. J. Kimble. Real-time cavity QED with single atoms. *Phys. Rev. Lett.*, **80**, 4157–4160 (1998).

C. J. Hood, H. J. Kimble, and J. Ye. Characterization of high finesse mirrors: loss, phase shifts and mode structure in an optical cavity. *Phys. Rev. A*, **64**, 033804 (2001).

C. J. Hood, T. W. Lynn, A. C. Doherty, A. S. Parkins, and H. J. Kimble. The atom-cavity microscope: Single atoms bound in orbit by single photons. *Science*, **287**, 1457 (2000).

P. Horak, G. Hechenblaikner, K. M. Gheri, H. Stecher, and H. Ritsch. Cavity-induced atom cooling in the strong coupling regime. *Phys. Rev. Lett.*, **79**, 4974–4977 (1997).

P. Horak, H. Ritsch, T. Fischer, P. Maunz, T. Puppe, P. W. H. Pinkse, and G. Rempe. An optical kaleidoscope using a single atom. *Phys. Rev. Lett.*, **88**, 043601 (2002).

Peter Horak, Stephen M. Barnett, and Helmut Ritsch. Coherent dynamics of Bose-Einstein condensates in high-finesse optical cavities. *Phys. Rev. A*, **61**, 033609 (2000).

Z. Hu and H. J. Kimble. Observation of a single atom in a magneto-optical trap. *Opt. Lett.*, **19**, 1889–1890 (1994).

Tetsuya Ido, Yoshitomo Isoya, and Hidetoshi Katori. Optical-dipole trapping of Sr atoms at a high phase-space density. *Phys. Rev. A*, **61**, 061403 (2000).

E. T. Jaynes and F. W. Cummings. Comparison of quantum and semiclassical radiation theories with application to the beam maser. *Proc. IEEE*, **51**, 89 (1963).

Brian Julsgaard, Jacob Sherson, J. Ignacio Cirac, Jaromir Fiurášek, and Eugene S. Polzik. Experimental demonstration of quantum memory for light. *Nature*, **432**, 482 (2004).

Matthias Keller, Birgit Lange, Kazuhiro Hayasaka, Wolfgang Lange, and Herbert Walther. Continuous generation of single photons with controlled waveform in an ion-trap cavity system. *Nature*, **431**, 1075 (2004).

E. Knill, R. Laflamme, and G. J. Milburn. A scheme for efficient quantum computing with linear optics. *Nature*, **409**, 46–52 (2001).

A. Kreuter, C. Becher, G. P. T. Lancaster, A. B. Mundt, C. Russo, H. Haffner, C. Roos, J. Eschner, F. Schmidt-Kaler, and R. Blatt. Spontaneous emission lifetime of a single trapped Ca^+ ion in a high finesse cavity. *Phys. Rev. Lett.*, **92**, 203002 (2004).

D. Kruse, C. von Cube, C. Zimmermann, and Ph. W. Courteille. Observation of lasing mediated by collective atomic recoil. *Phys. Rev. Lett.*, **91**, 183601 (2003).

A. Kuhn, M. Hennrich, and G. Rempe. Deterministic single-photon source for distributed quantum networking. *Phys. Rev. Lett.*, **89**, 067901 (2002).

S. Kuhr, W. Alt, D. Schrader, M. Müller, V. Gomer, and D. Meschede. Deterministic delivery of a single atom. *Science*, **293**, 278–280 (2001).

Joe Leach and P. R. Rice. Cavity QED with quantized center of mass motion. *Phys. Rev. Lett.*, **93**, 103601 (2004).

T. Legero, T. Wilk, A. Kuhn, and G. Rempe. Time-resolved two-photon quantum interference. *Appl. Phys. B*, **77**, 797 (2003).

Thomas Legero, Tatjana Wilk, Markus Hennrich, Gerhard Rempe, and Axel Kuhn. Quantum beat of two single photons. *Phys. Rev. Lett.*, **93**, 070503 (2004).

V. S. Letokhov and V. G. Minogin. Laser radiation pressure on free atoms. *Physics Reports*, **73**, 1–65 (1981).

P. Lett, R. Watts, C. Westbrook, W. Phillips, P. Gould, and H. Metcalf. Observation of atoms laser cooled below the Doppler limit. *Phys. Rev. Lett.*, **61**, 169 (1988).

Benjamin Lev, Kartik Srinivasan, Paul Barclay, Oskar Painter, and Hideo Mabuchi. Feasibility of detecting single atoms using photonic bandgap cavities. *Nanotechnology*, **15**, S556–S561 (2004).

L. A. Lugiato. Theory of optical bistability. In E. Wolf, editor, *Progress in Optics*, volume XXI, pages 71–216. Elsevier Science Publishers, B. V. (1984).

M. D. Lukin, S. F. Yelin, and M. Fleischhauer. Entanglement of atomic ensembles by trapping coherent photon states. *Phys. Rev. Lett.*, **84**, 4235–4238 (2000).

H. Mabuchi, Q. A. Turchette, M. S. Chapman, and H. J. Kimble. Real-time detection of individual atoms falling through a high-finesse cavity. *Opt. Lett.*, **21**, 1393–1395 (1996).

M. Matsumoto and T. Nishimura. Mersenne twister: A 623-dimensionally equidistributed uniform pseudorandom number generator. *ACM Trans. on Modeling and Computer Simulation*, **8**, 3–30 (1998).

P. Maunz, T. Puppe, T. Fischer, P. W. H. Pinkse, and G. Rempe. Emission pattern of an atomic dipole in a high-finesse optical cavity. *Opt. Lett.*, **28**, 46–48 (2003).

P. Maunz, T. Puppe, I. Schuster, N. Syassen, P. W. H. Pinkse, and G. Rempe. Cavity cooling of a single atom. *Nature*, **428**, 50 (2004).

P. Maunz, T. Puppe, I. Schuster, N. Syassen, P. W. H. Pinkse, and G. Rempe. Normal-mode spectroscopy of a single-bound-atom–cavity system. *Phys. Rev. Lett.*, **94**, 033002 (2005).

Peter Maunz. *Photoneninduzierte Bewegung einzelner Atome in einem optischen Resonator*. Diplomarbeit, Universität Konstanz (1999).

J. McKeever, A. Boca, A. D. Boozer, R. Miller, J. R. Buck, A. Kuzmich, and H. J. Kimble. Deterministic generation of single photons from one atom trapped in a cavity. *Science*, **303**, 1992–1994 (2004a).

J. McKeever, J. R. Buck, A. B. Boozer, A. Kuzmich, H.-C. Nägerl, D. M. Stamper-Kurn, and H. J. Kimble. State-insensitive cooling and trapping of single atoms in an optical cavity. *Phys. Rev. Lett.*, **90**, 133602 (2003).

J. McKeever, J. R. Buck, A. D. Boozer, and H. J. Kimble. Determination of the number of atoms trapped in an optical cavity. *Phys. Rev. Lett.*, **93**, 143601 (2004b).

Harold J. Metcalf and Peter van der Straten. *Laser Cooling and Trapping*. Springer-Verlag, New York (1999).

Pierre Meystre and Murray Sargent, III. *Elements of Quantum Optics*. Springer-Verlag, Berlin, third edition (1999).

K. Mølmer, Y. Castin, and J. Dalibard. Monte Carlo wave-function method in quantum optics. *J. Opt. Soc. Am. B*, **10**, 524–538 (1993).

C. Monroe. Quantum information processing with atoms and photons. *Nature*, **416**, 238–246 (2002).

P. Münstermann, T. Fischer, P. Maunz, P. W. H. Pinkse, and G. Rempe. Dynamics of single-atom motion observed in a high-finesse cavity. *Phys. Rev. Lett.*, **82**, 3791–3794 (1999a).

P. Münstermann, T. Fischer, P. Maunz, P. W. H. Pinkse, and G. Rempe. Observation of cavity-mediated long-range light forces between strongly coupled atoms. *Phys. Rev. Lett.*, **84**, 4068–4071 (2000).

P. Münstermann, T. Fischer, P. W. H. Pinkse, and G. Rempe. Single slow atoms from an atomic fountain observed in a high-finesse optical cavity. *Opt. Comm.*, **159**, 63–67 (1999b).

Peter Münstermann. *Dynamik einzelner Atome in einem Resonator höchster Finesse*. Ph.D. thesis, Fakultät für Physik, Universität Konstanz (1999).

Karim Murr. On the suppression of the diffusion and the quantum nature of a cavity mode. optical bistability: forces and friction in driven cavities. *J. Phys. B*, **36**, 2515–2537 (2003).

B. Nagorny, Th. Elsasser, and A. Hemmerich. Collective atomic motion in an optical lattice formed inside a high finesse cavity. *Phys. Rev. Lett.*, **91**, 153003 (2003).

W. Neuhauser, M. Hohenstatt, P. E. Toschek, and H. Dehmelt. Localized visible Ba^+ mono-ion oscillator. *Phys. Rev. A*, **22**, 1137–1140 (1980).

T. Pellizzari, S. A. Gardiner, J. I. Cirac, and P. Zoller. Decoherence, continuous observation, and quantum computing: A cavity QED model. *Phys. Rev. Lett.*, **75**, 3788–3791 (1995).

William D. Phillips. Nobel lecture: Laser cooling and trapping of neutral atoms. *Rev. Mod. Phys.*, **70**, 721 (1998).

P. W. H. Pinkse, T. Fischer, P. Maunz, and G. Rempe. Trapping an atom with single photons. *Nature*, **404**, 365–368 (2000).

T. Puppe, P. Maunz, T. Fischer, P.W.H. Pinkse, and G. Rempe. Single-atom trajectories in higher-order transverse modes of a high-finesse optical cavity. *Physica Scripta*, **T112**, 7–12 (2004).

E. L. Raab, M. Prentiss, A. Cable, S. Chu, and D. E. Pritchard. Trapping of neutral sodium atoms with radiation pressure. *Phys. Rev. Lett.*, **59**, 2631 (1987).

J. E. Reiner, H. M. Wiseman, and H. Mabuchi. Quantum jumps between dressed states: A proposed cavity-QED test using feedback. *Phys. Rev. A*, **67**, 042106 (2003).

J. P. Reithmaier, G. Sek, A. Löffler, C. Hoffmann, S. Kuhn, S. Reitzenstein, L. V. Keldysh, T. L. Reinecke, and A. Forchel. Strong coupling in a single quantum dot-semiconductor microcavity system. *Nature*, **432**, 197 (2004).

G. Rempe. One atom in an optical cavity: spatial resolution beyond the standard diffraction limit. *Appl. Phys. B*, **60**, 233–237 (1995).

G. Rempe, R. J. Thompson, H. J. Kimble, and R. Lalezari. Measurement of ultralow losses in an optical interferometer. *Opt. Lett.*, **17**, 363–365 (1992).

M. Riebe, H. Häffner, C. F. Roos, W. Hänsel, J. Benheim, G. P. T. Lancester, T. W. Körber, C. Becher, F. Schmidt-Kaler, D. F. V. James, and R. Blatt. Deterministic quantum teleportation with atoms. *Nature*, **429**, 734–737 (2004).

F. Ruschewitz, D. Bettermann, J. L. Peng, and W. Ertmer. Statistical investigations on single trapped neutral atoms. *Europhys. Lett.*, **34**, 651–656 (1996).

J. J. Sanchez-Mondragon, N. B. Narozhny, and J. H. Eberly. Theory of spontaneous-emission line shape in an ideal cavity. *Phys. Rev. Lett.*, **51**, 550 (1983). Erratum ibid, p. 1925.

J. A. Sauer, K. M. Fortier, M. S. Chang, C. D. Hamley, and M. S. Chapman. Cavity QED with optically transported atoms. *Phys. Rev. A*, **69**, 051804(R) (2004).

T. A. Savard, K. M. O'Hara, and J. E. Thomas. Laser-noise-induced heating in far-off resonance optical traps. *Phys. Rev. A*, **56**, R1095 (1997).

N. Schlosser, G. Reymond, I. Protsenko, and P. Grangier. Sub-poissonian loading of single atoms in a microscopic dipole trap. *Nature*, **411**, 1024–1027 (2001).

H. R. Schwarz. *Numerische Mathematik*. B. G. Teubner, 4th edition (1997).

P. W. Shor. Polynomial-time algorithms for prime factorization and discret logarithms on a quantum comupter. *SIAM Journal on Computing*, **26**, 1484–1509 (1997).

Anders S. Sørensen and Klaus Mølmer. Measurement induced entanglement and quantum computation with atoms in optical cavities. *Phys. Rev. Lett.*, **91**, 097905 (2003a).

Anders S. Sørensen and Klaus Mølmer. Probabilistic generation of entanglement in optical cavities. *Phys. Rev. Lett.*, **90**, 127903 (2003b).

S. M. Spillane, T. J. Kippenberg, K. J. Vahala, K. W. Goh, E. Wilcut, and H. J. Kimble. Ultrahigh-q toroidal microresonators for cavity quantum electrodynamics. *Phys. Rev. A*, **71**, 013817 (2005).

B. Sun, M. S. Chapman, and L. You. Atom-photon entanglement generation and distribution. *Phys. Rev. A*, **69**, 042316 (2004).

Niels Syassen. *Linear and nonlinear spectroscopy of a strongly-coupled atom-cavity system.* Master's thesis, Max-Planck-Institut für Quantenoptik and Technische Universität München (2003).

R. J. Thompson, G. Rempe, and H. J. Kimble. Observation of normal-mode splitting for an atom in an optical cavity. *Phys. Rev. Lett.*, **68**, 1132–1135 (1992).

Q. A. Turchette, C. J. Hood, W. Lange, M. Mabuchi, and H. J. Kimble. Measurement of conditional phase shifts for quantum logic. *Phys. Rev. Lett.*, **75**, 4710–4713 (1995).

K. J. Vahala. Optical microcavities. *Nature*, **424**, 839–846 (2003).

S. J. van Enk, J. I. Cirac, and P. Zoller. Photonic channels for quantum communication. *Science*, **279**, 205 (1998).

S. J. van Enk, J. McKeever, H. J. Kimble, and J. Ye. Cooling of a single atom in an optical trap inside a resonator. *Phys. Rev. A*, **64**, 013407 (2001).

D. W. Vernooy, A. Furusawa, N. Ph. Georgiades, V. S. Ilchenko, and H. J. Kimble. Cavity QED with high-Q whispering gallery modes. *Phys. Rev. A*, **57**, R2293 (1998).

D. W. Vernooy and H. J. Kimble. Well-dressed states for wave-packet dynamics in cavity QED. *Phys. Rev. A*, **56**, 4287–4295 (1997).

V. Vuletić and S. Chu. Laser cooling of atoms, ions, or molecules by coherent scattering. *Phys. Rev. Lett.*, **84**, 3787–3790 (2000).

A. Wallraff, D. I. Schuster, A. Blais, L. Frunzio, R.-S. Huang, J. Majer, S. Kumar, S. M. Girvin, and R. J. Schoelkopf. Strong coupling of a single photon to a superconducting qubit using circuit quantum electrodynamics. *Nature*, **431**, 162 (2004).

D. J. Wineland and W. M. Itano. Spectroscopy of a single Mg^+ ion. *Phys. Lett.*, **82A**, 75–78 (1981).

H. M. Wiseman and G. J. Milburn. Interpretation of quantum jump and diffusion processes illustrated on the Bloch sphere. *Phys. Rev. A*, **47**, 1652 (1993).

J. Ye, D. W. Vernooy, and H. J. Kimble. Trapping of single atoms in cavity QED. *Phys. Rev. Lett.*, **83**, 4987 (1999).

X. X. Yi, X. H. Su, and L. You. Conditional quantum phase gate between two 3-state atoms. *Phys. Rev. Lett.*, **90**, 097902 (2003).

T. Yoshie, A. Scherer, J. Hendrickson, G. Khitrova, H. M. Gibbs, G. Rupper, C. Ell, O. B. Shchekin, and D. G. Deppe. Vacuum Rabi splitting with a single quantum dot in a photonic crystal nanocavity. *Nature*, **432**, 200–203 (2004).

Y. Zhu, J. Gauthier, S. E. Morin, Q. Wu, H. J. Carmichael, and T. W. Mossberg. Vacuum Rabi splitting as a feature of linear-dispersion theory: Analysis and experimental observations. *Phys. Rev. Lett.*, **64**, 2499–2502 (1990).

Stefano Zippilli, Giovanna Morigi, and Helmut Ritsch. Suppression of Bragg scattering by collective interference of spatially ordered atoms with a high-Q cavity mode. *Phys. Rev. Lett.*, **93**, 123002 (2004).

Publications

P. Maunz, T. Puppe, I. Schuster, N. Syassen, P.W.H. Pinkse, and G. Rempe, Normal-mode spectroscopy of a single-bound-atom–cavity system, *Physical Review Letters* **94**, 033002 (2005).

P. Maunz, T. Puppe, I. Schuster, N. Syassen, P.W.H. Pinkse, and G. Rempe, Cavity cooling of a single atom, *Nature* **428**, 50-52 (2004).

T. Puppe, P. Maunz, T. Fischer, P.W.H. Pinkse, and G. Rempe, Single-atom trajectories in higher-order transverse modes of a high-finesse optical cavity, *Physica Scripta*, **T112**, p 7-12 (2004).

P. Maunz, T. Puppe, T. Fischer, P. W. H. Pinkse, and G. Rempe, Emission pattern of an atomic dipole in a high-finesse optical cavity, *Optics Letters* **28**, 46 (2003).

T. Fischer, P. Maunz, P. W. H. Pinkse, T. Puppe and G. Rempe, Feedback on the Motion of a Single Atom in an Optical Cavity, *Physical Review Letters* **88**, 163002 (2002).

P. Horak, H. Ritsch, T. Fischer, P. Maunz, T. Puppe, P.W.H. Pinkse and G. Rempe, An optical kaleidoscope using a single atom, *Physical Review Letters* **88**, 043601 (2002).

T. Fischer, P. Maunz, T. Puppe, P.W.H. Pinkse and G. Rempe, Collective light forces on atoms in a high-finesse cavity, *New Journal of Physics*, **3**, (2001).

P.W.H. Pinkse, T. Fischer, P. Maunz, T. Puppe, and G. Rempe, How to catch an atom with single photons, *Journal of Modern Optics* **47**, 2769-2787 (2000).

P. Münstermann, T. Fischer, P. Maunz, P.W.H. Pinkse, and G. Rempe, Observation of cavity-mediated long-range light forces between strongly coupled atoms, *Physical Review Letters* **84**, 4068-4071 (2000).

P.W.H. Pinkse, T. Fischer, P. Maunz, and G. Rempe, Trapping an atom with single photons, *Nature* **404**, 365-368 (2000).

P. Münstermann, T. Fischer, P. Maunz, P.W.H. Pinkse, and G. Rempe, Dynamics of single-atom motion observed in a high-finesse cavity, *Physical Review Letters* **82**, 3791 (1999).

Symbols

β Friction coefficient. The velocity-dependent force in first order of the atomic velocity is $\langle F \rangle_1 = -\beta v$, page 24.

c Speed of light in vacuum, $c = 299792458\,\mathrm{m/s}$, page 15.

D_{dp} Momentum diffusion due to fluctuations of the dipole force, page 23.

D_{se} Momentum diffusion due to spontaneous emission of photon from the atom, page 23.

Δ Detuning between atomic and cavity resonance, $\Delta = \omega_c - \omega_a$, page 16.

Δ_a Atom probe detuning, $\Delta_a = \omega_p - \omega_a$, page 21.

$\Delta_{a,\mathrm{eff}}$ Effective atom detuning between the probe laser and the Stark shifted atomic resonance assuming a two-level atom, $\Delta_{a,\mathrm{eff}} = \Delta_a - 2\Delta_S$, page 33.

$\tilde{\Delta}_a$ Generalised atom probe detuning, $\tilde{\Delta}_a = \Delta_a + i\gamma$, page 21.

Δ_c Cavity probe detuning, $\Delta_c = \omega_p - \omega_c$, page 21.

$\tilde{\Delta}_c$ Generalised cavity probe detuning, $\tilde{\Delta}_c = \Delta_c + i\kappa$, page 21.

Δ_S Stark shift of the far-detuned trapping field, $\Delta_S = n_{\mathrm{trap}} \times 100\,\mathrm{Hz}$, page 67.

Δ_{eff} Detuning between the probe laser and the Stark shifted atomic resonance frequency, $\Delta_{\mathrm{eff}} = \Delta - 2\Delta_S$, page 102.

ϵ_0 Vacuum permittivity, $\epsilon_0 = \frac{1}{4\pi c^2}\, 10^7 \frac{\mathrm{C}^2}{\mathrm{Nm}^2}$, page 15.

η Pump strength of the incident beam. For $\eta = \kappa$ leads to one photon in the empty resonant cavity ($n_e = 1$), page 17.

$\mathcal{F}$ Cavity finesse, $\mathcal{F} = 4.4 \times 10^5$, page 66.

FSR Free spectral range of the high-finesse cavity, $\mathrm{FSR} = \pi c/l = 1.232\,\mathrm{THz}$, page 66.

g Coupling strength between atom and cavity mode. The maximal coupling at an antinode, $g(\mathbf{r}) = g_0\phi(\mathbf{r})$, $g_0 = 2\pi \times 16\,\mathrm{MHz}$, page 15.

γ Polarisation decay rate of the $5P_{3/2}$ excited state of ^{85}Rb, $\gamma = 2\pi \times 3\,\mathrm{MHz}$, page 18.

κ Cavity field decay rate, $\kappa = 2\pi \times 1.4\,\mathrm{MHz}$, page 66.

l Cavity length, $l = 156\,\lambda_{780} \approx 121.7\,\mu\mathrm{m}$, page 66.

λ Wavelength of the probe laser, $\lambda = 780.243\,\mathrm{nm}$, page 58.

λ_{trap} Wavelength of the trapping light field, $\lambda_{\mathrm{trap}} = 785.28\,\mathrm{nm}$, page 67.

m Mass of ^{85}Rb, $m = 84.91\,\mathrm{u}$, page 20.

$\mathcal{L}$ Absorption of the high-finesse mirrors, $\mathcal{L} = 4.5\,\mathrm{ppm}$, page 62.

$\mathcal{T}$ Transmission of the high-finesse mirrors, $\mathcal{T} = 2.6\,\mathrm{ppm}$, page 62.

n_e Photon number in the empty resonant cavity which is generated by the driving, $n_e = \frac{P_p}{6.8\,\mathrm{pW}}$, page 66.

n_{trap} Intracavity photons in the far-detuned trapping field, $n_{\mathrm{trap}} = \frac{P}{0.9\,\mathrm{pW}}$, page 66.

ω_a Resonance frequency of the atomic atomic transition, page 15.

ω_c Resonance frequency of the cavity, page 15.

ω_p Frequency of the pump laser, page 17.

ϕ Spatial modefunction of the cavity, $\phi(\mathbf{r}) = \cos(kz)e^{-(x^2+y^2)/\mathrm{w}_0^2}$, page 20.

P_p Probe power incident on the cavity. A probe power of $P_p = 6.8\,\mathrm{pW}$ produces one intracavity photon on average in the empty resonant cavity, $n_e = 1$. This in turn generates a transmission of $0.9\,\mathrm{pW}$ corresponding to a detector count rate of $1\,\mathrm{MHz}$, page 92.

U_{trap} Depth of trapping potential of the far-detuned dipole trap, $U_{\mathrm{trap}} = n_{\mathrm{trap}} \times 5\,\mathrm{nK}$, page 67.

P Transmission of the trapping field, $P = n_{\mathrm{trap}} \times 0.9\,\mathrm{pW}$, page 67.

w_0 Cavity beam waist, $w_0 = 30\,\mu\mathrm{m}$, page 61.

ξ Quantum efficiency for the detection of photons transmitted by the cavity, $\xi = 30\%$, page 66.

Danksagung

Die letzte Seite dieser Arbeit ist all denen gewidmet, ohne die das Gelingen dieser Arbeit nicht möglich gewesen wäre.

Meinem Doktorvater Gerhard Rempe, der mich seit den ersten Studiensemestern in Konstanz immer wieder neu für die Physik begeistert hat, danke ich dafür, daß er mir die Arbeit an diesem außergewöhnlichen Experiment ermöglicht, und mir dabei viele Freiheiten gelassen und eigenverantwortliche Forschungsarbeit ermöglicht hat. Ich bedanke mich für guten Rat, viel Geduld und stetes Nachfragen, das wesentlich zum Erfolg des Experimentes beigetragen hat.

Ein so komplexes Experiment läßt sich nur im Team entwickeln, aufbauen und bedienen. Ich hatte das große Glück von Peter Münstermann und Thomas Fischer eine Apparatur übernehmen zu können, die sich dank ihrer umsichtigen und soliden Konstruktion gut verändern und erweitern ließ. Dafür bin ich ihnen sehr dankbar. Ganz besonders bedanke ich mich bei Thomas Puppe, Ingrid Schuster, Niels Syassen und Pepijn Pinkse, die mit mir das Experiment zu dem gemacht haben, was es heute ist. Ich danke für viele Diskussionen, die Arbeit im Labor, das Durchhaltevermögen in den langen Meßnächten und nicht zuletzt für die kritische Korrektur dieser Arbeit. Helmut Ritsch, Axel Kuhn und Karim Murr danke ich für interessante Diskussionen. Allen Mitarbeitern der Abteilung Quantendynamik danke ich für das hervorragende Arbeitsklima und die Erfahrung, sich auf jeden Einzelnen verlassen zu können. Beim Max-Planck-Institut für Quantenoptik in Garching bedanke ich mich für die exzellenten Arbeitsbedingungen, die den Aufbau dieses Experimentes ermöglicht haben.

Aber auch in dieser Doktorarbeit gab es schwere Zeiten, die ich ohne Musik und Tanz nicht so leicht durchgestanden hätte. Hierfür bedanke ich mich bei all jenen, die mein Interesse dafür geweckt haben und mir durch ihren hervorragenden Unterricht, der mir auch fachlich weitergebracht hat, eine neue Welt eröffnet haben. Meinen Freunden und Mitbewohnern danke ich für ihre Unterstützung, ihre Geduld und Freundschaft, die manchmal strapaziert wurde.

Ganz herzlich bedanke ich mich auch bei meinem Vater und meiner Schwester Brigitte für ihr Vertrauen, ihre bedingungslose Unterstützung und ihr Interesse an dieser Arbeit.